An NMR Study of Aqueous Isopolytungstate, Molybdotungstate and Tungstovanadate Solutions

by

Jeremy Joseph Hastings

Submitted for the Degree of Doctor of Philosophy

The University of Warwick

Department of Chemistry

October 1993

Contents.

List of Tables

Chapter 1

Chapter 4

Chapter 5

Chapter 6

List of Figures

Chapter 1

Chapter 4

Chapter 5

Chapter 6

Chapter 7

List of Schemes

Acknowledgements

I wish to express my gratitude to Dr. O. W. Howarth for advice, guidance and encouragement which he extended during the course of this research. Further my sincere thanks for his generous allocation of instrument time and access to his word processor.

I would like to thank Dr. L. Pettersson (and his colleagues) at Umeå University, Sweden for providing extremely good computer fits to my NMR data and for his encouragement and helpful discussions.

I would like to thank Dr. I. Sadler and Dr. D. Reed for access to the Ultra-High Field NMR service at Edinburgh University.

Also my thanks to the other members of academic staff at Warwick University for their helpful discussions and in particular I would like to thank Dr C. J. Samuel for his help and access to his laser printer.

I would also like to thank the members of NMR team past and present for their support and assistance.

Finally, and most importantly, I gratefully acknowledge the forbearance and support of my family and especially my wife, Julie and my daughter, Emma.

Declaration

The work described in this thesis is the original of the author, except where acknowledgement has been made to results and ideas previously published. The work was carried out at the Department of Chemistry, University of Warwick, between October 1989 and October 1993 and has not been submitted previously for a degree at any institution.

Summary

Isopolytungstates have been studied in aqueous solution between pH≈ 8-1, using ^{183}W, ^{17}O, ^{7}Li and ^{1}H NMR spectroscopy. The first isopolyanions to form upon acidification are the paratungstates-A and -B. Their resonances are largely assigned, and paratungstate-B is shown to protonate with pK_a = 4.59. Its protonated form has at least two isomers separated by a detectably slow proton-exchange process. On further acidification, paratungstate-B loses one tungsten atom to give an anion with no symmetry, which is identified as the solution form of ψ-metatungstate. This in turn protonates with pK_a =2.65. Six metatungstate species with Keggin structures are also observed at lower pH values. Two have the β-Keggin structures. In each case direct structural information is provided from the solution state. The rotational correlation times and average interproton distances of the α- and β-$[H_2W_{12}O_{40}]^{6-}$ species are deduced from their ^{1}H NMR relaxation data, and similar data are used to assist in identifying the three internally monoprotonated α- and β- Keggin anions.

Using ^{183}W and ^{95}Mo NMR spectroscopy, molybdotungstates in aqueous solution have been examined over a wide range of metal-ion ratios in the pH range 3-6. Molybdenum is shown to substitute into heptatungstate forming a range of isomers $[Mo_xW_{7-x}O_{24}]^{6-}$ (x=1 to 6) with a positional preference for the "ends" and least for the "central" W atoms. Assignments for 19 of the isomers present have been proposed. The ratios of the equilibrium constants for a given mixed-metal species with respect to the separate constants for the formation of heptatungstate from tungstate, and heptamolybdate from molybdate have been determined using the least-squares computer program LAKE. Mo is also shown to substitute only once into paratungstate-B and the α-Keggin species. Structures for these anions have been proposed and the substituted paratungstate-B is shown to protonate with pK_a = 4.9.

Tungstovanadates in aqueous solution have been investigated using ^{51}V, ^{183}W and ^{17}O NMR spectroscopy over a wide range of metal-ion concentration and temperature in the range pH 1.2-7. The structures of the anions *fac*-$[W_3V_3O_{19}]^{5-}$, *cis*-$[W_4V_2O_{19}]^{4-}$, *cis*-$[HW_4V_2O_{19}]^{3-}$, $[W_5VO_{19}]^{3-}$ and α-$[H_2W_{11}VO_{40}]^{7-}$ have been confirmed. Sound evidence is presented for species *mer*-$[W_3V_3O_{19}]^{5-}$ and *trans*-$[W_4V_2O_{19}]^{4-}$. ^{51}V-^{51}V correlation spectroscopy has established the unequivocal assignment of the $[WV_9O_{28}]^{5-}$ species with the tungsten replacing one of the "capping" vanadium atoms. $[WV_9O_{28}]^{5-}$ is also shown to protonate primarily at the bridging oxygens furthest away from W, with pK_a=2.1. Tentative evidence is also presented for the solution species $[W_8V_2O_{32}]^{6-}$, and more heavily substituted α- and β- metatungstates. Calculations on quantitative ^{51}V NMR data (25°C, 0.6 mol dm^{-3} NaCl) using the least-squares computer program LAKE have established the formation constants for the major species. The chemical speciation is illustrated in distribution diagrams.

Glossary

Symbols

B_0	static magnetic field strength of NMR spectrometer
B_L	local magnetic field (components B_{xL}, B_{yL}, B_{zL}) - of random field or dipolar origin
1D	one dimension
2D	two dimensions
I	nuclear spin quantum number
$^nJ_{AB}$, $^nJ(AB)$	nuclear spin-spin coupling constant through n bonds (in Hz) between nuclei A and B.
ln	natural logarithm (base e)
log	logarithm (base 10)
M	(i) molar, (ii) molecular weight.
M_0	equilibrium macroscopic magnetisation of a spin system in the presence of B_0
$M_{z(0)}$	initial component of macroscopic magnetisation about the z axis
$M_{z(\tau)}$	component of macroscopic magnetisation about the z axis after time τ
pH	-log[H^+]
pK_a	activation equilibrium constant (= $-\log_{10} K_a$)
p,q,r	notation for the p of moles of H^+ , q of moles of MO_4^{x-} and r of moles of NO_4^{x-} , where p,q,r are integers
q	electric field gradient
Q	nuclear quadrupole moment
R	dipolar coupling constant
r	general symbol for distance
S	signal height
$S_{(\infty)}$	signal height after a time greater than T_1
$S_{(\tau)}$	signal height after time τ
T_1	spin-lattice relaxation time
T_2	spin-spin relaxation time
T_d	pulse delay time
β_{pqr}	stability formation constant for a polynuclear metal cation
γ	gyromagnetic ratio (rad T^{-1} s^{-1})
δ_X	chemical shift (for the resonance) of nucleus of element X. (ppm)
ε	1/sweepwidth
η	asymmetry factor

θ	angle - especially for that between a given vector and $\mathbf{B}_0$
λ_{max}	wavelength corresponding to the maximum point of the absorption band
μ	magnetic dipole moment
μ_0	magnetic dipole moment (component μ_z along $\mathbf{B}_0$)
π	a 180° pulsewidth
$\Delta\sigma$	(i) anisotropy in ($\Delta\sigma = \sigma_{\|\|} - \sigma_{\perp}$), (ii) difference in σ for two different situations
$\sigma_{\|\|}$,$\sigma_{\perp}$	components of σ components parallel and perpendicular to a molecular symmetry axis
τ	time between radio frequency pulses
τ_c	correlation time
τ_{null}	recovery time sufficing to give zero signal after a 180° pulse
ω	angular frequency expressed in rad s^{-1}

Abbreviations

COSY	correlation spectroscopy
CW	continuous wave
DANTE	delays alternating with nutation excitation
DD	dipole dipole
EMF	electromotive force
ESR	electron spin resonance
FID	free induction decay
FT	Fourier transform
(n,m)	for the species $[M_nV_mO_x]^{(2x-6n-5m)-}$
NMR	nuclear magnetic resonance
ppm	parts per million
rf	radio frequency
SA	shielding anisotropy
TSP	3-(trimethylsilyl)propionic acid, sodium salt
UV	ultra violet
ca.	*circa* (about)
e.g.	*exempli gratis* (for instance)
et al.	*et alli* (and others)
e.t.c.	*et ceteri* (and so forth)
fac-	facial
i.e.	*id est* (that is)
mer-	meridional

Units

Å	Angström = 10^{-10} m	min	minute
cm^{-1}	wavenumber	mol	mole
Hz	hertz	rad	radian (360°/2π)
J	joule	s	seconds
l	litre	T	temperature (K)
m	metre		

Fundamental constants

B	magnetic field strength (400 MHz for ^1H) = 9.3950 tesla(T)
e	charge on an electron $=1.602 \times 10^{-19}$ C
h	Planck constant = 6.626×10^{-34} J s
k	Boltzmann constant = 1.38×10^{-23} J K^{-1}
R	Universal gas constant = 8.31451 J K^{-1} mol^{-1}
γ_H	magnetogyric ratio of proton = 2.675197×10^8 rad s^{-1} T^{-1}
γ_W	magnetogyric ratio of tungsten = 1.1283×10^7 rad s^{-1} T^{-1}
μ_0	permeability constant = $4\pi \times 10^{-7}$ kg m s^{-2} A^{-2}
π	3.14159
ω_0	spectrometer operating at 400 MHz = 2.513×10^9 rad s^{-1}

1. INTRODUCTION

Even though several structures of isolated isopolytungstates have been reported [1-10], the chemistry of aqueous isopoly- and heteropolytungstate solutions is poorly understood, as is that of molybdotungstates and tungstovanadates. This is partly because tungstate systems are slow to reach equilibrium and because of the relative inaccessibility of the NMR spectra of ^{183}W and ^{17}O in comparison with *e.g.* ^{1}H or ^{51}V. The aim of this work has been to establish the speciation of isopolytungstates, molybdotungstates and tungstovanadates in aqueous solution over the available pH range and to determine the structures of the main species present using multinuclear NMR techniques.

1.1. Polyanions

Although most metal oxides are insoluble, or have a poorly defined or limited solution chemistry, the isopoly- and heteropolyoxoanions of the early transition elements form an important exception. Such polyoxometallate anions form structures based very largely on quasi-octahedrally coordinated metal atoms. It is therefore, often best, to describe these structures in terms of aggregations of metal-centred MO_n polyhedra that are linked by shared corners, edges and (rarely) faces.

1.2. Structures, Bonding and Mechanisms

The chemistry of isopoly- and heteropolyanions has barely progressed insofar as the stabilities and molecular and electronic structures of these species can be said to be well understood, or that mechanisms for their formation and interconversions are really understood at all. There have, of course, been attempts to address these matters, although they have been hampered by the deficiency of reliable data and appropriate experimental methods.

Most attempts to rationalise the structures of isopoly- and heteropolyanions are based upon coulombic principles, *i.e.*, an application of "Pauling's Rules" for ionic aggregates. Pauling himself first proposed that a 12-metallate polyanion might adopt a structure of corner shared MO_6 octahedra [11]. In fact, it has transpired that edge-sharing of octahedra is a more common feature of polyoxoanion structures, and that even coulombically unfavourable face-shared octahedra are not forbidden.

Kepert [12] has argued that clusters of edge-shared octahedra accrete in such a way as to minimise $M^{n+}...M^{n+}$ repulsions. The repulsions in the dimer M_2O_{10} are reduced by the metal ions moving from the centres of their octahedra. In trimers or large clusters off centre displacements are more readily accommodated if the octahedra form non-linear arrangements (M-M-M angles of 90° or, better 60°).

Moore [13], Goiffen and Spinner [14] developed Kepert's ideas in order to explain polyoxoanion structures. However, the majority of the structures they proposed were not viable models for polyoxoanions. In fact, of the 144 structures that Moore considered, 87 were up to clusters of seven, and only three of those satisfied the Lipscomb Principle, *i.e.* that no octahedron should have more than two unshared vertices. Only these three anions have been observed in nature: M_7O_{24} (both heptamolybdate and the Anderson isomers) and the M_5O_{18} unit has been observed in both $[W_{10}O_{32}]^{4-}$ and $[X(W_5O_{18})_2]^{n-}$. So rather than just considering cation-cation repulsion, the Lipscomb Principle also takes into account the importance of metal-terminal oxygen π-bonding for the stabilisation of such structures.

Early insights into the mechanisms of polyanion formation were made by Baker [15,16]. Based on isotope exchange studies involving $[H_6CrMo_6O_{24}]^{3-}$ and $[H_6FeMo_6O_{24}]^{3-}$ these workers proposed that molybdenum exchange between the heteropolyanions and $[Mo_7O_{24}]^{6-}$, involved MoO_4^{2-} or $HMoO_4^-$ tetrahedra. Kepert, [1] around the same time proposed that isopolytungstate formation might involve a simple (and rapid) addition of WO_4 tetrahedra. Initially, the WO_4 would act as a

bidentate ligand to a second WO_4 and consequently it expands its coordination number to six. Polymerisation is then said to be initiated by protonation of WO_4^{2-} to HWO_4^-, which stretches one of the WO bonds in each tetrahedron. Tytko and Glemser have elaborated on Kepert's addition mechanism [17-21]. Sadly very little experimental evidence is available to support Tytko and Glemser's detailed mechanism, although it is certainly reasonable to suppose that polymerisation involves the addition of WO_4 tetrahedra.

1.3. Methods of Investigation of Polyanions in Solution

Very exacting demands upon experimental techniques and upon interpretation of results are required to unravel these complex polyoxometallate systems. As recently as 1971 only a handful of good-quality structures had been identified [22]. Since then there has been a considerable increase in the number of new polyanion structures derived mainly as before by X-ray crystallography of isolated crystalline solids. However, in solution the identification and structural characterisation of species is complicated by a number of problems. There may be more than one complex present that may also undergo either rapid or slow exchange, or exhibit fluxional behaviour. Furthermore, the solute species may bear no structural relationship to the materials that can be induced to crystallise from such solutions. Therefore in general polyoxoanions in solution have been analysed by a combination of experimental techniques. The more popular methods are briefly described below.

1.3.1. Equilibrium Analysis

Sillén *et al.* [23] have pioneered the application of precise EMF measurements to the study of polyanion formation. The technique in essence is simply to measure the hydrogen ion concentration of polyanion solutions as a function of added acid (or base) and the total metal ion concentration. In practice, great care must be taken to ensure that true equilibrium has been reached for each measurement.

Isopolyvanadate, -niobate, -molybdate and -tungstate solutions have been investigated by this method, and more recently three component (heteropoly) systems have been studied. With the latter systems a third variable is introduced which places further requirements upon the accumulation of precise experimental data. So recent investigations have always coupled equilibrium analysis with techniques aimed at structure determination [24-26].

1.3.2. Vibrational Spectroscopy

Infrared and Raman spectroscopy are extensively used in polyoxometallate chemistry either for "finger printing" purposes, or, in favourable cases, for structural elucidation [27,28] and the determination of force constants. The metal-oxygen stretching vibrations form the most characteristic region of the spectrum at *ca.* 1000-400 cm^{-1}. Similarities of spectral band positions, shapes and relative intensities for two complexes strongly indicate that they have identical structures. Good agreement between the spectra of crystalline and dissolved polyanions implies that the structure of the solute anion is the same as that observed in the crystal. Raman spectroscopy has been of considerable value in this connection [9,29-32].

1.3.3. Electron Spin Resonance

ESR spectroscopy can impart information regarding site symmetry and electronic structure of a paramagnetic metal atom in a polyoxoanion. This technique has been particularly helpful for the study of heteropoly blues [11].

1.3.4. Nuclear Magnetic Resonance

Prior to the development of pulsed Fourier Transform (FT) techniques the application of NMR spectroscopy to polyoxoanions was effectively restricted to broadline ^{1}H solid state measurements and high resolution spectra of a few nuclei (^{1}H, ^{31}P, ^{51}V) of sufficient sensitivity. That situation has now changed with the

availability of multinuclear high-field FT NMR spectrometers. The use of NMR spectroscopy has recently had, and will have, a profound impact upon our knowledge of polyoxometallates, particularly on their solution structures and dynamics. However, the reliability and usefulness of heteronuclear NMR spectra of polyoxoanions depends strongly upon the lability of the polyanion.

High resolution proton NMR of wholly inorganic polyoxoanions is of limited value since in most cases rapid exchange with solvent protons takes place. However, there are examples where exchange is restricted, and separate signals are observed. The metatungstate anion α-$[(H_2)W_{12}O_{40}]^{6-}$ exhibits a single proton resonance, (δ_H =6 ppm) equivalent to two protons [33].

^{17}O NMR spectroscopy is more demanding to perform due to the low abundance and quadrupole moment of the ^{17}O nucleus, however, its large chemical shift range does compensate [34]. Moderate extents of isotopic enrichment (1- 5 atom %) are generally required for adequate signal to noise in all but concentrated solutions of single species. Linewidths are not usually a serious problem except in the case of chemical exchange, or for large, slowly-tumbling polyanions. For the simple anions MoO_4^{2-} and VO_4^{3-} spin-spin couplings to ^{95}Mo and ^{51}V have been resolved in low viscosity solvents [35,36] and in polyanions, coupling to ^{51}V is shown by anomalous line shapes. Previous studies have shown that oxygen chemical shifts are determined largely by the metal-oxygen bond order (and by the metal), and occasionally it is possible to assign resonances by inspection of the anion structure, where this possesses symmetry. In the main, the more highly bridging oxygen atoms have the smaller (high field) chemical shifts. It is also possible to correlate chemical shift and the energy of the first charge-transfer band in polyoxoanions [37] since the chemical shift is dominated by the "paramagnetic" component σ_p. ^{17}O NMR spectroscopy has been successfully used to indicate slow site-selective oxygen processes [38,39] and to determine or verify structures of polyanions [40-42]. Furthermore, when an oxygen site is protonated, the metal-oxygen bonds are

weakened, leading to a decrease in chemical shift. This phenomenon has located the protonation sites in *e.g.* $[V_{10}O_{28}]^{6-}$, $[V_2W_4O_{19}]^{4-}$ [39,41].

Apart from ^{183}W, the magnetic nuclei of other atoms found in polyoxometallates (^{51}V,^{93}Nb,^{95}Mo,^{181}Ta) have quadrupole moments. The greatest number of NMR measurements has been made on ^{51}V [43-51], a highly receptive nucleus which, in diamagnetic polyanions gives spectra with linewidths ranging from 10 to 800 Hz. A recent review on ^{51}V NMR has also been published [52]. The chemical shifts of the isopoly- and heteropolyvanadates fall in the range δ_V -400 to -600 ppm relative to $VOCl_3$. The chemical shifts and linewidths of ^{51}V NMR resonances depend on both solvent and temperature. Large chemical shift changes with different solvents cannot be solely accounted for by volume susceptibility differences and so specific interactions must be occurring. For example, δ_V shifts by 16 ppm for $[W_5VO_{19}]^{3-}$ from water to acetonitrile [53]. In aqueous solutions the vanadium chemical shifts are not highly sensitive ($\Delta\delta_V < 2$ ppm) to counterion identity and concentration, polyanion concentration, and buffer identity, unless the anion protonates. The latter process then usually results in a lower frequency (δ_V more negative) and increased linewidth. Within the temperature range 30-80°C the frequency increases (δ_V more positive) by 3-7 ppm and linewidths decrease by about 60% [53]. As yet no resonances for ^{93}Nb or ^{181}Ta in oxoanions have been observed, presumably because of excessive linewidths as a result of large quadrupole coupling constants [11].

Although molybdenum has two magnetic nuclei, ^{95}Mo has a quadrupole moment that is an order of magnitude smaller than that of ^{97}Mo, and is therefore the preferred nucleus. At high pH, molybdate solutions contain the tetrahedral MoO_4^{2-} anion, which yields a narrow line (≈1Hz) in the ^{95}Mo NMR spectrum [11]. However, below pH 9 the linewidth broadens greatly (179 Hz at pH 5.4) as a result of protonation, polymerisation and chemical exchange [54,55]. Since the site symmetry of Mo is always low in polymolybdates and the sites are generally liable to exchange processes, the Mo linewidths are large [11].

Recently, ^{183}W NMR has been directly observed in a number of polytungstates [56-63]. Despite having a very low receptivity ($1.04x10^{-5}$) it does have $I=½$, and so yields spectra with extremely narrow lines. Also the chemical shifts are large enough to distinguish between all structurally distinct tungsten atoms in the polyanions so far examined. For example the ^{183}W NMR chemical shifts and relative integrals for $[W_7O_{24}]^{6-}$ are, δ_W = 269.2 (1W), -91.8 (4W) and -178.9 (2W) ppm [64].

1.4. Applications

The applications of polyoxometallates generally rest on their unique properties, including size, mass, electron- and proton transfer/storage abilities, thermal stability, lability of "lattice oxygen", and high Brønsted acidity of the corresponding acids. An additional advantage with heteropoly acids is that they can also be separated or enriched into organic solvents. Pope and Müller [65] have recently reviewed some of the new developments and the growing number of applications of polyoxometallates. Some of these applications are briefly described below with references cited from the review.

1.4.1. Catalysis and Photocatalysis

Heteropolyanions are extensively used as oxidation and acid catalysts. These catalysts are widely used in the oxidation of aldehydes to produce carboxylic acids, and dehydrogenation of alcohols, aldehydes and carboxylic acids to form C=C and C=O bonds.

Heterogeneous catalytic oxidation processes involving well-characterised polyoxometallates have been reviewed [66-68]. Among the more important are the commercial vapour phase oxidation of methacrolein to methacrylic acid (80, 000 tons per year) [69] and methane oxidation [70]. Recently further developments have

included the synthesis of bifunctional catalysts *e.g.* $[(Ph_3P)_2Rh(CO)]_4[SiW_{12}O_{40}]$, which can be used for sequential hydroformylation and oxidation of olefins [71].

Homogeneous oxidative catalytic activity [72] has been shown for both thermal [73] and photochemical dehydrogenation and H_2 evolution from RX-type (*e.g.* $X=CH_2OH$, COOH) species, including water-splitting processes [74-76] and for oxygen transfer to alkanes [77]. Polymolybdovanadates have been used as reoxidants in Wacker chemistry (oxidation of alkenes, coupling of aromatics) and may themselves be reoxidised with oxygen [78] (equations (1.1) and (1.2)). Use of the heteropolyanion instead of the normal $CuCl_2$ oxidants avoids corrosion by HCl.

$$Pd^0 + [HPA]_{ox} + 2H^+ = Pd^{II} + H_2[HPA]_{red} \qquad (1.1)$$

$$H_2[HPA]_{red} + \tfrac{1}{2}O_2 = [HPA]_{ox} + H_2O \qquad (1.2)$$

1.4.2. Solid-State Applications: Electronic and Protonic Conductors

In the crystalline state, polyoxometallates retain many of their solution state properties since the large anions tend to have a low affinity for counter-cations and solvent molecules. More specifically, their electron- and proton-transfer characteristics are usually preserved in the solid state. Thus heteropoly acids have been used as solid electrolytes in fuel cells [79].

1.4.3. Medicine: Antitumoral, Antiviral and Antiretroviral Activity

Many polyoxometallate salts have been shown to be biologically active. Such activity includes highly selective inhibition of enzyme function [80,81], in vitro and in vivo antitumoral activity [82], antiviral activity (*e.g.* against rabies [83] and

scrapie, the sheep version of "mad cow disease" [84]), and antiretroviral activity (*e.g.* against HIV infections, connected with AIDS, SAIDS [80]). One particular heteropoly tungstate HPA-23 $[(Na)(Sb_3O_7)_2(SbW_7O_{24})_3]^{18-}$ [85] has been used to treat AIDS patients in France. Research in this area is particularly vigorous.

1.5. Tungstates

The study of aqueous polytungstate equilibria is complicated by the extreme range of rates observed. The formulae of some polytungstates are not well understood because of the anion's inherent metastability with pH. The qualitative Scheme 1 below describes the sequence of reactions in aqueous solutions at moderate to high ionic strengths which were known before our investigation [11]. The vertical arrows indicate equilibria that are established quickly (mins or secs) whilst the other processes are slow (hours - weeks).

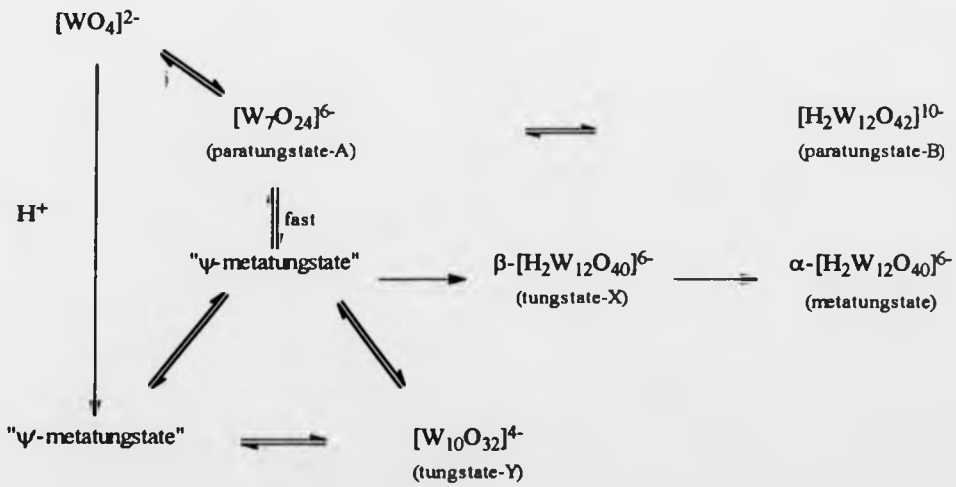

Scheme 1. Known aqueous tungstate polymerisation equilibria.

The processes involved in the polycondensation of $[MoO_4]^{2-}$ and $[WO_4]^{2-}$ anions have been the subject of a large number of studies, the results of which have been critically reviewed [1,21]. Burtseva *et al.* [86] have examined the processes that occur when these solutions are acidified from $[H]^+/[WO_4]^{2-}$ = 1 to 1.2. The enthalpies of formation of isopolyanions with different compositions were calculated, from which the authors concluded that the tungstates were more stable than those of the corresponding isopolymolybdates of the same composition. Within each homologous series, the isopolyanions containing fewer metal atoms were more stable and when the number of metal atoms were the same, the anion with most the oxygen atoms were more stable.

1.5.1. Mono- and Ditungstates

X-ray crystallography has shown the monomer, WO_4^{2-}, to have tetrahedral geometry [1]. Also Woodward and Robert [87] using Raman spectroscopy have demonstrated that the anion is stable and retains its tetrahedral structure in aqueous solution. Even though there is no direct evidence for their existence as stable solute species, tetrameric orthotungstate anions, $[W_4O_{16}]^{8-}$ have been observed in the crystal structure of $Li_{14}(WO_4)_3W_4O_{16}\cdot 4H_2O$ [2]. Presently, only one ditungstate, $Na_2W_2O_7\cdot 5H_2O$, has been obtained from solution [88].

1.5.2. Paratungstates

Potentiometric titrations of aqueous alkali metal tungstate solutions with acid gives pH inflections at $[H]^+/[WO_4]^{2-}$ = 1.1 to 1.2 and 1.5. The first is in accord with the formation of "paratungstates" and the latter to the metatungstates [11].

Early "equilibrium" studies [1,21] were in agreement that the first hydrolysis product was a hexamer, so-called paratungstate-A "$[HW_6O_{21}]^{5-}$". However, recent X-ray [89] and NMR [64] studies have demonstrated that this long held belief was

incorrect and it was in fact a heptamer similar to the molybdate [90] (see Figure 1(a)).

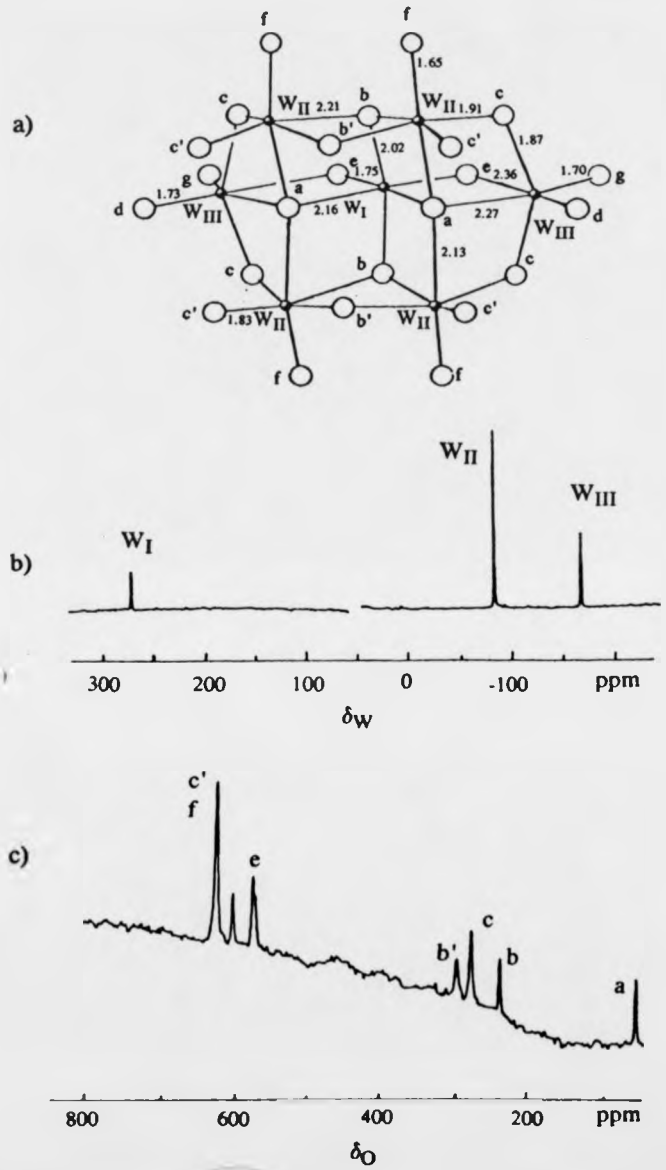

Figure 1. a) The structure and averaged bond lengths/Å [89] of paratungstate A, $[W_7O_{24}]^{6-}$. **b)** 12.5 MHz tungsten-183 NMR spectrum of aqueous $Na_6[W_7O_{24}]\cdot 14H_2O$ recorded at pH≈ 7 (293K) and **c)** 40.7 MHz oxygen-17 NMR spectrum of the same solution at 330K. Letters are based on an established [34] labelling scheme for decavanadate, with primes added to indicate nearness to "missing" octahedra [91].

The ^{183}W NMR spectrum (Figure 1(b)) reported by Maksimovskaya and Burtseva [64], was readily assigned, as it had three resonances in the ratio 1:4:2, δ_W = 269.2 W_I, -91.8 W_{II} and -178.9 ppm W_{III}. (The counterion was Na^+ at pH 7). The oxygen spectrum shown in Figure 1(c) was assigned on the principle that ^{17}O NMR shifts correlate with the O-W bond length, with greater lengths, corresponding to a lower frequency [51]. However, the correlation was insufficient for Maksimovskaya and Burtseva [64] to differentiate between three of the signals of equal intensity at δ_O=590, 595 and 624 ppm ($2O_d$, $2O_e$ and $2O_g$) because the corresponding bonds have nearly the same length. The oxygen shifts and their assignments are listed in Table 1.

Alongside the heptamer a dodecameric anion also formed, paratungstate-B. Lipscomb [3] was the first to suggest the open structure shown in Figure 2(a) as an alternative interpretation of Lindqvist's [4] earlier X-ray study. This proposed structure has been confirmed by further X-ray studies of five different salt hydrides [5-7,92] and Maksimovskaya and Burtseva [64] have obtained concordant ^{183}W and ^{17}O NMR results. The ^{183}W NMR spectrum of aqueous paratungstate-B shown in Figure 2(b) yielded four resonances in the area ratio 1:2:1:2; δ_W = -108.2 (2W), -110 (4W), -114.5 (2W) and -141.4 ppm (4W), but no assignment for these was offered. The ^{17}O NMR spectrum of this anion became more complex when the solution was heated because the $[H_2W_{12}O_{42}]^{10-}$ anions partly transformed into $[W_7O_{24}]^{6-}$. Further transformation occurred at low ionic strengths. However, with freshly prepared supersaturated solutions of $[H_2W_{12}O_{42}]^{10-}$, the rate of decomposition to $[W_7O_{24}]^{6-}$ was sufficiently reduced so that they were able to record the ^{17}O NMR spectrum. This spectrum is shown in Figure 2(c) and their assignments are listed Table 1.

In the central cavity of $[H_2W_{12}O_{42}]^{10-}$ two protons were shown to reside, and Evans *et al.* proposed that these helped to stabilise the structure by their charge and by hydrogen-bonding [93]. Lunk *et al.* [94] calculated a 2.22±0.02 Å interproton

separation according to broad line NMR. In contrast to the metastable anions (see below) these protons were accessible to and exchanged either reasonably or very rapidly with solvent water [95].

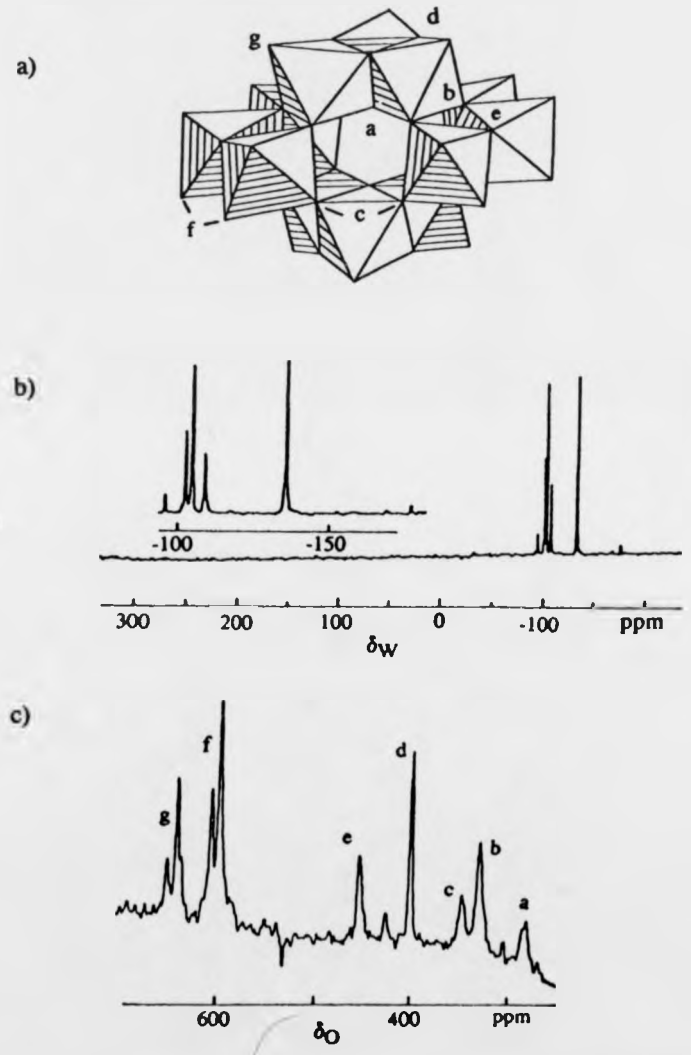

Figure 2. a) Structure of paratungstate B, $[H_2W_{12}O_{42}]^{10-}$. b) 12.5 MHz tungsten-183 NMR spectrum of an aqueous Li_2WO_4 solution acidified to ≈ pH 6 (293K) and c) 40.7 MHz oxygen-17 NMR spectrum of the same solution at 330K.

Table 1. Oxygen chemical shifts and relative integrals for paratungstate A and B.

peak label	A,$[W_7O_{24}]^{6-}$ δ_O		peak label	B,$[H_2W_{12}O_{42}]^{10-}$ δ_O	
a[a]	71	(2)[b]	a[a]	271	
b	254	(2)	b	323[c]	
b'	314	(2)	c	343	
c	295	(4)			
c'	648[d]	(4)	d	398	(4)
d	590 or 624	(2)	e	457	(4)
e	595	(2)			
f	648[d]	(4)	f	607[c]	(12)
g	590 or 624	(2)	f	613[c]	
			g	651	(6)
			g	663	

[a] Peak labelling as per Figures 1(a) and 2(a); referenced to solvent water δ_O=0 at 330K.[b] Is the relative peak intensity.[c] Peaks overlapped.[d] The lines enhanced during oxygen exchange with water enriched with ^{17}O.

Evans [92] located the protons in $(NH_4)_{10}[H_2W_{12}O_{42}]\cdot 4H_2O$ using neutron diffraction. The H atom lay 0.10 Å from the plane defined by O_b and two O_g oxygen atoms towards the molecular centre. The dimensions of this arrangement are shown in Figure 3. The distance they observed between the two H atoms in the molecule is 2.14 Å, in good agreement with the above.

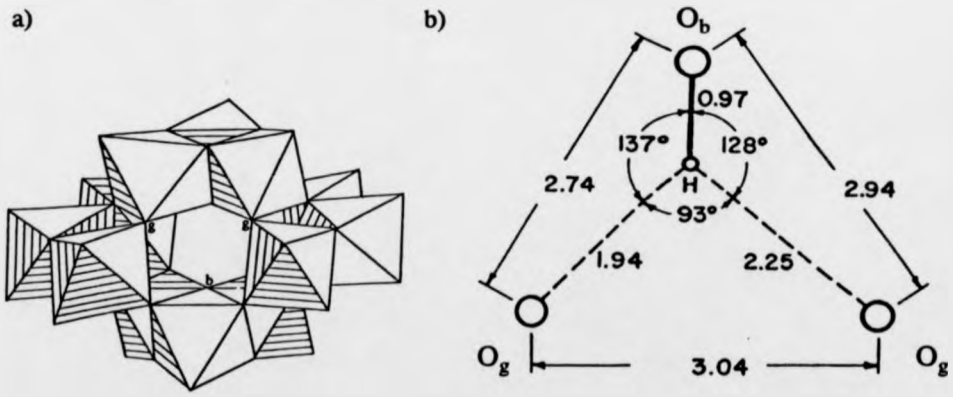

Figure 3. **a)** Structure of paratungstate-B showing the location of the three oxygen atoms. **b)** Projection of the four central atoms; H, and the plane defined by O_b and two O_g oxygen atoms, showing the interatomic distances in Å and angles at the H atom. Estimated errors of distances are ± 0.03 Å for O-O, ± 0.05 Å for O-H.

Maksimovskaya and Burtseva [64] have made some interesting observations upon the equilibrium between paratungstates A and B by using ^{17}O and ^{183}W NMR spectroscopy. With sodium as the counter ion, solutions containing $[W_7O_{24}]^{6-}$ and excess $[WO_4]^{2-}$, the anions remained unchanged after three months' storage at 293K. Also, in the solution with the same concentration of W^{VI} prepared from $Na_{10}[H_2W_{12}O_{42}] \cdot 27H_2O$ and stored for three months at 293K, nearly complete conversion to heptatungstate occurred. However, in freshly acidified 2M Li_2WO_4 solutions containing $[W_7O_{24}]^{6-}$, conversion into the $[H_2W_{12}O_{42}]^{10-}$ anion occurred in a matter of hours at room temperature, but on raising the temperature the transformation was incomplete and developed more slowly. In the presence of Li^+ the $[H_2W_{12}O_{42}]^{10-}$ anions remained in solution.

The ^{183}W chemical shifts of the $[H_2W_{12}O_{42}]^{10-}$ differed from those in the presence of sodium by 10 to 15 ppm toward high field. Because of this Maksimovskaya and Burtseva [64] concluded that there must be a stronger association of the Li^+ ion with polyanions, as compared with Na^+.

At low ionic strengths and high acidity $[H]^+/[WO_4]^{2-} > 1.5$, a third paratungstate was also detected, "tungstate-Y" [11]. This was characterised by its UV spectrum (λ_{max} = 320 nm) and its polarogram [11]. At first it was considered to be dodecamer and the isolated potassium salt was formulated as "$K_5HW_{12}O_{39} \cdot 4H_2O$" on the evidence of polarography and ultracentrifugation [96,97]. In aqueous solution the tungstate-Y was metastable with respect to both pH and ionic strength, and either formed ψ-metatungstate, β-$[H_2W_{12}O_{40}]^{6-}$ or $[W_7O_{24}]^{6-}$ [98]. Subsequently, comparison of the UV spectra [99] and redox properties [100] of tungstate-Y with those of acetonitrile solutions of the salt $(Bu_3NH)_4W_{10}O_{32}$ which were precipitated from aqueous solutions of potassium tungstate-Y, confirmed the decameric structure. The decatungstate anion was indefinitely stable in non-aqueous solution and the structure of the tri-n-butylammonium salt has been determined [8]. Figure 4

shows the structure of the salt and the ^{17}O NMR chemical shifts reported by Filowitz *et al.* [101].

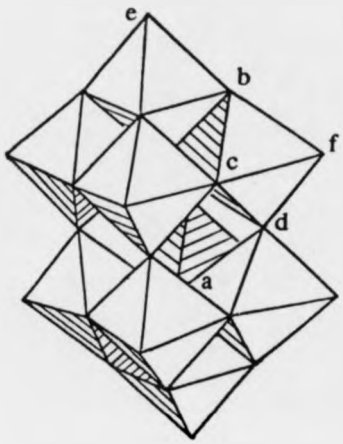

Assignments	δ_O(ppm)
a	-6
b, c, d	430, 416
e, f	762

Figure 4. Structure of decatungstate, tungstate-Y, $[W_{10}O_{32}]^{4-}$ and its oxygen chemical shifts at 298K.

1.5.3. Metatungstates

The second pH inflection at $[H]^+/[WO_4]^{2-} = 1.5$ corresponded to the formation of pseudometatungstate-ψ. This metastable anion formed rapidly in solution and then slowly mutated into "tungstate-X" (see Figure 5(a)), which then evolved into the more thermodynamically stable product α-$[H_2W_{12}O_{40}]^{6-}$, (see Figure 5(b)). These three products have been distinguished by their polarograms [98]. At 50°C, some 15 days were required for a 5mM aqueous tungstate solutuion to completely convert to metatungstate; at 80°C and pH 3 the half-lives of ψ to X and X to metatungstate were both about 70 min. [98].

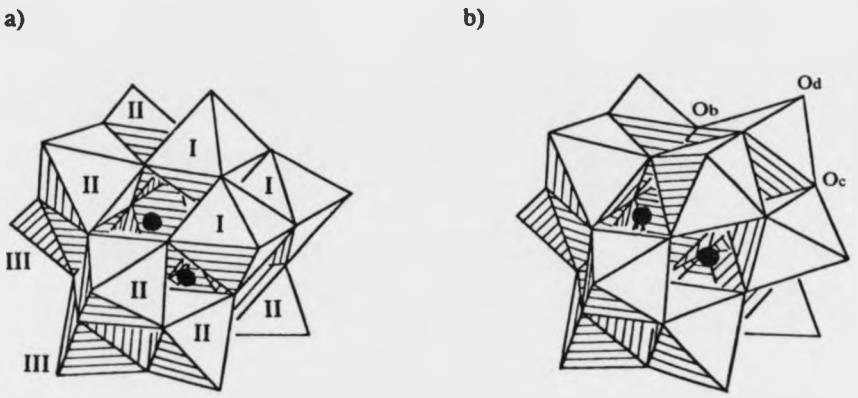

Figure 5. Structure of **a)** β-Keggin $[H_2W_{12}O_{40}]^{6-}$, tungstate-X; **b)** α-Keggin $[H_2W_{12}O_{40}]^{6-}$.(• =H) (oxygen O_a which are bound to three W are not indicated in the figure).

As early as 1909 Copaux [102] realised the importance of the isomorphism between metatungstic and the heteropoly acids with the Keggin structure, and Signor and Gross [103] later proposed that the two hydrogen atoms acted in lieu of the heteroatom. Recent X-ray analysis [9] has confirmed the α-Keggin structure. The metatungstate ion was in fact isolated as a triprotonated anion, but it has only been known to be diprotonated in solution [11]. Fuchs *et al.* [9] further proposed that this additional protonation occurred internally. Also evidence that the two protons were in the centre of the anion, and therefore not susceptible to rapid exchange with the solvent water, was provided by the observation a separate narrow ^1H NMR signal (δ_H = 6 ppm) in aqueous solutions of metatungstate [33]. Subsequent broad line NMR studies of solid metatungstates showed $r_{H\text{-}H}$ = 1.92 ± 0.03 Å [104]. A deprotonated form has also been reported, α-$[HW_{12}O_{40}]^{7-}$, which has only one internal proton characterised by its ^1H NMR (δ_H = 5.2 ppm) [95]. However, proton exchange with these species has not been completely ruled out, since Launay [105] has demonstrated that this deprotonated form converts into the diprotonated species, by a first order process which has a half life of *ca.* 50 min. at pH≤2.

Since "tungstate-X" is an intermediate species in the transformation of ψ-metatungstate into metatungstate, it has not yet been isolated in pure form. Ultracentrifugation [106] suggested that it was a dodecamer. The ^1H NMR [95] implied two non-exchangeable protons. The redox chemistry of the anion paralleled that of the metatungstate anion α-$[H_2W_{12}O_{40}]^{6-}$ [107]. On this evidence Launay *et al.* [95] concluded that tungstate-X was the β-isomer of metatungstate. Subsequently Lefebvre *et al.* [62] recorded ^{183}W NMR spectra for β-$[SiW_{12}O_{40}]^{4-}$ and $[H_2W_{12}O_{40}]^{6-}$. These confirmed the β-Keggin structure, because they both showed three resonances in the area ratio 1:2:1. The spectrum of β-Keggin $[H_2W_{12}O_{40}]^{6-}$ is illustrated in Figure 6. The coupling constants observed fall into two well-defined classes, couplings between two tungsten atoms within the same W_3O_{13} moiety, an *inter-group* coupling (W-O_c-W bond), ≈8Hz and an *extra-group* coupling between one tungsten of the rotated (β) W_3O_{13} group and one central W (W-O_b-W bond) ≈20Hz. Unfortunately, due to the broadness of the resonances in $[H_2W_{12}O_{40}]^{6-}$, the *inter-group* coupling expected on δ_W =-130.6 ppm (W_{III}) was not resolved, however, the *extra-group* coupling was clearly evident, 19Hz on the δ_W = -107.2 (W_I) and δ_W = -120.9 (W_{II}) ppm peaks. (Labels as per Figure 5(a)).

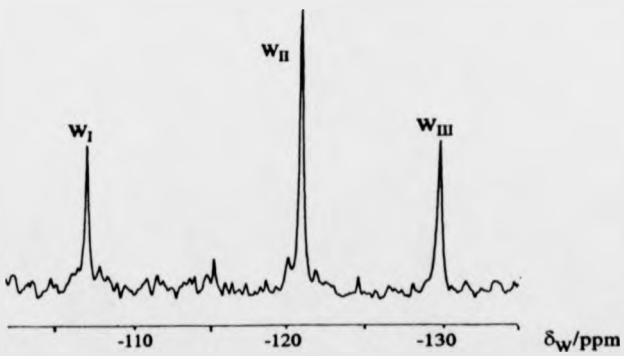

Figure 6. 10.42 MHz tungsten-183 NMR spectrum of tungstate-X, β-Keggin $[H_2W_{12}O_{40}]^{6-}$, a partial conversion to α-Keggin can be detected (δ_W -117.5 ppm).

Very little is known about the ψ-metatungstate anion. Ultracentrifugation studies implied a dodecamer [106], however, recent evidence from an X-ray analysis [10] suggested an undecameric structure $K_6H_4W_{11}O_{38}\cdot 11H_2O$ (an ion with σ_v symmetry only known in the crystalline state). (See Figure 7).

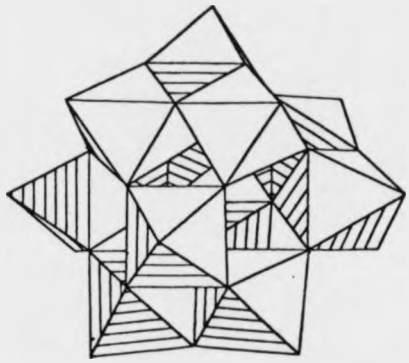

Figure 7. Structure of the undecameric anion $K_6H_4W_{11}O_{38}\cdot 11H_2O$ in the crystalline state.

1.6. Molybdates

In the main, the molybdenum exhibits a distorted octahedral coordination geometry. Exceptions are $[Mo_2O_7]^{2-}$, $[HMo_5O_{17}]^{3-}$ and α-$[Mo_8O_{26}]^{4-}$ (non-aqueous species) which contain one or more MoO_4 tetrahedra, and $[Mo_{36}O_{112}(H_2O)_{16}]^{8-}$ with seven-coordinate molybdenum atoms. Equilibria involving MoO_4^{2-} and polymolybdates in aqueous solution are established rapidly [11]. Several precise EMF studies [30,108,109] of molybdate solutions in the near neutral pH range were consistent with the presence of monomers and heptamers as the major solute species. Under acidic conditions the EMF data was ambiguous, but the bulk of other evidence (see below) indicated the presence of Mo_8 and, ultimately, Mo_{36} species.

1.6.1. Mono- and Dimolybdates

In both the crystalline state and in aqueous solution the MoO_4^{2-} anion adopts tetrahedral coordination [110-112]. Despite numerous attempts, no intermediate has been unambiguously characterised in the aqueous polymerisation of MoO_4^{2-} to $[Mo_7O_{24}]^{6-}$, although tetrameric and hexameric species have been proposed [21].

1.6.2. Aqueous Polymolybdates : $[Mo_7O_{24}]^{6-}$, β-$[Mo_8O_{26}]^{4-}$ and $[Mo_{36}O_{112}(H_2O)_{16}]^{8-}$

In millimolar concentrations and at pH 3 to *ca.* 5.5 the predominant molybdate solute species in aqueous solution was the heptamolybdate ("paramolybdate") anion $[Mo_7O_{24}]^{6-}$ or its protonated forms. The heptamolybdate anion shown in Figure 8(a) has been characterised by numerous solution studies [21] and by the structures of $[NH_4]_6Mo_7O_{24}\cdot 4H_2O$ [113], $K_6Mo_7O_{24}\cdot 4H_2O$ [90] and $Na_6Mo_7O_{24}\cdot 14H_2O$ [114] all of which were crystallised from aqueous solution. Raman spectroscopy [30,31,115] and X-ray scattering measurements [115] confirmed that the same structure was retained in aqueous solution.

The ^{17}O NMR spectra of aqueous heptamolybdate (VI) $[Mo_7O_{24}]^{6-}$ solutions have exposed an oxygen exchange process [91]. The initial spectra observed by Howarth and Kelly [91] (Figure 8(b)) were inconsistent with the known structure, in that eight oxygen atoms yielded no visible resonance. However, two further broad resonances were observed by reducing the temperature to 280K (Figure 8(c)). One in the bridging region (δ_O 356 ppm) and another, most likely composite, in the (mainly) terminal region at *ca.* δ_O 735 ppm. The ^{17}O chemical shifts observed at 293K and pH 5.4 were: δ_{O_a} 121.7, δ_{O_b} 338.6, $\delta_{O_{b'}}$ 395.2, δ_{O_c} 358, δ_{O_d} with δ_{O_g} *ca.*735, δ_{O_e} 754.4, $\delta_{O_{e'}}$ with δ_{O_f} 815.4 ppm relative to solvent water at zero. (Peaks labelled as per Figure 8 (a)). It is evident from Figures 8(b) and 8(c) that this exchange process only involved terminal and bridging oxygens, since on raising the temperature the other resonances narrowed. Thus, in contrast to decavanadate [39],

the heptamolybdate anion exhibits oxygen exchange without any overall breakdown of its structure. Furthermore, the narrow $[MoO_4]^{2-}$ resonance at δ_O 529 ppm in Figure 8(c) demonstrates that the monomeric anion does not participate in this low temperature exchange process.

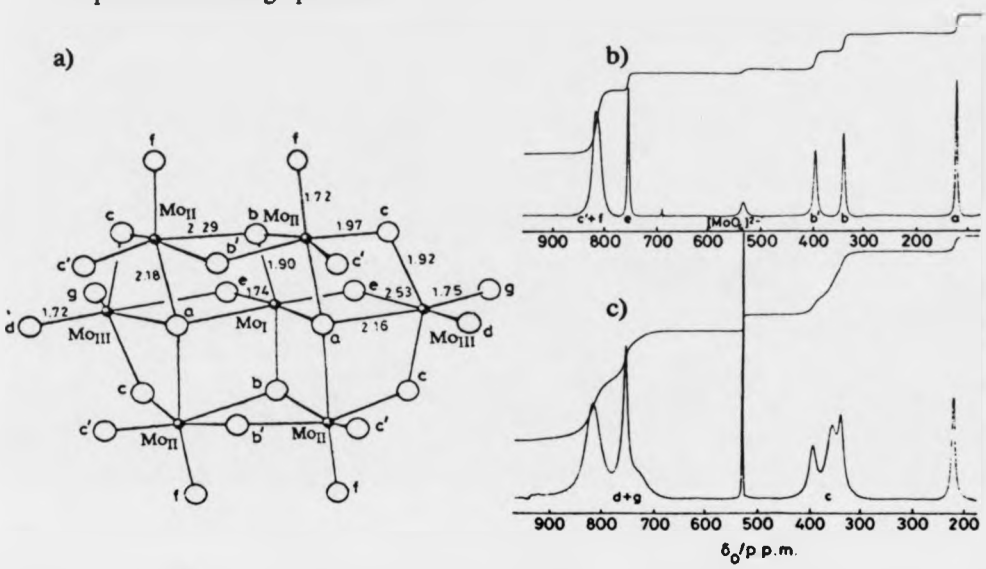

Figure 8. a) Structure and averaged bond lengths/Å in the heptamolybdate anion. b) 54.2 MHz oxygen-17 NMR spectra of aqueous $[Mo_7O_{24}]^{6-}$, 10% ^{17}O at pH 5.0, 319K and c) pH 5.7, 280 K [91].

The large π-pulse required for these solutions enabled Howarth and Kelly [91] to achieve selective irradiation because this reduced the spectral range to 100 ppm either side of the spectrum centre in quadrature mode. Therefore, with the centre on the broad bridging ^{17}O NMR resonance and interleaving $(\pi\text{-}\tau\text{-}\pi/8\text{-}0.1s)_n$ experiments with $\tau=3$ ms and a dummy with $\tau=100$ ms, the authors observed saturation transfer to the terminal region and *vice versa*. However, upon irradiating the water resonance no saturation transfer was observed, thus proving that this was an internal process rather than one involving solvent water. They also proposed that the three already long bonds broke, namely (labelling as per Figure 8(a)): O_c-Mo_{II},1.97; O_e-Mo_{III},2.53; O_a-Mo_{III},2.16 Å, where Mo_{III} was the partly detached molybdenum. In the transition state, the Mo_{III} atom is only attached to the

rest of the polyanion via one oxygen atom, O_c, to Mo_{II} and therefore the MoO_3 unit is free to rotate so that O_c, O_g and O_d can interchange.

Howarth *et al.* [116] have also performed a series of ^{17}O and ^{95}Mo NMR spectra of aqueous molybdate solutions over the pH 6 to 1.2 range. Initially, heptamolybdate $[Mo_7O_{24}]^{6-}$ formed. On protonation the proton was shown to either bridge between O_b and $O_{b'}$ in $[HMo_7O_{24}]^{5-}$, or else it protonated each site in turn. On further acidification the anion decomposed (pH *ca.*3.5) before the second protonation step.

Below pH 4 new broad resonances appeared which they attributed to $[H_3Mo_8O_{28}]^{5-}$, this then protonated further, eliminated water and rearranged to yield β-$[Mo_8O_{26}]^{4-}$. Figure 9, shows the mechanism Howarth *et al.* [116] proposed for the interconversion of heptamolybdate *via* a hypothetical intermediate based on their earlier work [47] discussed above. On acidification one of the octahedra in heptamolybdate (I) becomes labile, namely A or A'. The three long Mo-O bonds are broken and the resulting MoO_4 tetrahedron remains attached only at one oxygen, O_c. Because of this, and also the known acid-catalysed exchange process between molybdate and heptamolybdate, they proposed that further acidification would detach this tetrahedron, giving structure (II), in an unknown state of protonation. This hexamolybdate structure is unknown in the solid state, however, Fuchs [117] has recently reported an X-ray crystal structure of this type for hexatungstate. Presumably in the tungstate case the equilibration is slow enough for this metastable species to crystallise. In the faster molybdo equilibrium this hexamolybdate species may only exist as an intermediate on the way to structure (III), in which a "Mo_2O_5" unit has been added. The distinct dependence of the linewidths of (III) upon concentration also supported the proposal that at least two species were involved, such as (I) or (II). Structure (IV) is then derived by a folding in of the two "labile" octahedra, as indicated by the arrows. Structure (IV) received further support from the very good correlation of the oxygen shifts they observed with those reported by Klemperer [34] for β-$[Mo_8O_{26}]^{4-}$ in acetonitrile.

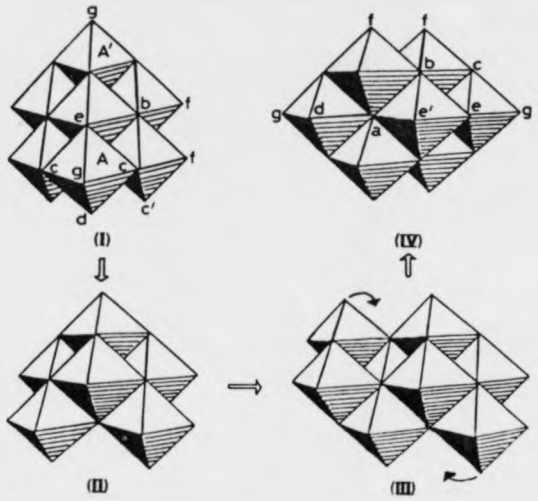

Figure 9. Structure, labelling scheme, and proposed mechanism of interchange of the species described in text. **(I)** $[Mo_7O_{24}]^{6-}$ and $[HMo_7O_{24}]^{5-}$; **(II)** hypothetical intermediate based on ref. [91]; **(III)** $[H_3Mo_8O_{28}]^{5-}$; **(IV)** β-$[Mo_8O_{26}]^{4-}$.

Further oxygen exchange processes present in these new solutions at lower pH were then examined by applying the saturation-transfer technique described above with selective inversion being performed at many different resonance positions. However, in contrast to their earlier results, Howarth *et al.* [116] observed that all the oxygen exchanges in these solutions were dominated by exchange with the solvent. Even heptamolybdate experienced such an exchange below pH 4, and at 328K its resonances became very broad indeed.

Below pH 2.8 a white precipitate of $[MoO_3]$ formed in 2 mol dm^{-3} solutions. However, diluting the solution to 0.4 mol dm^{-3} an ^{17}O NMR spectrum was just possible, but, due to exchange they were unable to assign the spectrum except to say that it was loosely consistent with $[Mo_{36}O_{112}(OH_2)_{16}]^{8-}$.

Because the quadrupole moment of ^{95}Mo is relatively large, molybdenum spectra were only useful as complementary information. Howarth *et al.* [116] observed one

resonance at δ_{Mo} = 26.8 ppm for heptamolybdate, and one at δ_{Mo} = 100 ppm which they attributed to β-$[Mo_8O_{26}]^{4-}$.

1.7. Molybdotungstates

The early literature of these anions is contradictory, however more recent aqueous studies using ultracentrifugation, polarography and UV spectroscopy have suggested the existence of complexes with Mo/W = 1/1, 1/5 and 1/11 formulated respectively as $[Mo_6W_6O_{41}]^{10-}$, $[Mo_3W_{15}O_{60}H_3]^{9-}$ and $[H_2MoW_{11}O_{40}]^{6-}$ [118,119]. In mixed aqueous organic solvents the anions $[Mo_3W_3O_{19}]^{2-}$ and $[HMo_2W_{10}O_{40}]^{5-}$ have been reported [120]. The latter species was regarded on the basis of its IR spectrum as a molybdenum-substituted "tungstate-Y". Recently, tetrabutylammonium salts of the anions $[MoW_5O_{19}]^{2-}$ and $[Mo^VW_5O_{19}]^{3-}$ have also been characterised [11].

Maksimovskaya *et al.* [121] have analysed mixed aqueous complexes of molybdenum and tungsten using ^{17}O NMR and to a lesser extent ^{183}W NMR. The solutions were prepared in the pH 5 to 8.9 range corresponding to paramolybdate $[Mo_7O_{24}]^{6-}$ and the paratungstates $[W_7O_{24}]^{6-}$ and $[H_2W_{12}O_{42}]^{10-}$.

In the titration of mixed Mo:W (1:1) solutions, the ^{17}O NMR spectra showed a decrease in the intensity of the signals of the tetraoxo-anions. This initially occurred at pH 8.9, to a greater extent for WO_4^{2-} (δ_O = 422 ppm) than for MoO_4^{2-} (δ_O =533 ppm), and was accompanied by the appearance of lines characteristic of the spectrum of $[W_7O_{24}]^{6-}$ (see Figure 10). A new resonance ($\delta_O \approx 80$ ppm) appeared in the range associated with four-coordinate O_a type oxygen atoms. On further acidification the quantity of Mo involved in polycondensation increased, and two new signals appeared in the same range with ($\delta_O \approx 90$ and ≈ 105 ppm). Simultaneously, the other resonances of the $[W_7O_{24}]^{6-}$ spectrum underwent displacement, broadening, and splitting, associated with the appearance of resonances from $[Mo_7O_{24}]^{6-}$.

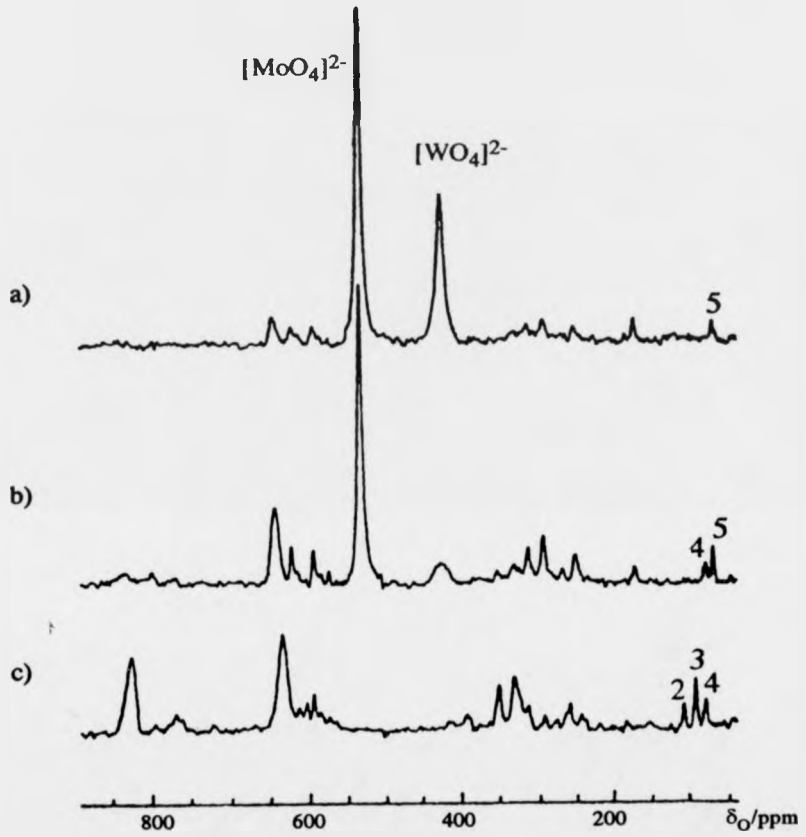

Figure 10. 54.2 MHz oxygen-17 NMR spectra of solutions with Mo:W = 1:1 at; a) pH 8.9, b) pH 8.5 c) pH 5, [Mo+W] = 2M.

Thus, instead of simply just two signals from O_a (at 121 and 70 ppm), five were observed. (See Figure 11). The five signals were assigned to O_a oxygen atoms with different local environments. The assignments and occasions where these local environments occur within the range of mixed heptametallates are shown in Table 2. Also a range of bridging oxygen resonances were observed with chemical shifts

intermediate between those for the pure heptametallates, indicating that the corresponding O atoms had mixed Mo-W environments, *i.e.* mixed heptametallates with the general formula $[Mo_xW_{7-x}O_{24}]^{6-}$ (x = 1 to 6) were produced.

Maksimovskaya *et al.* [121] have suggested the following assignments:

Table 2. Possible environments of the O_a atoms in heptametallates with different compositions, and the corresponding signals in the oxygen-17 NMR spectrum (δ, ppm).

Isopolyanion	OMo_4	OMo_3W	OMo_2W_2	$OMoW_3$	OW_4
	δ_O	δ_O	δ_O	δ_O	δ_O
	122[a] (1)[b]	105[a] (2)[b]	91[a] (3)[b]	80[a] (4)[b]	68[a] (5)[b]
$[Mo_7O_{24}]^{6-}$	+				
$[Mo_6WO_{24}]^{6-}$	+	+			
$[Mo_5W_2O_{24}]^{6-}$	+	+	+		
$[Mo_4W_3O_{24}]^{6-}$	+	+	+	+	
$[Mo_3W_4O_{24}]^{6-}$		+	+	+	+
$[Mo_2W_5O_{24}]^{6-}$			+	+	+
$[MoW_6O_{24}]^{6-}$				+	+
$[W_7O_{24}]^{6-}$					+

[a] Oxygen-17 shifts at 300K referenced to solvent water at $\delta_O = 0$. [b] The numbers refer to the labelling of the resonances in Figure 11.

Even with the Mo:W=9:1 and 1:9 solutions where the predominant mixed anions were $[Mo_6WO_{24}]^{6-}$ and $[MoW_6O_{24}]^{6-}$ respectively, the spectra were complicated by the presence of more than one isomer.

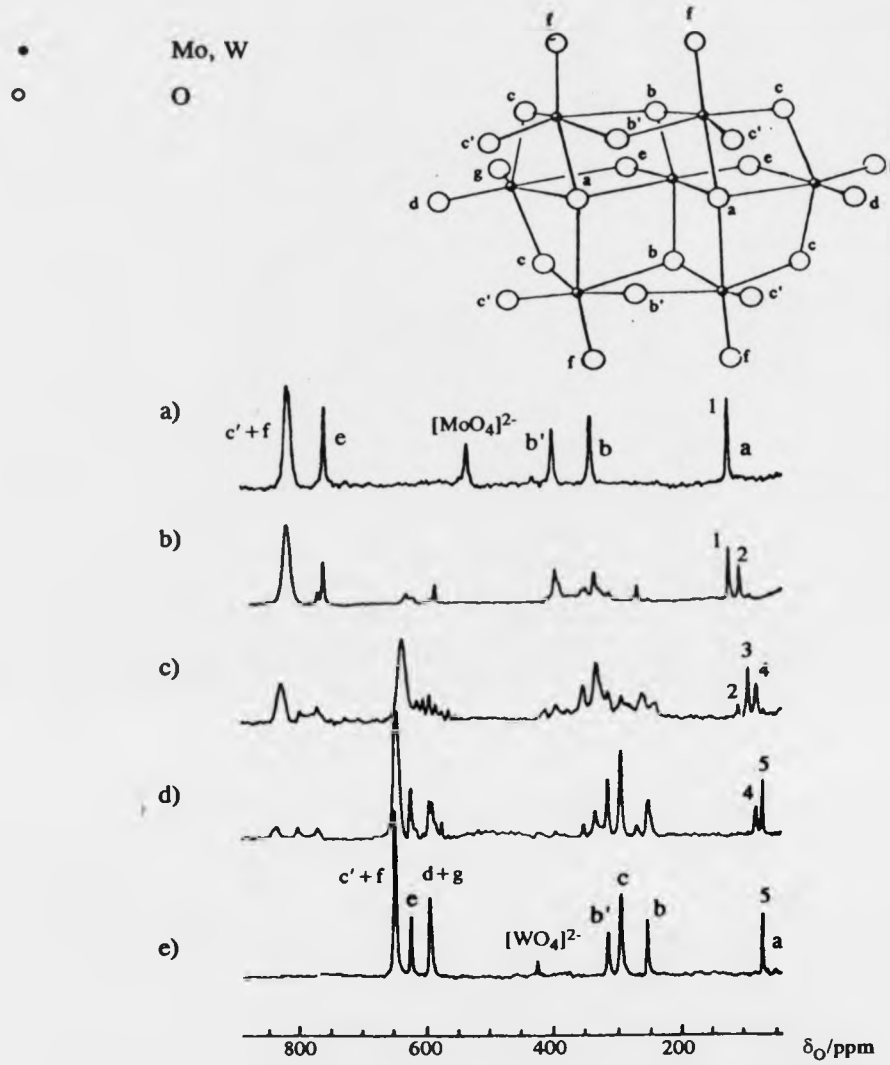

Figure 11. The structure of $[M_7O_{24}]^{6-}$ and the 54.2 MHz oxygen-17 NMR spectra of solutions of **a)** $[Mo_7O_{24}]^{6-}$, **e)** $[W_7O_{24}]^{6-}$, and Mo-W solutions at pH 6 with Mo:W ratios **b)** 9:1, **c)** 2:3, and **d)** 1:9; the numbering of the resonances of O_a corresponds to that in Table 2.

The assignments of the ^{17}O and ^{183}W NMR chemical shifts proposed by Maksimovskaya *et al.* [121] are shown in Tables 3 and 4 respectively. From the relative tungsten integrals they concluded that tungsten preferred the W_I (central)

and W_{II} (capping) sites, in Mo_6W, whereas molybdenum, preferred the Mo_{II} (capping) and Mo_{III} (end) sites in W_6Mo. In the latter case the ^{17}O NMR spectrum recorded at 330K (Figure 11(d)) contained resonances due to the O_f atoms, which were not observed under the same conditions for $[Mo_7O_{24}]^{6-}$ because of the lability of this fragment of the polyanion [91].

Table 3. Oxygen chemical shifts of $[W_7O_{24}]^{6-}$, $[Mo_7O_{24}]^{6-}$, $[Mo_6WO_{24}]^{6-}$ and $[MoW_6O_{24}]^{6-}$.

Peak[a]	$[Mo_7O_{24}]^{6-}$	$[Mo_6WO_{24}]^{6-}$	$[MoW_6O_{24}]^{6-}$	$[W_7O_{24}]^{6-}$
	δ_O	δ_O	δ_O	δ_O
a	121	122, 105	68, 80	70
b	340	334	312, 271	254
			271, 250	
b′	397	397, 350	315, 334	314
c	354[b]	355	298, 352	295
e	757	767, 759	591, 576	595
			767	
d+g	750[b]		624, 596	624, 590
			801	
c′+f	818	817	644	648
		626,617	835	

[a] Peak labelling as per Figure 1(a). [b] Observed at T < 286K

Table 4. Tungsten chemical shifts of $[W_7O_{24}]^{6-}$, $[Mo_6WO_{24}]^{6-}$ and their relative integrals.

peak[a]	$[W_7O_{24}]^{6-}$		$[Mo_6WO_{24}]^{6-}$	
	δ_W		δ_W	
I	271	(1)[b]	264	(1)[b]
II	-92	(4)	-47	(1)
III	-179	(2)	-170	(<.5)

[a] Peak labelling as per Figure 1(a). [b] Relative integrals.

Over the range of mixed heptametallate species, five types of environment are possible for the four-coordinate O_a atoms (Table 2). Anions with different metal ratios may have O_a atoms with identical local environments. Thus each of the five resonances from the O_a atoms may correspond to several (up to four) species with different metal ratios and each metal ratio having to 2-4 resonances due to positional isomerism.

It is also evident from Table 2 that the O_a chemical shift is determined by the immediate environment, and this changes approximately in an additive fashion by 11 to 15 ppm when one metal atom is replaced. Because of the similarity in the properties and the equal charges of Mo and W, the overall composition of the anion and the position replaced, (I, II or III) influences the magnitude of the chemical shift for the O_a signal only within the limits of the linewidth ($\pm$2 ppm). Thus the resonances for the O_a atoms of the mixed polyanions were broader than those for the pure forms, and represented the superposition of several signals with similar δ values. The concomitant change in the ratio of the intensities of the five signals for the O_a atoms, and the chemical shifts of the terminal oxygen resonances with the change in the Mo:W ratio indicated that the heptametallates formed covered the full range of metal ratios *ie.* $[Mo_xW_{7-x}O_{24}]^{6-}$ (x= 1 to 6).

Burtseva and Kochubei [122] have analysed the composition of fractions of crystals precipitated from molybdotungstate solutions of various metal ratios. They have shown that along side the full range of $[Mo_xW_{7-x}O_{24}]^{6-}$ (x = 1 to 6) isomers, molybdenum also replaced up to two tungsten atoms in paratungstate-B yielding $[H_2MoW_{11}O_{42}]^{10-}$ and $[H_2Mo_2W_{10}O_{42}]^{10-}$. When there was an excess of tungsten, species based on the paratungstate-B $[H_2W_{12}O_{42}]^{10-}$ structure were favoured, but as the fraction of tungsten was reduced, the mixed heptametallate anions dominated.

1.8. Vanadates

There is a wide range of vanadate (V) anions in solution. Their relative concentrations depend on pH, overall metal concentration, and ionic strength. A typical distribution of these species versus pH can be seen in Figure 12.

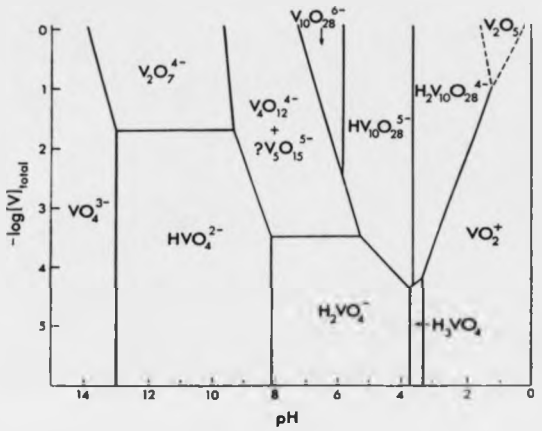

Figure 12. Distribution diagram for isopolyvanadates [11].

1.8.1. Mono- and Divanadates

In the solid state the species VO_4^{3-} and $V_2O_7^{4-}$ were shown to have tetrahedrally coordinated metal atoms [11]. In solution, infrared [123] and Raman [124] spectra were consistent with a tetrahedral structure for VO_4^{3-}. The $V_2O_7^{4-}$ anion adopts a structure analogous to that of $P_2O_7^{4-}$ in solution [11].

1.8.2. Metavanadates

Metavanadates are colourless anions with the empirical formula VO_3^- that predominate in aqueous vanadate solutions at pH *ca.* 6.5-8. Solution studies have indicated the presence of both trimeric and tetrameric anions [11]. Depending on which experimental technique was used arguments were made in favour of one or

the other of these species. UV spectroscopy suggested a trimer [125,126], EMF measurements were interpreted in terms of both $[V_3O_9]^{3-}$ and $[V_4O_{12}]^{4-}$ [127], whilst ultracentrifugation [128] and diffusion measurements [129] supported a tetramer. The crystal structure [130] of a tetra-n-butylammonium salt, $(Bu_4N)_3HV_4O_{12}$ isolated from a solution of V_2O_5 in alcoholic Bu_4NOH, revealed a cyclic anion of corner-shared VO_4 tetrahedra.

Heath and Howarth [51] have recorded ^{51}V and ^{17}O NMR spectra of metavanadate solutions and interpreted these to show the presence of VO_4^{3-}, (δ_V -541.2 ppm), $V_2O_7^{4-}$, (δ_V -561.0 ppm), cyclic $[V_4O_{12}]^{4-}$ (δ_V -577.6 ppm), $[V_5O_{15}]^{5-}$ (δ_V -586 ppm), with minor quantities of $[V_6O_{18}]^{6-}$ (δ_V -589.4 ppm) and linear V_3 and V_4 anions.

1.8.3. Decavanadate

Metavanadate solutions acidified to pH 6 or below yield orange solutions containing the decavanadate anion $[V_{10}O_{28}]^{6-}$ [11]. Numerous X-ray studies [131-135] have determined the decavanadate structure shown in Figure 13. Solution state ^{51}V NMR spectroscopy [47,54] has shown that the structure of the anion corresponds to that in the solid, with three structurally distinct vanadiums in the ratio 1:2:2.

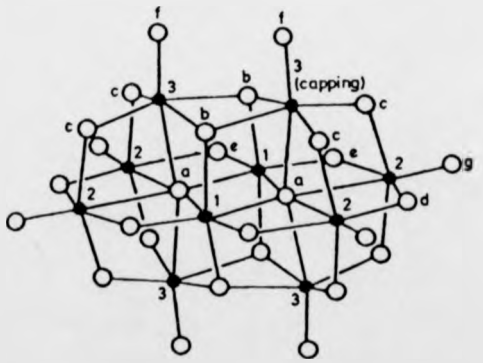

Figure 13. Structure of decavanadate $[V_{10}O_{28}]^{6-}$ labelled according to reference [39] (● = V, ○ = O).

In Klemperer and Shum's [39] early ^{17}O NMR investigation they had assigned all the resonances except those of O_f and O_g, and found that the predominant protonation site was at O_b, and to a lesser extent O_c. Subsequently, Klemperer *et al.* [136] performed $^{17}O\{^{51}V\}$ decoupling experiments and have unequivocally assigned V_2, V_3 and also the ^{17}O NMR resonances f and g to O_f and O_g .

More recently Day *et al.* [53] have characterised the protonation sites of $[H_3V_{10}O_{28}]^{3-}$ both in solid, and solution (non-aqueous) state using single crystal X-ray diffraction and multinuclear NMR techniques including ^{51}V and ^{1}H. Previous solution investigations of the $[V_{10}O_{28}]^{6-}$ protonation sites had been performed in aqueous solvents where proton exchange is fast on the NMR time scale, thus removing the possibility of observing any proton signals.

1.8.5. Species with Keggin Structures

Howarth and Pettersson [137] have demonstrated that vanadium [V] can form a transient species $[H_{12}V_{13}O_{40}]^{3-}$, with 12 V atoms arranged in a Keggin structure around a central tetrahedrally coordinated V atom. The NMR data clearly indicated a symmetrical Keggin species (half-life of 80 min. at 298K) consistent with either an α- or ε- isomer. The ^{17}O NMR spectrum also revealed three new resonances consistent with either an α- or ε- isomer which decayed at the same rate as the corresponding vanadium resonances.

1.9. Tungstovanadates

Early investigations of the tungstovanadates firmly established the structures of $[W_5VO_{19}]^{3-}$, *cis*-$[W_4V_2O_{19}]^{4-}$ [138], and more recently *fac*-$[W_3V_3O_{19}]^{5-}$ [139,140] and a series of tungstovanadates based on the Keggin structure [53]. (For convenience, the above may be abbreviated using the notation (n,m) as shorthand for the species $[M_nV_mO_x]^{(2x-6n-5m)-}$). On the evidence of low field NMR and UV spectroscopy, Pope *et al.* [141] proposed Scheme 2 for the interconversion of

aqueous tungstovanadates. The product of each reaction in the scheme was identified by crystallisation of sparingly soluble salts. Many of the reactions they observed were slow and they did not attempt to determine reaction the stoichiometries. At pH>8 all the tungstovanadates decomposed to HVO_4^{3-} and WO_4^{2-} at varying ratios. The complexes X identified in the scheme were phases that consisted of lustrous orange leaflets or red parallelepipeds that were obtained as by products in the preparations [142] of $K_6V_4W_9O_{40}$ and $K_5V_3W_{10}O_{40}$. The two phases were interconvertible by recrystallisation (leaflets at pH 2-3, parallelepipeds at pH 0-1, mixtures of these at pH 1-2) but were not observed to convert to the $[V_4W_9O_{40}]^{6-}$ or $[V_3W_{10}O_{40}]^{5-}$ complexes.

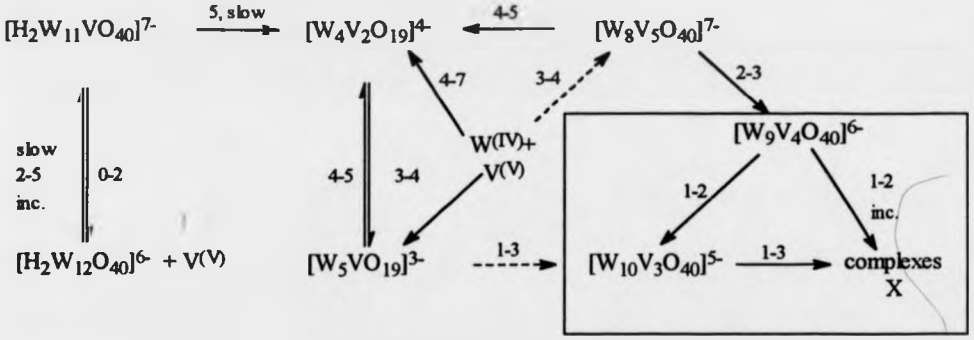

Numbers indicate the range of pH for each reaction. Broken arrows denote slow reactions that occurred in concentrated solutions. The complexes enclosed in the box were extracted by ether from very acidic solutions; the resulting free acids slowly decomposed to give oxide precipitates.

Scheme 2. Interconversion of tungstovanadates [141].

1.9.1. Hexametallates

The (5,1) anion, $[W_5VO_{19}]^{3-}$ (Figure 14(a)) is stable in aqueous solution at pH 2-3 and exhibits a single, pH independent, ^{51}V NMR resonance at δ_V =-523.2 ppm (at 303K) [143]. Domaille [144] has reported a ^{183}W $\{^{51}V\}$ NMR spectrum for the

$[(n\text{-}C_4H_9)_4N]_3(5,1)$ anion in acetonitrile, which has two peaks in the area ratio 4:1, δ_W= 76.4 and 75.9 ppm respectively. The ^{51}V NMR resonance was sufficiently sharp that the ^{183}W satellites were visible with $^2J_{W\text{-}O\text{-}V}$ =11.1Hz. Recently, Pope and Leparulo-Loftus [143] also observed a similar doublet $^2J_{W\text{-}O\text{-}V}$ = 10.8 Hz. at 80°C, using natural abundance ^{183}W NMR. However, with enriched ^{183}W (82.5%) solutions they obtained an envelope of resonances which was satisfactorily simulated by the sum of the appropriate multiplets (46% quintet, 39% quartet, 13% triplet) each with the same J value. Thus indicating that only the *cis*- related tungsten atoms coupled.

The (4,2) species, *cis*-$[W_4V_2O_{19}]^{4-}$ formed rapidly in aqueous solution at pH 4-5. Its ^{51}V NMR shift was at δ_V=-508.5 ppm (at 303K) and on protonation δ_V=-524.4 ppm [143]. Maksimovskaya and Chumachenko [145] have reported the anion protonated with a $pK_a \approx 3.3$ (W:V, 3:1 [V]=0.004M) somewhat less than the molybdo analogue $pK_a \approx 4.7$. Presumably this indicates that the tungstovanadate species prefers a higher anionic charge because of stronger π-bonding from the oxygen to the tungsten. The orientational disorder of the (4,2) anion rendered all metal atoms equivalent and consequently X-ray analysis [146] failed to determine whether either the *cis*-, *trans*-, or a mixture of both isomers were present. Although the ^{51}V NMR data do not directly address the problem of structure elucidation, the relatively large effect of protonation upon the vanadium chemical shift ($\Delta\delta_V$ = 13.5 ppm) [144] is consistent with protonation at the unique V-O-V oxygen atom as proposed earlier [47]. Subsequent ^{183}W and ^{17}O NMR [41,47,50] investigations have demonstrated that only the *cis*- isomer formed (Figure 14(b)).

The ^{183}W NMR resonances that Domaille [144] observed in aqueous solution were broad for the (4,2) anion. However, decoupling the vanadium resonances, two equally intense ^{183}W lines at δ_W = 70.3 and 69.4 ppm were observed, consistent with the *cis*- isomer. No additional line attributable to a *trans*- isomer was observed.

Satellite isotopomer lines were not observed either because of close spacing, broad lines, and the lower signal-to-noise ratios.

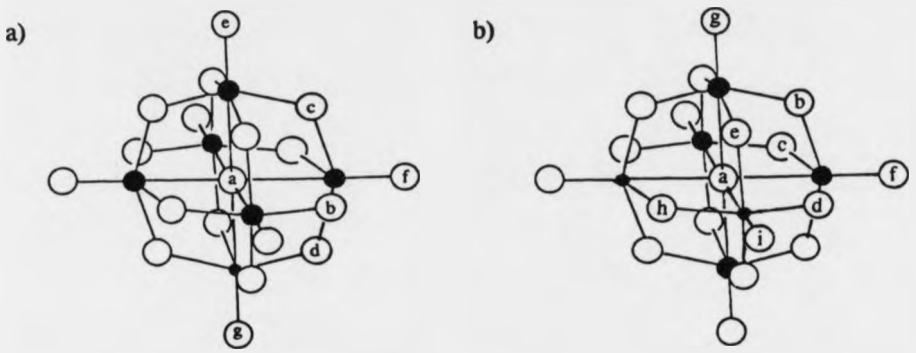

Figure 14. Structures of **a)** $[W_5VO_{19}]^{3-}$ and **b)** *cis*-$[W_4V_2O_{19}]^{4-}$. (●=V, ●=W, ○=O).

Further evidence for the *cis*- geometry of the vanadium atoms was provided by the ^{17}O NMR spectrum reported by Klemperer and Shum [41] (see Figure 15(c) and Table 5). The peak at δ_O=848 ppm was in the range expected for V-O-V oxygens [39] and two resonances were observed in the W-O-W region (δ_O=371 and 384 ppm). Resonances for the (4,2) anion were assigned after delineation of the chemical shift ranges for oxygens in similar OV, OW, OV_2, OW_2 and OVW environments. This was accomplished by measuring spectra for the $[W_6O_{19}]^{2-}$ and the (5,1) anions (see Figure 15(a) and 15(b)). The ^{17}O NMR spectrum of $[W_6O_{19}]^{2-}$ was readily assigned by the ratio of the integrals. The ^{17}O NMR resonances of the oxygen atoms bonded to vanadium in the (5,1) anion were easily identified by their unusual line shapes caused by ^{51}V-^{17}O spin-spin coupling [30,41]. Comparison of the unprotonated (4,2) anion's spectrum recorded at 25°C (discussed above) with the spectrum of the protonated anion at 0°C revealed a marked upfield shift for the V-O-V resonance δ_{Oh}=848 to 610 ppm on protonation. This unambiguously identified the protonation site (Figure 15(d)). At elevated temperatures (Figure 15(e)) the linewidths are reduced.

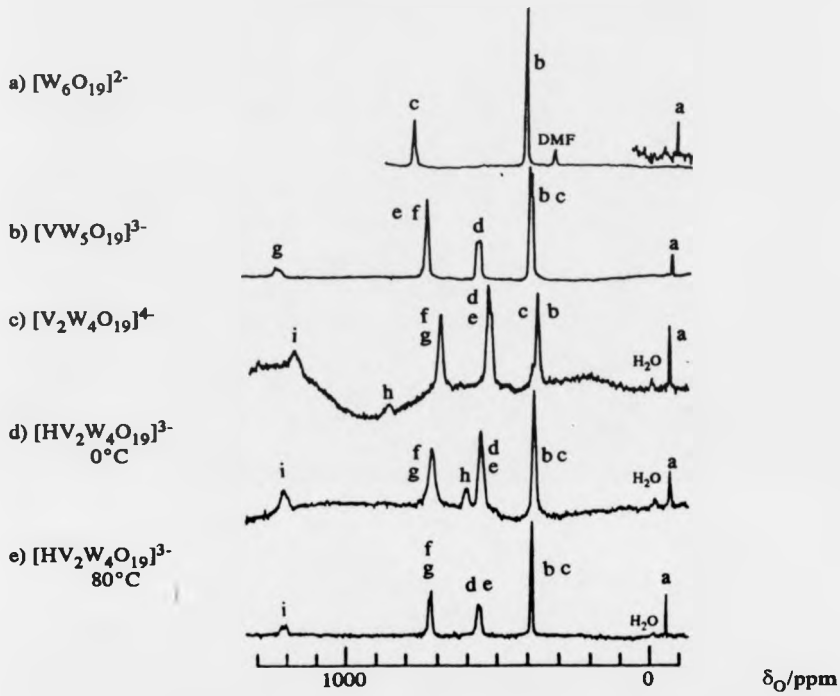

Figure 15. 13.5 MHz oxygen-17 NMR spectra of hexametallate anions discussed in text. Resonances are labelled using the lettering schemes given in Figure 14.

Salts of the $[W_3V_3O_{19}]^{5-}$ anion have been reported [147] and recently ^{51}V NMR spectroscopy revealed a single resonance at δ_V=-500 ppm [143] associated with the facial (*fac*-) isomer. Pope and Leparulo-Loftus [143] repeated Il'yasova's [147] preparation of $[W_3V_3O_{19}]^{5-}$ crystals, their initial ^{51}V NMR spectra indicated a mixture of *cis*-$[W_4V_2O_{19}]^{4-}$ (δ_V = -508.5 ppm), and metavanadates $[V_4O_{12}]^{4-}$ and $[V_5O_{15}]^{5-}$ (δ_V = -574 and -583 ppm), [51] together with traces of a species with δ_V *ca.* -500 ppm. However, if the spectrum was recorded within minutes of dissolution, the -500 ppm resonance was the major feature. They also noted that the

ratio of the *cis*-$[W_4V_2O_{19}]^{4-}$ and metavanadate peaks remained equal during the course of the evolution of the spectrum, and, thus concluded that there must be a decomposition of a polyanion in which the mole ratio of W:V is 1:1, *e.g.*

$$2H^+ + 4[W_3V_3O_{19}]^{5-} = 3[W_4V_2O_{19}]^{4-} + 6VO_3^- + H_2O \qquad (1.3)$$

The close similarity of the IR spectrum of the crystals to that of *cis*-$[W_4V_2O_{19}]^{4-}$ salts supported the assignment as a hexametallate *i.e.* $[W_3V_3O_{19}]^{5-}$, and the single ^{51}V NMR resonance implied the *fac*- isomer (Figure 16(a)). They also reported a further small resonance at δ_V = -515 ppm which disappeared as the solution aged at pH 7.5, and which they tentatively assigned to one of the non-equivalent vanadium atoms in the meridional (*mer*-) isomer (Figure 16(b)).

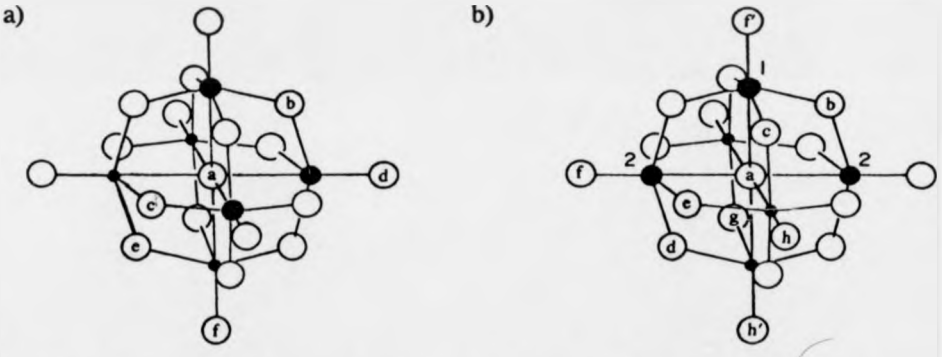

Figure 16. Structures of a) *fac*-$[W_3V_3O_{19}]^{5-}$ and b) *mer*-$[W_3V_3O_{19}]^{5-}$. (●=V, ●=W, ○=O)

Maksimovskaya *et al.* [148] have reported ^{17}O NMR data for the *fac*- (3,3) anion. Figure 17 shows the ^{17}O NMR spectrum of the *fac*-(3,3) anion which was readily assigned by analogy to that of the *cis*-(4,2) species. Although in the spectrum there is evidently only one W=O resonance which one would anticipate for a symmetrical species, Maksimovskaya *et al.* [148] tabulated two chemical shifts with no explanation. See Table 5.

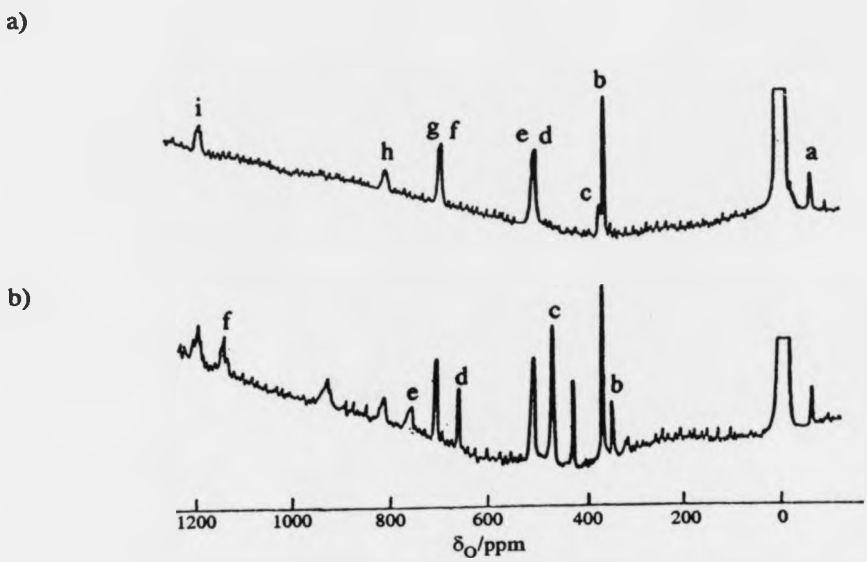

Figure 17. 40.7 MHz oxygen-17 NMR spectrum of 0.2 M solutions of **a)** $Na_4W_4V_2O_{19}\cdot 14H_2O$ and **b)** $Na_5W_3V_3O_{19}\cdot 18H_2O$ at 300K.

A distribution of vanadium versus pH has been compiled for a tungstovanadate solution (W:V, 3:1 [V]=0.004M) using ^{51}V NMR spectra [145] (See Figure 18).

1 $[VO_3]^-$, $[H_2V_2O_7]^{2-}$, $[H_2VO_4]^-$
2 $[W_4V_2O_{19}]^{4-}$
3 $[HW_4V_2O_{19}]^{3-}$
4 $[W_5VO_{19}]^{3-}$
5 $[VO_2]^+$

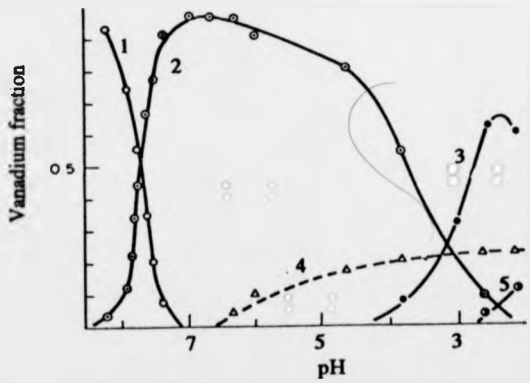

Figure 18. Distribution diagrams of $V^{(V)}$ for Na_2WO_4-$NaVO_3$ (W:V, 3:1 [V]=0.004M) versus pH.

Figure 18 shows that just above pH 7 the metavanadates dominate the ^{51}V NMR spectrum whereas, just below, the (4,2) species accounts for all the vanadium present. Below pH 4.2 the *cis*-(4,2) anion protonates, and this protonated form maximises to ≈65% of the vanadium present at pH≈ 2.5, below pH 2 this becomes less stable. The (5,1) anion starts to compete with the *cis*-(4,2) species at *ca.* pH 6 and represents ≈20% of the vanadium present below pH 3. At low pH>3, VO_2^{2+} steadily increases to ≈15%.

Table 5. Oxygen chemical shifts of the known hexametallate tungstovanadates at 303K/ppm.

peak	$[W_6O_{19}]^{2-a}$	$[W_5VO_{19}]^{3-b}$	$[W_4V_2O_{19}]^{4-c}$	$[HW_4V_2O_{19}]^{3-d}$	$[W_3V_3O_{19}]^{5-e}$
	δ_O	δ_O	δ_O	δ_O	δ_O
a	-81 (1)[f]	-75 (1)	-65 (1) [-67][g]	-60 (1)	-67 (1)
b	413 (12)	389 (4)	371 (4) [361]	391 (4)	345 (3)
c	772 (6)	395 (4)	384 (1) [368]	391 (1)	467 (3)
d		562 (4)	530 (2) [510]	564 (2)	668, 656(3)
e		731 (1)	530 (4) [510]	564 (4)	764 (3)
f		731 (4)	687 (2) [695]	723 (2)	1132 (3)
g		1217(1)	687 (2) [698]	723 (2)	
h			848 (1) [814]	610 (1)	
i			1162(2) [1190]	1208 (2)	

[a] $(n\text{-}Bu_4N)_2\ W_6O_{19}$, 0.087 mol in DMF [41]. [b] $(n\text{-}Bu_4N)_3\ W_5VO_{19}$, 0.064 mol in CH_3CN [41]. [c] $(n\text{-}Bu_4N)_4\ W_4V_2O_{19}$, 0.089 mol in CH_3CN [41]. [d] $(n\text{-}Bu_4N)_3\ HW_4V_2O_{19}\cdot H_2O$, 0.15 mol in CH_3CN at 273K [41]. [e] Chemical shifts in aqueous solution at pH 7, 300K [148]. [f] is the relative intensity. [g] Chemical shifts in aqueous solution at pH 7, 300K [148].

1.9.2. Substitution into the Decavanadate Structure $[WV_9O_{28}]^{5-}$

Maksimovskaya and Chumachenko [145] have recently reported a (1,9) species with the tungsten substituting one of the "capping" vanadiums in decavanadate, using ^{51}V and ^{17}O NMR spectroscopy (see Figure 19, Tables 6 and 7). In their modified decavanadate ^{51}V NMR spectrum the two signals representing V_2 and V_3 were split into four 2:2:2:1 indicating that one of either was replaced by W. Although the

assignment for these vanadium resonances was vague, the authors were able to determine which vanadium atom had been replaced by ^{17}O NMR spectroscopy. Assignments were made by comparison with the (1,9) molybdo analogue and the known data of decavanadate anion [39]. The resolution of their spectra did not permit them to resolve whether a further substituted species also formed.

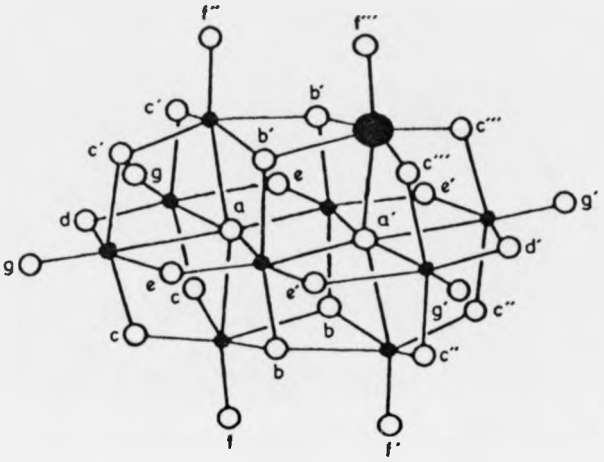

Figure 19. Structure of monotungstononavanadate, $[WV_9O_{28}]^{5-}$. (● = V, ● = W, ○ = O)

Table 6. Vanadium chemical shifts of $[V_{10}O_{28}]^{6-}$ and $[WV_9O_{28}]^{5-}$ at 303K/ppm in aqueous solution [145].

Peak	$[V_{10}O_{28}]^{6-}$ δ_V	$[WV_9O_{28}]^{5-}$ δ_V
I	-420 (2)[a]	-424 (2)[a]
II	-495 (4)	-492 (2) -503 (2)
III	-511 (4)	-511 (2) -522 (2)

[a] Is the relative integral.

Table 7. Oxygen chemical shifts of $[V_{10}O_{28}]^{6-}$ and $[WV_9O_{28}]^{5-}$ at 303K/ppm in aqueous solution [145].

peak[a]	$[V_{10}O_{28}]^{6-}$		$[WV_9O_{28}]^{5-}$	
	δ_O		δ_O	
a	63[a]	(2)[b]	14	(1)
a'	n.a.		82	(1)
b'	n.a.		298	(2)
b	397	(4)	439	(2)
c'''	n.a.		495	(2)
c'	n.a.		788	(2)
c	765	(8)	788	(2)
c''	n.a.		825	(2)
d	790	(2)	807	(1)
d'	n.a.		825	(1)
e	895	(4)	904	(2)
e'	n.a.		933	(2)
f'''	n.a.		[c]	
f	1140	(4)	1160	(2)
f'	n.a.		1174	(2)
f''	n.a.		1195	(3)
g	1150	(4)		
g'	n.a.			

[a] Referenced to solvent water $\delta_O = 0$. [b] Is the relative integral. [c] Omitted from their table.

1.9.3. Species with Keggin Structures

Further acidification and heating of these solutions leads to the darker coloured anions of the Keggin series $[W_{12-X}(V)V_XO_{40}]^{(3-X)-}$ (X = 2,3), which have been isolated as potassium and other salts [142] (see Figure 20). Members X = 0 and 1 are unknown [142]. Although not stable in solution, salts of the X = 4 member of the series have been reported [149] and an X-ray structural analysis of $K_7[W_8(V)V_4O_{40}]\cdot 12H_2O$ has been performed [150]. These formulae are written to indicate that the central, tetrahedrally coordinated atom in the α-Keggin structure is vanadium. Pope and Leparulo-Loftus [143] have identified the ^{51}V NMR

resonances of many isomers of members x = 2 and 3 (see Tables 8 and 9), which confirmed their earlier lower field ^{51}V CW-NMR investigation [50] and the findings of Maksimovskaya *et al.* [148]. The central vanadium resonances were generally sharper than the octahedrally coordinated vanadium, and fell in δ_V=-550 to -560 ppm range, with those for the $[W_9(V)V_3O_{40}]^{6-}$ complexes towards the higher δ values. The positions of the other vanadium resonances depended on their neighbours. Generally, isolated VO_6 octahedra tended to resonate between δ_V=-520 and -535 ppm, whilst those which shared a common edge with another VO_6 resonated around δ_V=-500 to -510 ppm. Even higher shifts were observed δ_V= -480 if a common vertex is shared in a cluster of three.

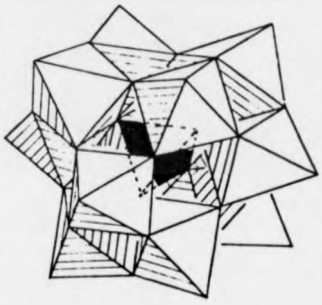

Figure 20. Structure of an α-Keggin anion with a tetrahedral vanadium in the centre.

Table 8. Vanadium chemical shifts, relative integrals and linewidths of $K_5VV_2W_{10}O_{40}$[a] [143]

δ_V[b]	Integral		Linewidth[c]
-505.3	3.8	0.38	76 ± 5
-527.3	1.0		180 ± 30
-530.2	9.7	1.2	43 ± 5
-532.3	1.3		76 ± 5
-536.0	5.4	0.54	67 ± 5
-558.2		1.0	32 ± 4
-558.8			
-559.1			22 ± 4
-559.4(sh)			
-559.9(sh)			

[a] In 0.5 M HSO_4^-/SO_4^{2-} (50% ^2H_2O, pH 2.0). Measured at T=30°C, [V]=0.06M. [b] ± 0.1ppm, measured with respect to $SiVW_{11}$ (assigned as -548.30 ppm) in 0.25 M NaOAc (pH 4.7, 50% ^2H_2O) by external substitution referencing. [c]measured at half peak height in Hz.

Table 9. Vanadium chemical shifts, relative integrals and linewidths of $K_6VV_3W_9O_{40}$[a] [143]

δ_V[b]	Integral	Linewidth[c]
-480.5	<0.1	110 ± 10
-502.5	1	160 ± 10
-505.2		130 ± 10
-507 ± 1(sh)		
-508.1		
-509.0		90 ± 10
-522.0	2	290 ± 50
-525.8		
-526.9(sh)		
-527.7		
-530.0		
-531.0		
-533.4		58 ± 4
-552.5 ± 0.2(sh)	1	
-552.8		20 - 30
-553.0 ± 0.2(sh)		
-553.1		20 - 30
-553.4 ± 0.2(sh)		
-554.0		20 ± 4

[a] In 0.25 M NaOAc (pH 4.0), T=30°C, and [V] = 0.08M. [b] ± 0.1ppm, measured with respect to $SiVW_{11}$ (assigned as -548.30 ppm) in 0.25 M NaOAc (pH 4.7, 50% ^2H_2O) by external substitution referencing. [c]measured at half peak height in Hz.

The assignment of the ^{51}V NMR spectrum of $[W_{10}(V)V_2O_{40}]^{5-}$ (Figure 21), was assisted by expansion of the central vanadium region at δ_V *ca.* -559 ppm and simulation of these resonances (Figure 22), revealed five isomers in the ratio : δ_V = -558.2 (30.4%),-558.8 (21.9%), -559.1 (41.7%), -559.4(4%) and -559.9(2%). This assignment was confirmed by the ratio of the combined integral of this group of lines, to the remainder being 1:2.1, and, the rest of the spectrum consisted of three major resonances (δ_V = -505.3, -530.2, and -536.0 ppm) and two minor peaks.

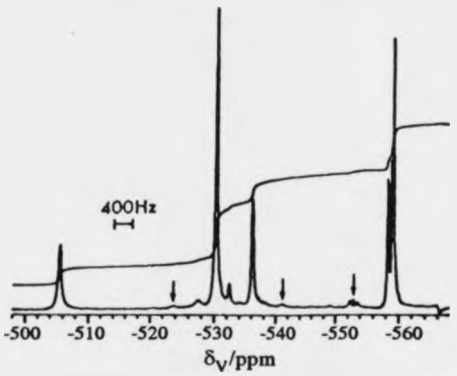

Figure 21. 131.4 MHz vanadium-51 NMR spectrum of $K_5W_{10}(V)V_2O_{40}$ (pH 2.0). The arrows indicating the impurity of $[W_9(V)V_3O_{40}]^{6-}$.

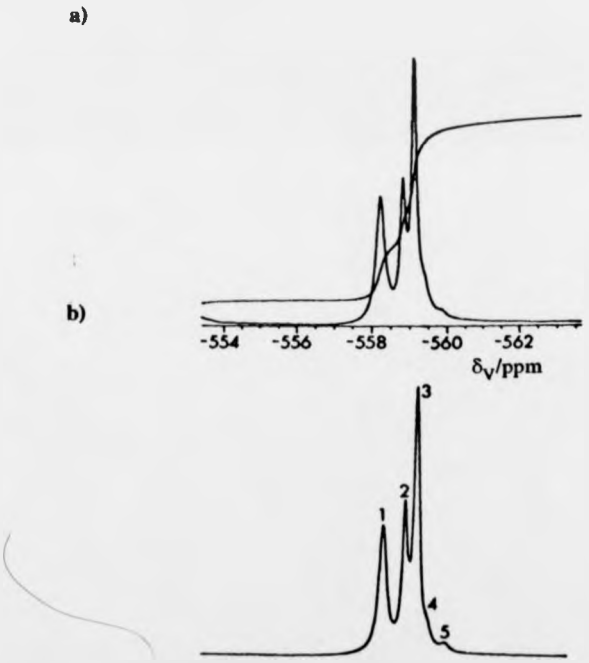

Figure 22. a) Expansion of the region between -554 and -563 ppm of the vanadium-51 NMR spectrum shown in Figure 21). b) Simulation of a) with lines at -558.2, -558.8, -559.4 and -559.9 ppm and relative integrated areas of 1). 30.4%, 2). 21.9%, 3). 41.7%, 4). 4.0% and 5) 2.0%.

When these authors expanded the region *ca.* δ_V -553 ppm (attributed to the central vanadiums) in the ^{51}V NMR spectrum of the $[W_9(V)V_3O_{40}]^{6-}$ anion, it revealed at least 7 of the 13 possible isomers. The ratio of the integral of these resonances to that of the remainder of the spectrum was 1:3 supported this assignment (see Figure 23).

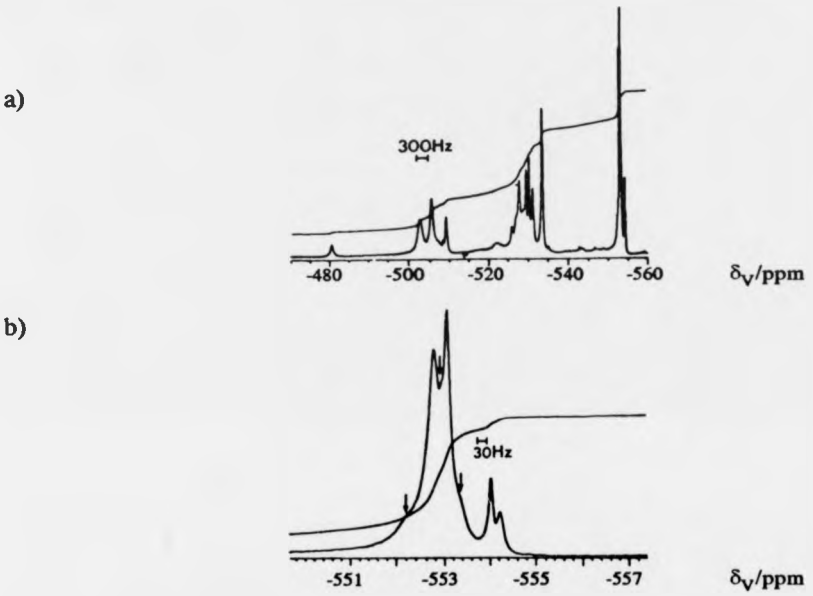

Figure 23. a) 131.4 MHz vanadium-51 NMR spectrum of $K_6W_9(V)V_3O_{40}$ (pH 4). **b)** Expansion of the region between -550 and -557 ppm. Arrows indicate unresolved shoulders.

The ^{17}O NMR spectrum of $[W_9(V)V_3O_{40}]^{6-}$ reported by Maksimovskaya *et al.* [148] is shown in Figure 24 and shifts are tabulated in Table 10. They noted that the spectrum was remarkably similar to that of $[W_9(P)V_3O_{40}]^{6-}$ [151] which indicated that the two anions were isostructural and an analogous interpretation was therefore applied. The intensity of the lines was consistent with that expected for a statistical distribution of the three V atoms between the 12 possible positions in the anion. They attributed the extra intensity in the V-O-W region (δ_O *ca.* 500 to 570 ppm) to the resonances from the oxygens bonded to the central tetrahedrally coordinated vanadium atom. These shifts were very close to the chemical shift of the free VO_4^{3-}

ion in solution (δ_O = 570 ppm). This closeness of the chemical shifts implied that there was very little interaction of these oxygen atoms with the surrounding tungsten "cage". Also when they correlated the chemical shifts of the terminal oxygen atoms with the bond length [152] separately for both V and W atoms, as distinct from the X-ray crystallography, the chemical shifts of the lines V=O and W=O corresponded approximately to 1.60 and 1.73 Å, respectively.

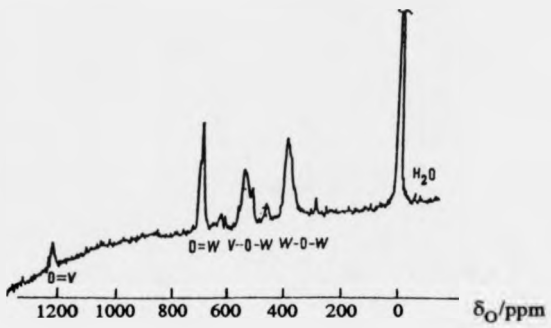

Figure 24. 40.7 MHz oxygen-17 NMR spectrum of a ≈ 0.2 M solution of $K_6W_9(V)V_3O_{40}{\cdot}24H_2O$; 345K.

Table 10. Oxygen chemical shifts (ppm) for $K_6W_9VV_3O_{40}$ assigned by oxygen type.

	O=V	O=W	V-O-W	W-O-W	VO_4
$[W_9(V)V_3O_{40}]^{6-}$ δ_O	1223[a]	706,698	545,517	567	395

[a] Referenced to solvent water δ_O=0.

The substituted metatungstate anion $[H_2W_{11}VO_{40}]^{7-}$ has also been characterised by ^1H and ^{51}V NMR spectroscopy [141]. The resonances from the internal protons were observed at δ_H=6.08 ppm, very close to the corresponding signal from the metatungstate anion at δ_H=6.09 ppm recorded under similar conditions. The ^{51}V

NMR resonance was observed at δ_V=-539 ppm and was about 60 Hz wide. When a solution of $[K_7H_2W_{11}VO_{40}]$ was acidified in the presence of ^2H_2O, the proton signal disappeared within 5 min.. This implied that the tetrahedral cavity of the Keggin structure opened up rapidly and permitted exchange with the solvent. The ^{51}V NMR spectra of acidified solutions of $[H_2VW_{11}O_{40}]^{7-}$, still exhibited the original signal at δ_V=-539 ppm after 4.5 hours, together with a new resonance at δ_V = -548 to -550 ppm (tentatively attributed to VO_2^+). In freshly acidified solutions they were in the ratio of about 2:1 (-539:-548) (after *ca.* 5 min.). Gradually, the peak at δ_V=-548 ppm increased in intensity on addition of more acid and prolonged standing. The peak at δ_V = -539 ppm broadened to 100 Hz which indicated that the anion had protonated. Pope *et al.* [141] proposed that the anion protonated at the oxygen atoms that bound the vanadium atom to the rest of the Keggin structure. It was then postulated that because of this protonation process one or more of the V-O-W bonds broke, which opened up the centre of the structure to proton exchange. They also observed that 0.02 mM solutions of $[H_2W_{11}VO_{40}]^{7-}$ decomposed completely within several hours at pH 2 or lower, yielding colourless or very pale yellow solutions with UV spectra characteristic of metatungstate. However, with a 2.0 mM solution at pH 2, decomposition was incomplete even after 40 days.

1.10. Molybdovanadates

Howarth *et al.* [25,26] performed a detailed study of aqueous molybdovanadate solutions over a wide range of metal ion ratios in the pH range 1-7 using multinuclear NMR spectroscopy and EMF measurements. As a result they have established the speciation, structures of the main anions present and have clarified the findings of Maksimovskaya and Chumachenko [145].

1.10.1. Substitution into the Decavanadate Structure

1.10.1.1. $[MoV_9O_{28}]^{5-}$

Figure 25 shows the structure of $[MoV_9O_{28}]^{5-}$ and a ^{51}V NMR spectrum of a solution of $[MoV_9O_{28}]^{5-}$ and $[HV_{10}O_{28}]^{5-}$ at pH 5 and room temperature, from which has been subtracted a spectrum of decavanadate at the same pH, ionic medium and temperature. This demonstrates the 2:2:2:1:1:1 peak area ratio, and this proves that Mo has replaced a "capping" V. Below pH 3 further resonances were observed which Howarth *et al.* [25] attributed to *cis*- and *trans*-(2,8) isomers. (See below).

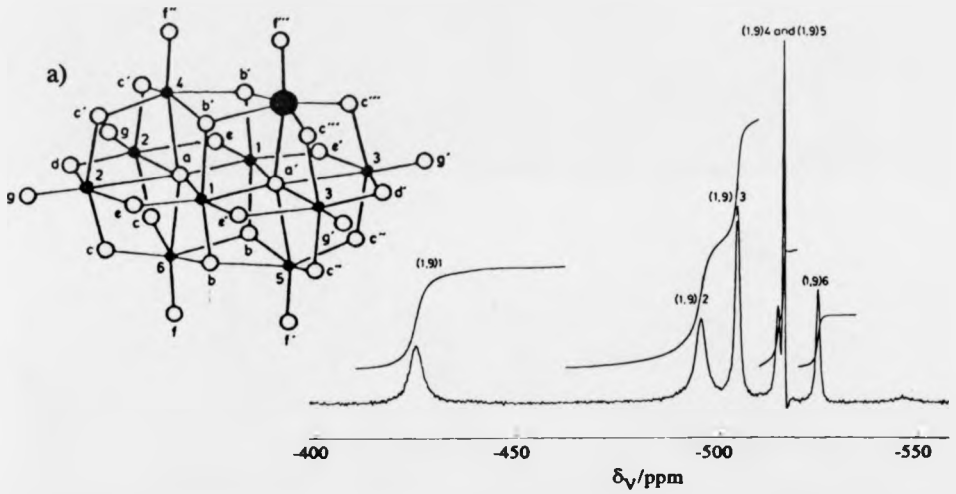

Figure 25. a) The structure of $[MoV_9O_{28}]^{5-}$ (●=V, ●=Mo, ○=O). **b)** 105.2 MHz vanadium-51 NMR spectrum, pH 5.0, 45 mmol dm^{-3} in V and 5 mmol dm^{-3} in Mo, 294K, from which has been subtracted a spectrum of decavanadate at the same pH, so as to show only the six peaks from $[MoV_9O_{28}]^{5-}$.

The ^{51}V NMR resonances of $[MoV_9O_{28}]^{5-}$ exhibited a common $pK_a = 2.77$ (293K) upon protonation which confirmed a single species. In Figure 25 the peaks assigned to $[MoV_9O_{28}]^{5-}$ and its protonated form are labelled (1,9)n, where n increases with decreasing δ_V. Table 11 shows the ^{51}V chemical shifts and assignments made for (1,9) and its protonated form. Retention of the decavanadate structure was further supported by the fact that peak (1,9)1 was very close in shift to (0,10)1, peak (1,9)2

close to (0,10)2 and peaks (1,9)4 and (1,9)5 close to (0,10)3, in the unprotonated state. The other peaks, however, were shifted by the molybdenum substitution by up to 10 ppm to lower frequency, presumably because of structural distortions created by the molybdenum. These assignments were then conclusively confirmed by 2D ^{51}V-^{51}V COSY .

Table 11. Vanadium Chemical Shifts of $[V_{10}O_{28}]^{6-}$, $[MoV_9O_{28}]^{5-}$ and $[HMoV_9O_{28}]^{4-}$ at 294K/ppm [25].

$[V_{10}O_{28}]^{6-}$			$[MoV_9O_{28}]^{5-}$			$[HMoV_9O_{28}]^{4-a}$
peak	$\delta_V{}^b$		peak	$\delta_V{}^b$		δ_V
(0,10)1	-425[c]	(2)[d]	(1,9)1	-425	(2)	-426
(0,10)2	-498	(4)	(1,9)2	-495.5	(2)	-510.6
	n.a.		(1,9)3	-505	(2)	-505
(0,10)3	-515	(4)	(1,9)4	-514.9	(1)	-524.2
	n.a.		(1,9)5	-516.2	(1)	-520.7
	n.a.		(1,9)6	-525.3	(1)	-530.4

[a] estimated composition from pH curve. [b] relative peak area for compound in question. [c] figures without decimal places are less accurate, *e.g.* due to overlap. [d] notional relative integral.

As with the decavanadate anion [53], protonation of the (1,9) species, was shown to occur at both O_b and O_c but with a preference for O_c; being further away from the added positive charge of the Mo^{VI}. The same electrostatic repulsion also removed $O_{b'}$ from the competition for H^+. Unfortunately Howarth *et al.* [25] were unable to distinguish O_c from $O_{c'}$ and concluded that either site was equally favourable. Table 12 shows the ^{17}O chemical shifts and assignments made for decavanadate and its mono- and dimolybdo substituted analogues *cis*- and *trans*-(2,8) (the *cis*- and *trans*-(2,8) species are discussed in the next section).

1.10.1.2. Further Substitution: *cis*-$[Mo_2V_8O_{28}]^{4-}$ and *trans*-$[Mo_2V_8O_{28}]^{4-}$

Using 2-dimensional spectroscopy Howarth *et al.* [25] assigned the remaining resonances to *cis*- and *trans*- (2,8). The isomer ratio of these was 9:11 respectively. These assertions were also confirmed by their parallel potentiometric study. The structures of *cis*- and *trans*- (2,8) are shown in Figure 26. Table 13 shows ^{51}V NMR chemical shifts for *cis*- and *trans*-(2,8) species. These species were present below pH 3 and their resonances were independent of pH.

Table 12. Oxygen chemical shifts of $[V_{10}O_{28}]^{6-}$, $[MoV_9O_{28}]^{5-}$, $[HMoV_9O_{28}]^{4-}$, *cis*-$[Mo_2V_8O_{28}]^{4-}$ and *trans*-$[Mo_2V_8O_{28}]^{4-}$ at 294K/ppm.

peak[a]	$[V_{10}O_{28}]^{6-}$	$[MoV_9O_{28}]^{5-}$	$[HMoV_9O_{28}]^{4-}$[b]	*cis*-$[Mo_2V_8O_{28}]^{4-}$	*trans*-$[Mo_2V_8O_{28}]^{4-}$
	δ_O	δ_O	δ_O	δ_O	δ_O
a	55[c]	27.6	41.4	n.a.	n.a.
a'	n.a.	80.2	74.7	77.2	47.7
b'	n.a.	337.2	343.6	279.4	n.a.
b	420	438.7	410.1	446.7	355.1
c'''	n.a.	604.4	614.2	n.a.	n.a.
c'	n.a.	786	720	622	622
c	765	786	720	726	845
c''	n.a.	825	835.7	n.a.	n.a.
d	785	806	846.3	832	832
d'	n.a.	806	835.7	n.a	n.a.
e	895	896.8	917.9	909.2	935
e'	n.a.	930.1	936	n.a.	n.a.
f''	n.a.	881.4	896.1	n.a.	n.a.
f	1125	1143	1187	1165	1198
f'	n.a.	1143	1187	922.2	916
f''	n.a.	1180	1200	n.a.	n.a.
g	1142	1170.8	1200	1207	1220
g'	n.a.	1191	1206.7	n.a.	n.a.
$\Sigma\ \delta_O$	22128	22002	22077	21310	21934

[a] Using labelling scheme of [136] with added dashes to indicate increasing proximity to Mo. [b] Approximately monoprotonated, but precise state not definable. [c] δ_O (solvent water) = 0. Values without decimal places were less precise, *e.g.* due to overlap. n.a. Not applicable because of higher symmetry.

Table 13. Vanadium chemical shifts of *cis*-$[Mo_2V_8O_{28}]^{4-}$ and *trans*-$[Mo_2V_8O_{28}]^{4-}$ at 294K/ppm [25].

	cis-$[Mo_2V_8O_{28}]^{4-}$			*trans*-$[Mo_2V_8O_{28}]^{4-}$		
peak	δ_V		peak	δ_V	
trans- (2,8)1	-427[a]	(2)[b]	*cis*-(2,8)1	-424	(2)
trans- (2,8)2	-505	(4)	*cis*-(2,8)2	-505	(4)
trans- (2,8)3	-516.2	(2)	n.a.		
	n.a.		*cis*-(2,8)3	-525.5	(2)

[a] figures without decimal places are less accurate, *e.g.* due to overlap. [b] relative peak area for compound in question.

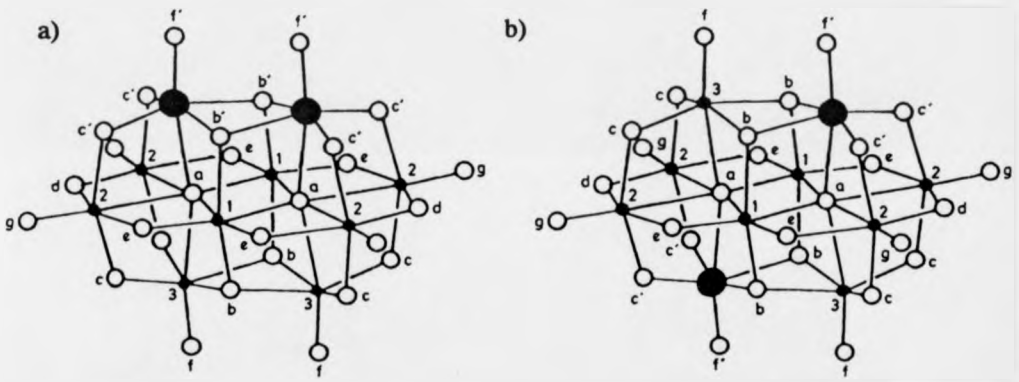

Figure 26. Proposed structures for a) *cis*-$[Mo_2V_8O_{28}]^{4-}$, and b) *trans*-$[Mo_2V_8O_{28}]^{4-}$. (● = V, ● = Mo, O = O)

Further confirmation of these structures was supplied by ^{17}O NMR spectroscopy. A portion of a typical spectrum is shown in Figure 27. Examination of the ^{17}O chemical shifts of the substituted decavanadate species in Table 12 revealed that the oxygens attached to the vanadium atoms were higher than those in decavanadate counter balancing the decrease around the molybdenum atoms. The authors therefore proposed that the sum of the oxygen chemical shifts may be a useful qualitative guide to structure.

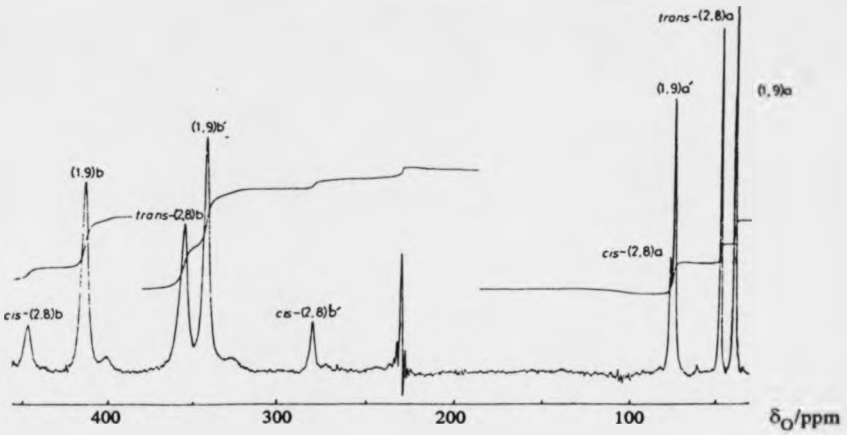

Figure 27. A portion of a typical 54.2 MHz oxygen-17 NMR spectrum of a solution *ca.* 1 mol dm^{-3} in V, 0.4 mol dm^{-3} in Mo, pH 2.0, 99°C, showing $[HMoV_9O_{28}]^{4-}$, *trans*-$[Mo_2V_8O_{28}]^{4-}$, and *cis*-$[Mo_2V_8O_{28}]^{4-}$ as the dominant species in decreasing order of abundance.

Distributions of vanadium as a function of pH for Mo:V ratios (a) 0.05:1 and (b) 0.25:1 were calculated from the combined NMR and EMF data using the computer program SOLGASWATER [153]. These are shown in Figure 28. Howarth *et al.* [25] assigned the ^{95}Mo NMR spectra by correlation with the ^{51}V NMR spectra as follows: $[MoV_9O_{28}]^{5-}$, 115.5; $[HMoV_9O_{28}]^{4-}$, 101; *trans*-$[Mo_2V_8O_{28}]^{4-}$, 92.4 and *cis*-$[Mo_2V_8O_{28}]^{4-}$, 110 ppm.

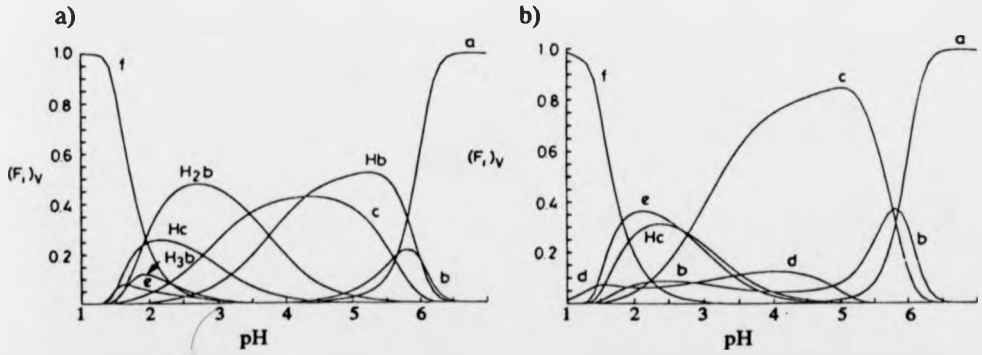

Figure 28. Diagrams showing the distribution of vanadium as a function of pH. The quantity $(F_i)_V$ is defined as the ratio between the vanadium in a species to the total vanadium. For clarity, $(F_i)_V$ <0.05 have been omitted. Mo:V ratio is 0.5:1 **a)** and 0.25:1 **b)** Species:- a = $[H_2VO_4]^-$ + $[V_4O_{12}]^{4-}$ + $[V_5O_{15}]^{5-}$; b = $[V_{10}O_{28}]^{6-}$; Hb = $[HV_{10}O_{28}]^{5-}$; c = $[MoV_9O_{28}]^{5-}$; Hc = $[HMoV_9O_{28}]^{4-}$; d = species with higher Mo:V ratios; e = *cis*- and *trans*-$[Mo_2V_8O_{28}]^{4-}$; f = $[VO_2]^+$.

1.10.2. High Mo:V Ratio Solutions

1.10.2.1. Hexametallates

The *cis*-(4,2) species, dominated the ^{51}V NMR spectrum and exhibited a single pK_a=3.8 (297K). Its shift was δ_V -498.0 and -512.5 ppm upon protonation [26]. Typical ^{51}V and ^{17}O NMR spectra are shown in Figures 29 and 30 respectively. The ^{17}O NMR assignments for the unprotonated *cis*-(4,2) anion are shown in Table 14. From the broadenings due to couplings with vanadium they deduced a *cis*-geometry. Even though the protonated species was less dominant and was partially replaced by (5,1) they were still able to demonstrate that protonation took place at the oxygen bridging the two vanadium atoms, as anticipated.

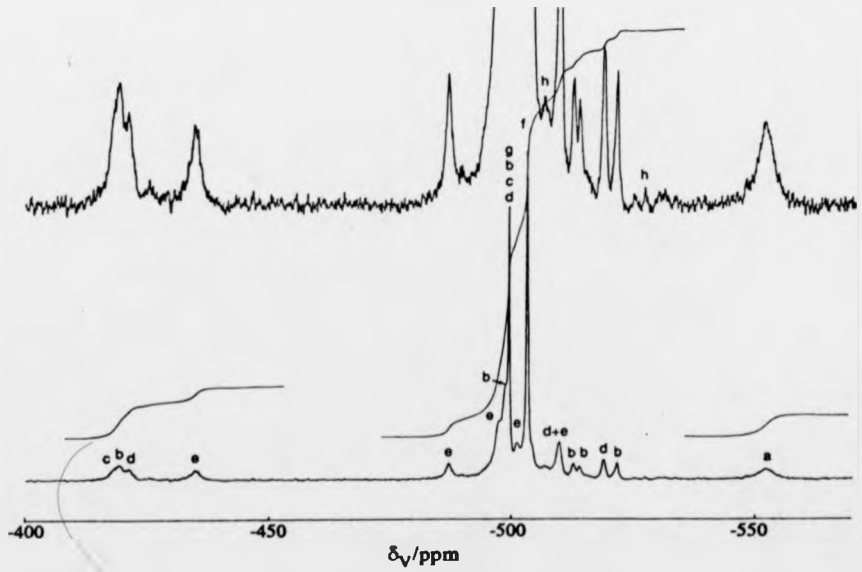

Figure 29. A typical 105.2 MHz vanadium-51 NMR spectrum plus x8 vertical expansion: 15.1 mmol dm^{-3} Mo, 10.0 mmol dm^{-3} V, 372K, room temperature pH 2.95. Species: a, (0,1)+(0,4); b, (1,9); c, *cis*-(2,8); d, *trans*-(2,8); e, (4,5); f, *cis*-(4,2); g, (5,1); h, probable (9,4) Keggin species.

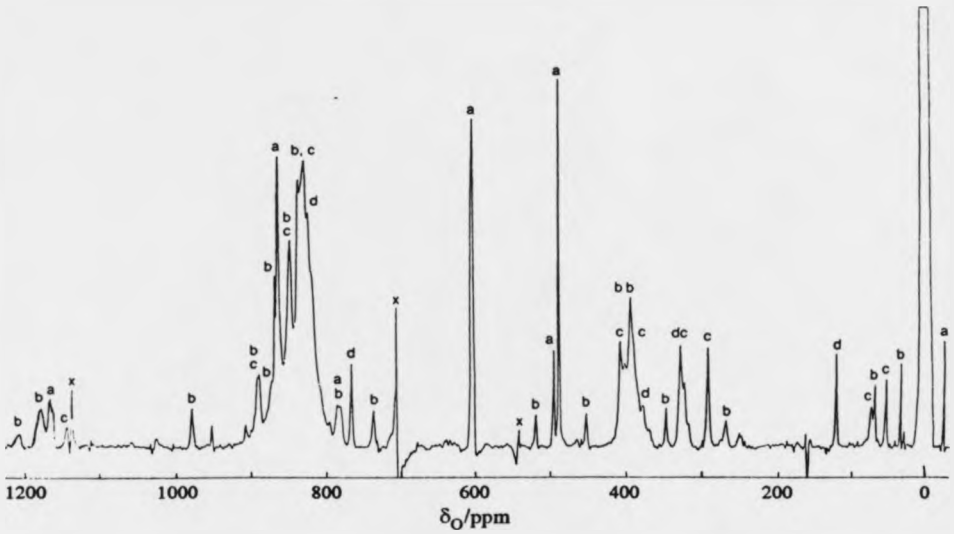

Figure 30. A typical 54.2 MHz oxygen-17 NMR spectrum, 294K, pH 4.8, obtained after a full equilibration of a saturated solution of species α-(6,2) in water enriched to 5 atom % in ^{17}O. Species: a, *cis*-(4,2); b (4,5); c, (1,7); d, (0,7); x, known spectrometer artefact.

The (5,1) species, gave a narrow ^{51}V NMR resonance at $\delta_V = -506.4$ ppm. This shift was independent of pH and the peak intensity reached a maximum between pH 1.5 and 4.0. The oxygen chemical shifts are given in Table 14. No (3,3) species were observed.

Table 14. Oxygen chemical shifts of the known hexametallate molybdovanadates at 294K/ppm

peak	$[MoV_5O_{19}]^{3-}$	$[Mo_2V_4O_{19}]^{4-}$
	δ_O	δ_O
a	-28[a]	-24[a]
b	518	486
c	520	496
d	640	603
e	908	603
f	908	861
g	1220	861
h	n.a.	787
i	n.a.	1166

[a] referenced to solvent water $\delta_O = 0$

1.10.2.2. $[Mo_4V_5O_{27}]^{5-}$ and $[HMo_4V_5O_{27}]^{4-}$

Interestingly, although a (3,7) species based on the decavanadate framework was not observed, a (4,5) species was, except that one of the corner vanadium atoms was removed. Despite its clear similarities and overlap with (1,9) and (2,8) Howarth *et al.* [26] managed to discern five ^{51}V NMR resonances of equal area at higher Mo:V ratios. ^{51}V-^{51}V COSY confirmed the assignments: V^1 -440.0, V^2 -491.6, V^3 -501.6, V^4 -504.4 and V^5 -518.6 ppm (labels as per Figure 31). ^{95}Mo NMR yielded four resonances which supplemented the above. By analogy with other similar species a prediction was made for the ^{17}O NMR assignments. The close correlation with the experimental data is shown in Figure 31. On acidification the (4,5) anion protonated once with $pK_a \approx 2.5$. Potentiometric measurements confirmed these findings.

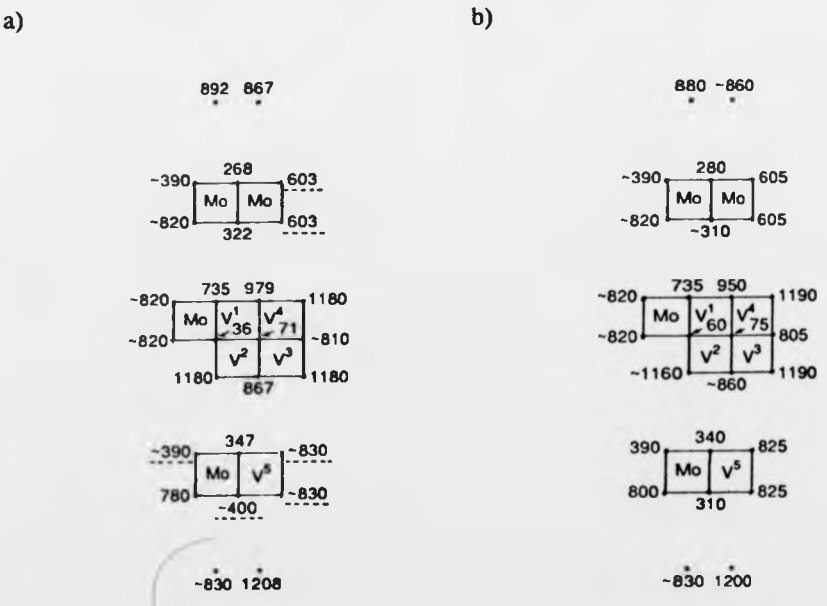

Figure 31. Successive layer diagram structures of species (4,5) with oxygen-17 shifts at 293K assigned as in the text: **a)** experimental data; **b)** shifts predicted by analogy with related species. Dotted underlining indicates an unresolved peak in a crowded region with adequate total intensity.

1.10.2.3. β-$[Mo_7VO_{26}]^{5-}$

A further new species was also characterised as β-(7,1). The structure of this species was based on the isomolybdate β-$[Mo_8O_{26}]^{4-}$ (see above) with one of the central molybdenum atoms replaced by a vanadium atom. It gave a fairly broad ^{51}V NMR resonance at -537.2 ppm independent of pH. With high Mo:V ratios this species dominated the spectrum and consequently Howarth *et al.* [26] were able to assign most of the ^{17}O NMR spectrum except in the very crowded region δ_O 820 to 860 ppm.

1.10.2.4. Other Minor Species

Table 15 summarises the remaining species proposed [26].

Table 15 The proposed vanadium chemical shifts, formulae and structures for the minor species

Formula	δ_V	Proposed Structure
α-$[HMo_6V_2O_{26}]^{5-}$	-500.2	
α-$[HMo_7VO_{26}]^{4-}$	-502.6	
$[HMo_{10}V_2O_{38}]^{5-}$	-526	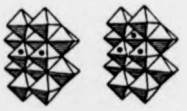
$[Mo_9V_3O_{38}]^{7-}$	-516	
$[HMo_9V_3O_{38}]^{6-}$	-525.8(2)	
	-522.6(1)	
$[HMo_9VO_{32}]^{4-}$	-515	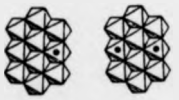
$[HMo_8V_2O_{32}]^{5-}$	-519	
$[Mo_4VO_{17}]^{5-}$	-567	
β-$[H_2Mo_6V_2O_{26}]^{4-}$	-539.3	
$[V(Mo_{10}V_2O_{40})]^{5-}$	-505	
	-525	
	-547.8	
	-548.0	

● = vanadium sites, O = alternative vanadium sites

1.11. The Present Work

A deficiency of the early research of polyoxometallates is that it has largely relied on the isolation of compounds, rather than on the methodical analysis of solutions, over the attainable range of pH. In particular X-ray crystallographic studies have been criticised for this limitation. Whilst X-ray crystallography may yield extremely valuable structural information of crystalline species they may not be representative of the solution species. For example, the crystal structures of only 6 molybdovanadate species have been determined, whereas a recent, comprehensive study in aqueous solution showed the presence of at least 22 stable molybdovanadates, when including the different states of protonation [26]. Moreover, only one of the crystallised species was also a major component of the solution. A second problem is that the species crystallised out of solution may not bear any resemblance to the solution species. An example of this is seen in the present work, ψ-metatungstate in aqueous solution is asymmetric but in the crystalline state it has a plane of symmetry.

In the field of solution chemistry the importance of studying a given system by more than one method has repeatedly been emphasised in the literature [11]. However, it is often difficult to apply two or more methods to a system one is going to investigate. In the present work ^{183}W, ^{51}V, ^{95}Mo, ^{1}H and, where possible, ^{17}O NMR have been employed to characterise isopolytungstate, molybdotungstate and tungstovanadate aqueous solutions. Unlike the isopolymolybdates, the isopolytungstates are inert to exchange on the NMR time-scale and a comprehensive analysis is possible. NMR spectroscopy of solutions has been successfully applied to simple vanadates [51], peroxo- [24] and sulphidovanadates [155], molybdo- [25] and tungstovanadates [143].

Of course other experimental techniques were considered such as infrared and Raman spectroscopy, X-ray crystallography and potentiometry. Whilst infrared and

Raman spectroscopy are useful for "finger printing" purposes of isolated species, little structural information can be gained from multi-component solutions. X-ray crystallographic methods have been successful in determining many structures of isopolyoxometallates, for example, decavanadate [131-135], paratungstates -A [89] and -B [3], and ψ-metatungstate [10]. However, with mixed metal species such as *cis*-$[W_4V_2O_{19}]^{4-}$ [146], disorder in crystal orientations rendered all the metal centres equivalent. A further problem with these multi-component solutions is controlling which species precipitates. Very often it is the species with the highest charge, and many of the interesting species are metastable, for example β-metatungstate transforms into the more stable α-metatungstate [11]. Potentiometry has been successfully coupled with NMR spectroscopy in the study of molybdovanadates [25,26] where it was possible to characterise the labile species that were not detected by NMR spectroscopy. However, with such slow equilibria in tungstate systems potentiometry becomes impracticable and in any case facilities were not available to measure EMF data to the precision necessary.

Many of the results from this present study have already been published [156-158] and copies of these are shown in the Appendix. The brief summary below highlights the species formed and some of their inter-relationships .

In respect of the paratungstates, our isopolytungstate study confirms the conclusions of Maksimovskaya and Burtseva [64], whilst also revealing the protonation of paratungstate-B and ruling out the simultaneous presence of any other major species. As the pH is lowered, paratungstate-B is transformed into a new and previously unsuspected anion with 11W atoms and no symmetry. In addition, 6 anions with either α- or β-Keggin structures can be identified. These vary in the sites and in the extent of their protonation.

Molybdenum is shown to substitute into heptatungstate forming a range of isomers $[Mo_xW_{7-x}O_{24}]^{6-}$ (x=1 to 6) with positional preference for the "ends" and least for

the "central" W atoms. In the same pH range as the heptametallates, paratungstate-B and mono-substituted paratungstate-B form. At lower pH α-metatungstate and mono-substituted α-metatungstate anions dominate the solutions.

As with the molybdovanadates the decavanadate structure dominates the solutions with high vanadium ratios, although only a single substitution occurs. The tungsten replacing one of the "capping" vanadium atoms. As the tungsten ratio is increased a series of hexametallates and Keggin structures are observed. The structures of the anions *fac*-$[W_3V_3O_{19}]^{5-}$, *cis*-$[W_4V_2O_{19}]^{4-}$, $[W_5VO_{19}]^{3-}$ and α-$[H_2W_{11}VO_{40}]^{7-}$ have been confirmed. Firm evidence is presented for species *mer*-$[W_3V_3O_{19}]^{5-}$ and *trans*- $[W_4V_2O_{19}]^{4-}$. Tentative evidence is also presented for the species $[W_8V_2O_{32}]^{6-}$ and more heavily substituted α- and β- metatungstates in the more acidic solutions.

2. THEORY

Since basic NMR theory and standard routine NMR experiments have been extensively covered in the literature [159-166], only aspects with particular relevance to the present work will be discussed. For example, it was necessary in one case to generate a selective pulse to pre-irradiate a tungsten resonance using the DANTE sequence [167]. Again, in a multinuclear NMR study it was interesting to examine the importance of different relaxation mechanisms for each nucleus. Also from spin-lattice relaxation data it was possible to obtain useful structural information in terms of bond lengths and tumbling rates. The derivation of the Henderson-Hasselbalch equation to yield pK_a values from chemical shifts is also summarised [168], along with the above three less standard applications of NMR theory.

2.1. Relaxation

In order for a spin system to return to equilibrium after being perturbed by *e.g.* a radio frequency pulse, there must be an interaction between the spins and the surroundings, or lattice, leading to a loss of excess energy. The rate at which the system returns to equilibrium will depend upon the ability of this interaction to convey energy into or out of the system. The return to equilibrium is not instantaneous but usually [163] occurs with a first-order rate constant, R_1. Since relaxation phenomena are usually studied by time dependence measurements, it is common to use the relaxation time constant, T_1 rather than the relaxation rate constant.

$$R_1 = 1/T_1 \qquad (2.1)$$

Once disturbed from equilibrium, the magnetisation may have components in the xy plane, and these will also relax to their equilibrium value zero. Inevitably, xy magnetisation will decay at least as rapidly as the rate at which spin-lattice relaxation returns the magnetisation to the z-axis. However, the xy magnetisation can also be lost by additional processes which cause components of the xy magnetisation to fan out or dephase, producing a net zero magnetisation in the xy plane. The time constant for the xy plane is given by T_2 and is often referred to as the spin-spin or transverse relaxation time.

Extensive mathematical and quantum mechanical derivations for T_1 and T_2 may be found in the literature [159,160] and therefore will not be discussed here.

2.1.1. T_1 Measurement

The common method for measuring T_1 is by a pulse sequence known as inversion recovery [169].

$$[180°\text{-}\tau\text{-}90°(\text{FID})\text{-}T_d]_n \qquad (2.2)$$

T_d is a delay time substantially longer than the longest T_1 to be measured. It must be included in order for the Boltzmann populations to be re-established between 180° pulses. The accumulated FID is Fourier transformed, and the evolution period τ is varied. Following the 180° pulse, the spin population is inverted. The recovery, therefore, goes from $-M_0$ to M_0, where M_0 is the Boltzmann equilibrium magnetisation, which is succeeded by purely spin-lattice relaxation, normally exponential [160]:

$$M_{z(\tau)} - M_0 = [M_{z(0)} - M_0]\exp(\tau/T_1) \qquad (2.3)$$

where $M_{z(\tau)}$, is the magnetisation left to recover and $M_{z(0)}$, is the initial magnetisation. But, at inversion then $M_{z(0)} = -M_0$, and the above may be rewritten as:

$$M_0 - M_{z(\tau)} = 2M_0[\exp(\tau/T_1)] \qquad (2.4)$$

Unfortunately, in a real experiment several things are not ideal. There are varying amounts of noise which causes the points to scatter. The noise makes it difficult to estimate M_0, and the initial value of magnetisation. However, these errors are small with a good signal noise ratio, and the above equation can be recast in the form of a general exponential decay replacing M, by the peak height S.

$$S_{(\tau)} = S_{(\infty)} - 2S_{(\infty)}[\exp(\tau/T_1)] \qquad (2.5)$$

Where $S_{(\tau)}$, represents the fraction of magnetisation left to recover at time τ, and $S_{(\infty)}$, is the peak height after a time greater than T_1 and contains information about the initial value of magnetisation. Using standard software T_1 may be evaluated. Alternatively, the natural logarithm of the peak height, S, for each peak may be plotted against τ, and thus T_1 is found according to equation (2.6).

$$\ln [S_{(\infty)} - S_{(\tau)}] = \ln 2 + \ln S_{(\infty)} - \tau/T_1 \qquad (2.6)$$

At short recovery times τ, the signal will appear negative, since in effect a 270° pulse has been applied. At long times, full recovery is obtained so that $S_0 = S_{(\infty)}$. At an intermediate stage the signal will be zero, this time, τ_{null}, can be used as an estimate of T_1 since :

$$T_1 = \tau_{null}/\ln 2 \qquad (2.7)$$

2.1.2. T_2 Measurement

T_2 is related quite simply to the linewidth [163] but this measurement is subject to inhomogeneity of the magnetic field:

$$T_2 = 1/\pi(\text{linewidth}) \qquad (2.8)$$

Alternatively a Hahn [170,171] echo sequence may be employed. An initial 90° pulse turns M_0 into the y direction in the system of rotating axes. The magnetic vectors from different portions of the sample then begin to fan out and the signal decays. A $180°_y$ pulse is then applied after time τ, which has the effect of rotating all the magnetisation vectors by 180° about y, *i.e.* reflecting them in the y direction [172]. Refocusing occurs at time 2τ. The amplitudes of successive echoes decay exponentially, due to relaxation, and the true value of T_2 can be found from the envelope of echoes.

$$90° [-\tau\text{-}180°\text{-}\tau\text{- echo -}]_n \qquad (2.9)$$

2.1.3. T_1 Minimum

In a mobile solution the molecules experience random molecular tumbling and the average time for a molecule to progress through one radian is given by τ_c, typically 10ps. The dependence of T_1 on the correlation time is given by [160]:

$$T_1^{-1} = \gamma^2 [B^0_{xl}]^2 \cdot 2\tau_c / (1 + \omega^2\tau_c^2) \qquad (2.10)$$

where γ is the magnetogyric ratio, B^0_{xl} is the x component of a local fluctuating magnetic field and ω is the spectrometer operating frequency expressed in rad s^{-1}. In the extreme narrowing condition when $\omega^2\tau_c^2 \ll 1$ the equation simplifies to:

$$T_1^{-1} = 2\gamma^2 [B^0_{xl}]^2 \tau_c \qquad (2.11)$$

This implies that the spin-lattice relaxation rate increases as τ_c increases, *i.e.* as mobility decreases. This occurs, for example, for molecular tumbling when the temperature is lowered. However, if τ_c increases sufficiently so that it becomes of the order of ω^{-1}, a new regime is entered. The full equation (2.10) predicts a maximum in T_1^{-1} (a minimum in T_1) as a function of τ_c. The T_1 minimum occurs when $\tau_c = \omega^{-1}$, *i.e.* between the two regimes.

2.2. Relaxation Mechanisms

There are several physical mechanisms which permit spin-lattice relaxation, such as, a magnetic interaction fluctuating at the resonance frequency. Contributions from these relaxation mechanisms then combine to yield the spin-lattice relaxation. Only brief interpretations will be given here; more rigorous treatments are in the literature [159,160].

2.2.1. Dipole-Dipole Interactions with other Nuclei

The nucleus experiences a fluctuating field due to the motion of neighbouring magnetic dipoles (unpaired electrons or other nuclei). The field due to a dipole of strength μ at a distance r and subtending an angle θ with respect to the $\mathbf{B}_0$ direction is given by:

$$\mathbf{B}_{DD} = \pm(\mu_0/4\pi)\mu\,(3\cos^2\theta - 1)/r^3 \qquad (2.12)$$

The sign of this field depends on the orientation of the dipole (with or against the magnetic field). Unpaired electrons have much stronger magnetic dipoles than nuclei, and samples with traces of paramagnetic transition metal compounds or free radicals or even dissolved paramagnetic oxygen gas can affect the spin-lattice relaxation times. The remaining dipolar fields originate from other nuclear spins in the immediate environment and can therefore provide information about molecular

structure or molecular motion. This mechanism is particularly relevant for spin I=½ nuclei such as ^{1}H. However, the ^{183}W (I=½) nucleus is mainly relaxed by chemical shift anisotropy (see below) and ^{51}V is quadrupolar (I=$^{7}/_{2}$) and therefore dipole-dipole relaxation contributes very little to their relaxation.

Thus, for ^{1}H nuclei, it is possible, using the appropriate equations to gain useful structural information. For example, if we assume that the internal protons in the Keggin structures principally relax by mutual dipole-dipole interactions and that it is possible to obtain the T_1 data either side of the T_1 minimum by varying the temperature, then because the rate of dipole-dipole relaxation between the two protons is given by: [173]

$$1/T_{1HH} = 3\mu_0^2\gamma_H^4(h/2\pi)^2/160\pi^2r_{HH}^6 \{(\tau_c/1+\omega^2\tau_c^2) + (4\tau_c/1+4\omega^2\tau_c^2)\} \quad (2.13)$$

where γ_H is the magnetogyric ratio of ^{1}H, then r_{HH}, the distance between the interacting protons can be calculated. For a T_1 minimum the expression in the brackets must be maximised and since ω is known, τ_c may be varied iteratively to achieve this. Furthermore, if the τ_c data exhibit Arrhenius behaviour [162] versus temperature, then the assumption made above is correct, and the activation energy may also be calculated:

$$\tau_c = Ae^{-B/RT} \quad (2.14)$$

where R is the universal gas constant, T, the temperature, A is a constant and B is the activation enthalpy. Also the above equation for T_1 may be developed further to calculate T_2 [173], provided that other T_2 mechanisms are of minimal importance.

$$1/T_{2HH} = 3\mu_0^2\gamma_H^4(h/2\pi)^2/320\pi^2r_{HH}^6 \{(5\tau_c/1+\omega^2\tau_c^2) +(2\tau_c/1+4\omega^2\tau_c^2)+ 3\tau_c\} \quad (2.15)$$

2.2.2. Chemical Shift Anisotropy

A second type of shielding arises because the chemical shielding of the nucleus depends on the orientation of the molecule with respect to $\mathbf{B}_0$ field direction. Shielding can be depicted as a weak secondary magnetic field generated by the electrons surrounding the nucleus precessing in the applied field $\mathbf{B}_0$. Hence the field is commensurate to $\mathbf{B}_0$ and fluctuates as the molecule tumbles. The resulting expressions for T_1 and T_2 (SA) are analogous to those for dipolar relaxation, except that the spin system is only two-level. In the present treatment we discount minor complications that arise from the possibility of asymmetry in the screening tensor. In the simple case of a symmetric tensor ($\sigma_{zz} \neq \sigma_{xx} = \sigma_{yy}$) [159].

$$1/T_1 = (1/15)\, \gamma^2 \mathbf{B}_0^2\, (\Delta\sigma)^2\, [2\tau_c/(1+\omega^2\tau_c^2)] \qquad (2.16)$$

and

$$1/T_2 = (1/90)\, \gamma^2 \mathbf{B}_0^2\, (\Delta\sigma)^2\, \{[6\tau_c/(1+\omega^2\tau_c^2)]+8\tau_c\} \qquad (2.17)$$

For protons, which have small chemical shifts, this relaxation mechanism may be ignored. However, it is significant with for example, ^{183}W, for this has a large chemical shift range, and hence a large $\Delta\sigma$. However, as before, there is little relevance to ^{51}V because this nucleus is quadrupolar ($I=7/2$) . Since the relaxation depends on the square of the appropriate field at the nucleus, the rate of spin-lattice relaxation by this mechanism increases as the square of the applied field strength $\mathbf{B}_0$ [159]. So this mechanism can dominate at high magnetic fields.

2.2.3. Spin-Rotation Interaction

As the molecule tumbles, the electrons surrounding the nuclei generate small electric currents which induce a small magnetic field at the nucleus. Although the charges of electrons and nuclei balance, the resulting fields do not quite cancel

because in general the "centre of gravity" of the electron charge does not coincide with that of the corresponding nucleus. This leaves a net field at the nucleus which fluctuates because the reorientational motion is not uniform, but proceeds by a series of random jumps. As the tumbling motion escalates the efficiency of the mechanism increases. Therefore, as distinct from the dipolar mechanism, spin-rotational relaxation is more effective for small molecules in low-viscosity solutions at high temperatures. This opposite temperature tendency may be used to distinguish these mechanisms. This mechanism is only relevant to very rapidly rotating molecules *e.g.* as found in the gas phase and consequently bears little relevance to heavy metal complexes in solution.

2.2.4. Quadrupolar Relaxation

All nuclei with $I > ½$ are nonspherical, according to physical theory, and therefore must possess nuclear electric quadrupole moments. The distribution of nuclear charge is of the form of an ellipsoid, and this can interact strongly with an electrostatic field gradient. Most chemical bonds generate such a gradient of the electrostatic field at the nucleus and the interaction fluctuates as the molecule reorients in solution. Spin-spin relaxation thus tends to be rapid, giving broad lines and making these nuclei unsuitable for high resolution work, since any small chemical shift difference is engulfed by the broad lines. However, heating the sample can reduce the linewidths, because T_2^{-1} decreases as the tumbling rate τ_c^{-1} increases with the increasing mobility at higher temperatures. T_1 and T_2 may derived from the standard equation [159]:

$$1/T_1 = 1/T_2 = (1/40)\,[(2I+3)/(I^2(2I-1))]\,\{(1+\eta^2/3)[(e^2Qq)/(h/2\pi)]^2\tau_c\} \quad (2.18)$$

where I and eQ are respectively the spin and quadrupole moment, eq is the electric field gradient, and η is the asymmetry parameter. This is the principal relaxation

mechanism for the quadrupolar nuclei ^{51}V, ^{17}O and ^{95}Mo. But since neither ^{1}H nor ^{183}W possesses a quadrupole moment they cannot relax by this mechanism.

2.3. DANTE Sequence

There are situations in which we wish to generate a selective pulse at a frequency for which a decoupler is not available *e.g.* to pre-irradiate a tungsten resonance. This can be achieved using the DANTE (Delays Alternating with NuTation Excitation) [167]. DANTE exploits a phenomenon which is, in most cases, a nuisance. If the pulse is long, there will be considerable precession during the pulse unless the pulse is exactly on resonance. The sequence consists of a train of short pulses separated by a delay, ε, of about a millisecond, followed by a non-selective pulse and acquisition. See below. If the pulses are on resonance, their effect will be additive; n pulses, each with a tip-angle of ϕ, are equivalent to one pulse (usually a transmitter π pulse length selectively inverting the magnetisation) with a tip-angle of $n\phi$, assuming that there is no relaxation between pulses. If the pulses are applied off-resonance, some precession will occur during ε, the net effect will in general cancel, and leave the magnetisation at, or at least near, equilibrium. In general then, only a small region of the spectrum is excited by the DANTE sequence. The sequence is most effective when there are at least 30 pulses.

Equilibrium delay -- (ϕ - ε)n -- Non selective pulse -- Acquire

In our tungsten case typically, the equilibrium delay = 0.5s, for selective inversion $n\phi = \pi$ (π =86μs, n = 60, ϕ = 1.5 μs), ε = 0.3 ms, determined by the 3000 Hz sweepwidth required for excitation (ε = 1/ sweepwidth).

2.4. Measurement of pK_a Values

There are many problems that arise which defeat the measurement of precise and accurate pK_a values. Sometimes equilibrations are slow and it can be very difficult to know if the true equilibrium condition has been attained in the experiment. This is particularly true of tungstate systems. It is also necessary to maintain a constant ionic strength and temperature since both these parameters affect the pK_a values obtained. In the case of the tungstovanadates the ionic strength is controlled by swamping the solutions with 0.6 M NaCl and maintaining a constant sodium ion concentration. Unfortunately in the isopolytungstate case, the very low sensitivity of tungsten NMR spectroscopy precluded any control of ionic strength.

When a species protonates, its ^{17}O, ^{51}V and ^{183}W NMR chemical shifts exhibit pH dependences. The observed chemical shift δ_O, may be defined as an average of the limiting shifts for the unprotonated salt at high pH δ_H, and the fully protonated acid species at low pH δ_L, and weighted according to the concentration of each species as in equation (2.19).

$$\delta_O = (\delta_L[\text{acid}] + \delta_H[\text{salt}])/([\text{acid}] + [\text{salt}]) \qquad (2.19)$$

With simple mono-protonation steps and sufficient data either side of the inflection it is possible to fit a Henderson-Hasselbalch type equation (2.20) using a least squares fit program and hence calculate a pK_a value for the species [168].

$$pH = pK_a + \log([\text{salt}]/[\text{acid}]) \qquad (2.20)$$

Rearrangement of (2.19), subtraction of $\delta_L([\text{acid}] + [\text{salt}])$ from both sides of the equation and substitution into (2.20) yields:

$$pH = pK_a + \log\{[(\delta_H - \delta_L)/(\delta_O - \delta_L)]-1\} \qquad (2.21)$$

Rearrangement of (2.21) gives:

$$\delta_O = \{(\delta_H - \delta_L)/(\text{EXP}[\ln 10\ (\text{pH}-\text{p}K_a)]+1)\}+\delta_L \qquad (2.22)$$

3. EXPERIMENTAL

3.1. Spectra

^{183}W, ^{51}V, ^{17}O, ^{7}Li and ^{1}H NMR spectra were obtained on a Bruker WH400 spectrometer equipped with a 10 mm multinuclear VSP and a 5 mm QNP probe, and operated at 16.65, 105.2, 54.2, 155.49 and 400.13 MHz respectively. However, towards the end of the project a Bruker ACP 400 spectrometer was used. Some ^{183}W NMR spectra were also run on a Varian VXR 600S at 24.996 MHz and I would like to thank Drs. I. Sadler and D. Reed of the University of Edinburgh for performing these. The ^{1}H 250.13 MHz spectra were obtained on a Bruker ACF 250 spectrometer equipped with a 5 mm VSP probe.

^{183}W NMR spectra were typically recorded using 2 mol dm^{-3} solutions at 20°C with a 15 μs (30°) pulse length, 20 kHz sweepwidth, 64K data points and 30,000 transients. A 2 mol dm^{-3} $Na_2[WO_4]$ capillary was the reference. The spectra were then processed by zeroing the first 40 data points to remove the spurious ringing signal and using a Gaussian window function with -1 Hz line broadening. The signal to noise was in most cases adequate for reliable integration. The error in measurement of these integrals was typically ±20%. Also by adding $Li[Cl]\cdot H_2O$ (BDH) as appropriate, the dependence of the ^{183}W shifts upon $[Li]^+$ was recorded. Some tungsten T_1 measurements were also made by the inversion recovery method [169] where the signal to noise permitted.

Complementary ^{95}Mo NMR spectra were performed on the molybdotungstate solutions at 89°C, 13 kHz sweepwidth, 4K data points and 2000 transients.

1D ^{51}V NMR spectra were typically recorded with a 12 μs (35°) pulse length, 28 kHz sweepwidth, 8K data points and 2,000 transients at both 20° and 89°C and referenced to a $VOCl_3$ capillary at 20°C. An exponential window function was then applied with 10 Hz line broadening. 2D ^{51}V-^{51}V COSY 90 [174] NMR spectra

were run as 256 x 1K (2048 scans each) at 89°C to minimise linewidths, and were processed with both sinebell windows, for maximum resolution, and also Gaussian windows with typically -200 Hz line broadening when it was necessary to enhance broader resonances.

^{17}O NMR spectra were obtained on the same solutions at both 20° and 89°C with typically 20,000 transients and referenced to internal $H_2{}^{17}O$. They were run on 4K data points, over a 83 kHz sweepwidth and repeated with altered offsets to identify spurious signals.

^{7}Li NMR spectra were recorded using the same isopolytungstate solutions with 4 mol dm^{-3} in LiCl at 20°C, with 2.5 kHz sweepwidth, 32K data points, 32 transients and referenced to an aqueous 2 mol dm^{-3} $LiClO_4$ capillary.

The ^{1}H NMR spectra were run on 32K data points with 3 kHz sweepwidth and referenced to a sodium 3-(trimethylsilyl)propionate (TSP) capillary. T_1 and T_2 measurements were made by the inversion-recovery method [169] and a Hahn echo sequence [172] respectively, followed by least-squares fitting.

3.2 Chemicals

Stock tungsten solutions were prepared from WO_3 (BDH) and $Li[OH]\cdot H_2O$ (Aldrich) in *ca.* 50% $^{2}H_2O$ and adjusted to one of two starting pH values, either 7.5 or 9 with dilute HCl, after filtration. Their volume was then reduced to requirements. 3 ml aliquots were then further acidified either directly to pH 3 or stepwise to cover pH 9 to 1 range. The appropriate conditions and the species obtained from these solutions are described in Chapter 4. An M84 meter (Copenhagen) was used for measuring pH values. It was calibrated at room temperature using pH 4 and pH 7 buffers. Solutions were then left for at least one day, to approach equilibrium, and their pH was recorded just after the spectra were obtained. Values of pK_a were obtained by linear regression analysis, using the

simultaneous fitting of several shifts as far as possible [168]. The very low sensitivity of tungsten NMR precluded any control of ionic strength. Solutions were generally 2 mol dm^{-3} in W. ^{17}O enrichment of two tungstate solutions at pH 6.5 to *ca.* 5% was performed by evaporation, followed by redissolution in $H_2{}^{17}O$ with added ^2H_2O. The first sample was acidified stepwise to pH *c.a.* 0.9 and a spectrum was recorded at each interval at 20 and 89°C. The second was acidified directly to pH 3 in order to observe the oxygen resonances of the metastable β-metatungstate at 20 and 89°C. A similar evaporation technique, using no isotopic enrichment initially, was used to prepare Keggin species with trapped protons, in ^2H_2O solution. The samples were degassed with nitrogen and it was also necessary to prepare these Keggin samples in plastic vessels rather than glass because it was suspected that some iron salts were leaching into the solution from the glass.

A series of molybdotungstate solutions were prepared from WO_3 (BDH), MoO_3 (AnalaR) and $Li[OH]\cdot H_2O$ (Aldrich) in the ratios (W:Mo) 11:1, 6:1, 5:2, 4:3, 1:1, 3:4, 2:5, 1:6 with *ca.* 10% ^2H_2O these were acidified to pH 7 with dilute HCl, after filtration. Their volume was reduced so that the total metal concentration was 2M and as above any control of the ionic strength had to rely upon self-buffering. 3 ml aliquots were then further acidified directly to cover the pH range pH 7 to 3. The more detailed investigation of the mixed heptametallate species was performed independently at pH 5 and 6 over the entire range of metal ratios. pH measurements were made as above. As the isopolytungstate species, unlike the isopolymolybdates, are known to take several hours to interconvert, all measurements were made on solutions that had had at least a day to reach equilibrium. Further checks were made after longer periods; these showed no further spectral or pH changes.

Attempts were also made to measure the rate of Mo substitution using both ^{183}W and ^{17}O NMR spectroscopy as 1 ml of 2M molybdate solution is added to 2 ml of 2M tungstate solution at pH 7.

The tungstovanadate solutions were prepared from $Na_2WO_4 \cdot 2H_2O$ (MB) and $NaVO_3$ (BDH) in the (V-W) ratios 20:80, 50:50, 80:20, 400:100, 250:250 and 100:400 mmol dm^{-3} in 0.6 mol dm^{-3} Na[Cl] (Fisons) medium and *ca.* 10% ^2H_2O. Using the same sample preparation procedure as with the tungstate solutions, 3 ml aliquots were then further acidified to cover the pH 7-1.5 range. Due to overlap at room temperature only a few pK_a values of resolved resonances could be obtained using regression analysis. It was therefore, necessary to minimise linewidths by raising the temperature to gain the other pK_a values. pH measurements were also made at these elevated temperatures. A 250:250 mmol dm^{-3} (W:V) ^{17}O enriched *ca.* 5% was prepared at pH 6.5 by evaporation and redissolved in $H_2{}^{17}O$ with added ^2H_2O. The sample was then acidified stepwise to pH 3 and a spectrum was recorded at each interval. A 1250:250 mmol dm^{-3} (W:V) ^{17}O enriched *ca.* 5% was also prepared at pH 2.75.

Two tungstovanadate solutions 1250:250 mmol dm^{-3} (W:V) were acidified to pH 2.65, one was immediately raised to 60°C for 20 min., whilst the other was not heated. The formation kinetics were then followed using ^{51}V NMR spectroscopy over a period of three months.

4. ISOPOLYTUNGSTATES

4.1. Isopolytungstate Results.

Figure 32 shows the tungsten chemical shifts observed at various pH values as aqueous $[WO_4]^{2-}$ is acidified. These shifts are found to depend quite strongly and linearly upon $[Li]^+$. The shift values for the component species, extrapolated where necessary, are reported in Table 16 along with their lithium dependence, where available, and their averaged relative integrals.

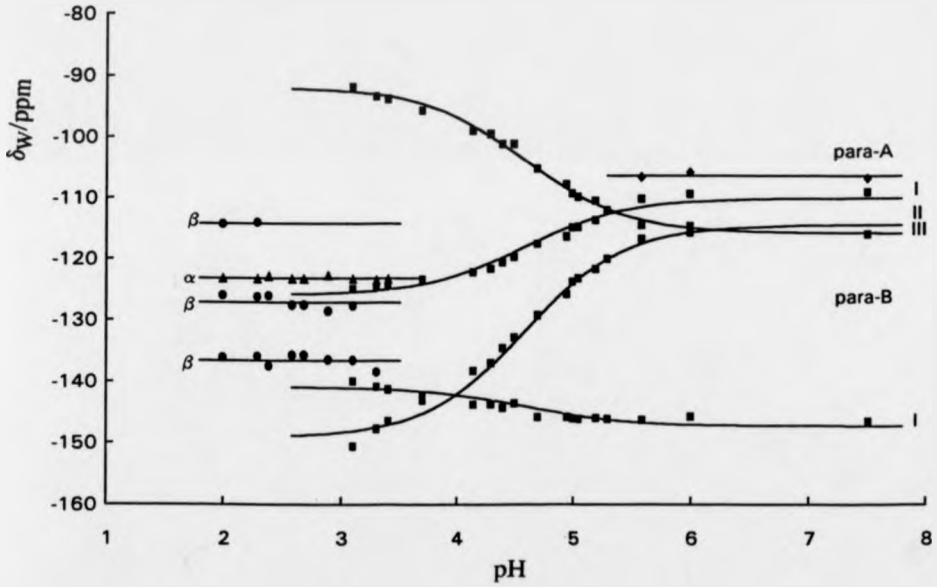

Figure 32. Tungsten chemical shifts *vs.* pH of species obtained by direct protonation of $[WO_4]^{2-}$ at 294K.

Table 16. Tungsten chemical shifts and relative integrals of the more stable species.

$[WO_4]^{2-}$	$[W_7O_{24}]^{6-}$	$[H_2W_{12}O_{42}]^{10-}$	$[H_3W_{12}O_{42}]^{9-}$
δ_W	δ_W	δ_W	δ_W
-9.5[a] (1W)[b] [-2.4][c]	268 (1.0W) [-0.42]	-109 (1.6W) [-0.92]	-125 (2W)
	-106 (4.2W) [-2.1]	-114 (2.2W) [-1.4]	-151 (2W)
	-189 (2.1W) [-1.8]	-116 (4.2W) [-0.96]	-91 (4W)
		-147 (4.0W) [-1.8]	-140 (4W)

$[H_7W_{11}O_{40}]^{7-}$	$[H_8W_{11}O_{40}]^{6-}$	α-$[HW_{12}O_{40}]^{7-}$	α-$[H_2W_{12}O_{40}]^{6-}$
δ_W	δ_W	δ_W	δ_W
-42 (0.9W)	-36[d]	-144	-123 [-0.83]
-104 (1W)	-85		
-120 (0.9W)	-114		
-120 (0.8W)	-126		
-127 (1W)	-118		
-137 (1W)	-135		
-140 (0.8W)	-148		
-164 (0.7W)	-152		
-170 (1W)	-166		
-178 (1W)	-180		
-200 (0.9W)	-209		

β-$[H_2W_{12}O_{40}]^{6-}$	$[W_{10}O_{32}]^{4-}$[e]
δ_W	δ_W
-112 (3W)	-27.6 (8.4W)
-127 (6.6W)	-172.3 (1.86W)
-136 (3.6W)	

[a] Tungsten chemical shift in ppm from external 2 mol dm^{-3} aqueous $Na_2[WO_4]$ at 293K. [b] Measured relative tungsten integral. [c] Shift change per mole dm^{-3} added $[Li]^+$. [e] Tetra n-butyl ammonium salt, in CD_3CN.

Figure 33 demonstrates the linearity of the Li^+ dependence. The resonances in Figure 32 are labelled in accord with the discussion below. The proportions of

paratungstate-A (see below for assignment) are maximal at pH≈ 6, at low concentration, at low ionic strength, and at high temperature. A coupling of 18.5 Hz is observed in paratungstate-B between tungstens II and IV. This is shown in Figure 34. The relative heights of the resonances show that tungsten II couples to either of two tungstens IV, at the naturally abundant isotope ratio $^{183}W/^{184}W$ = 0.168. The pH-dependent resonances in Figure 32 all fit to a pK_a of 4.59±0.03; the figure shows the fitted curves derived from a least squares fit to equation (2.22) (see Chapter 2, section 2.4). The resonances of monotungstate and of paratungstate-A are independent of pH and are shown in Figure 35.

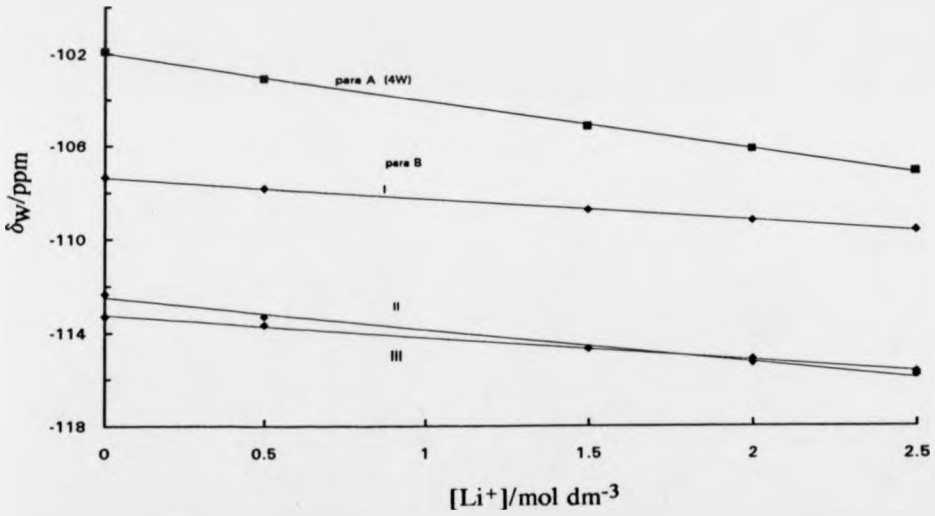

Figure 33. Typical dependence of tungsten chemical shifts upon the concentration of added Li^+. Upper line, paratungstate-A, 4W resonance; and lower three lines, paratungstate-B, resonance I, II and III.

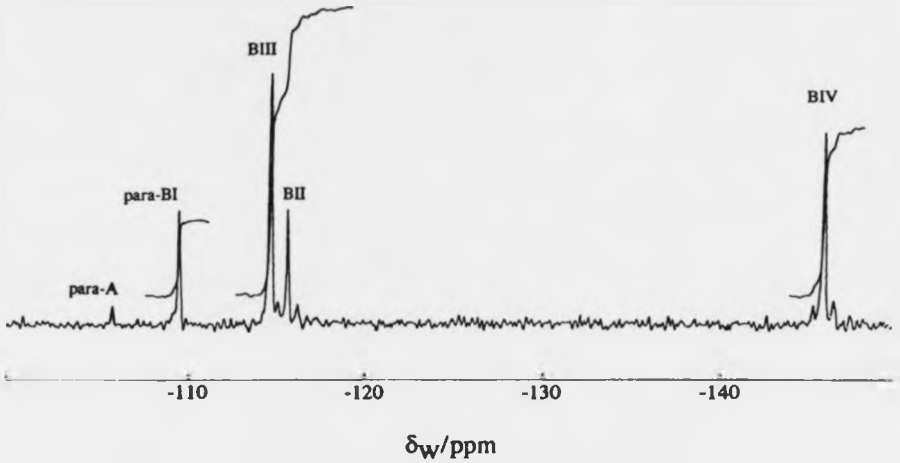

Figure 34. Tungsten-183 NMR spectrum of slightly acidified paratungstate-B, pH 6.0, 293K. Labels as in Figure 32.

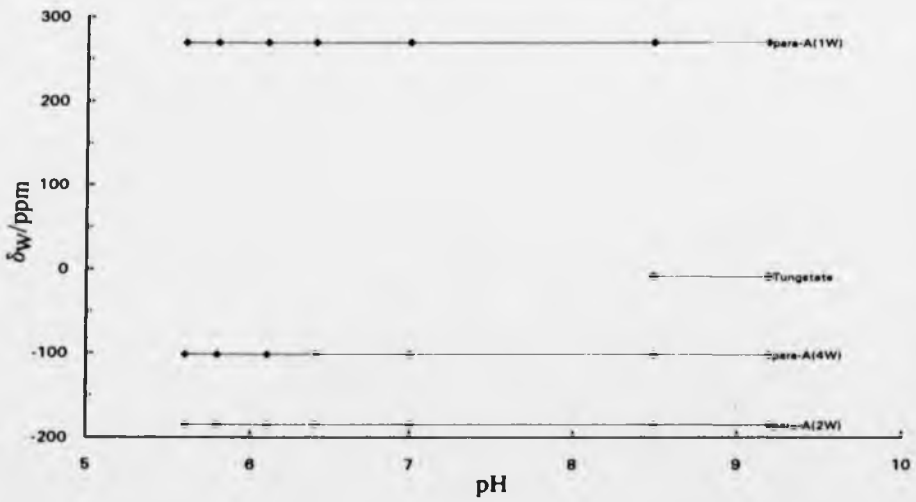

Figure 35. Tungsten chemical shifts of paratungstate-A $[W_7O_{24}]^{6-}$ are independent of pH.

The ^{183}W linewidths of paratungstate-B increase with its extent of protonation. This increase is particularly marked at lower temperatures, and also when the solvent is predominantly $^{2}H_2O$ rather than $^{1}H_2O$ (See Figure 36). The effect of deuteriation is to increase all the linewidths of paratungstate-B by a factor of *ca.* 2.5. Some representative linewidths are listed in Table 17. The added linewidths correlate approximately but not exactly with the protonation shift of the resonance in question.

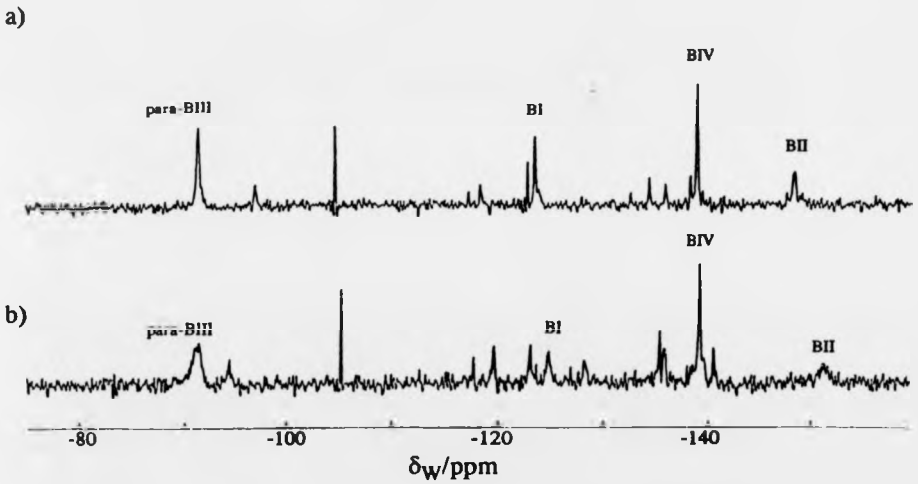

Figure 36. Tungsten-183 NMR spectrum of paratungstate-B at 283K illustrates the effect of deuteriation on the tungsten linewidths **a)** pH 3 solvent $^{1}H_2O$; **b)** pH 2.8 solvent $^{2}H_2O$.

Table 17. Linewidth variations in acidified paratungstate-B

Peak label	^2H_2O, 283K pH=2.8[a]	^1H_2O, 283K pH=3.1	^1H_2O, 283K pH=4.2[b]	^1H_2O, 268K pH=3.1	$^1H/^2H$ pH≈3
I	7.6[c]	3.4	3.0	6.0	2.8[d]
II	15.2	7.2	3.9	16.2	2.3
III	16.2	6.8	3.2	11.5	2.6
IV	5.2	3.0	2.3	4.6	2.8

[a] Almost fully protonated (*i.e.* H_3). [b] Just over half-protonated (*i.e.* $H_{2.6}$). [c] Width at half height in Hz, after removal of broadening due to window function. [d] Natural linewidth = 1Hz, as observed in the unacidified anion (*i.e.* H_2).

Table 17 also reports that the linewidths approximately double, assuming a natural linewidth of 1 Hz, when the temperature is lowered by 15K. Assuming Arrhenius behaviour and then using Arrhenius equation [162] in the form below (4.1) yields an energy of activation of *ca.* 30 kJ mol^{-1}.

$$\ln (k_1/k_2) = \Delta E (1/T_2 - 1/T_1)/R \qquad (4.1)$$

The ^{17}O resonances corresponding to the above species are listed in Table 18. Some of the integrals in this table are the combined contributions of overlapping peaks. It was convenient to separate the resonance sets for each species by the device of heating a pH 6 solution to 89°C for an hour, so as to maximise its proportion of paratungstate-A, and then to cool it to room temperature before obtaining the oxygen spectrum. Appropriate subtraction of this spectrum from that of the equilibrium mixture at the same temperature yielded integrable spectra for each species separately. The resulting ^{17}O NMR subtraction spectra are shown in Figure 37. The half-life for return to equilibrium under these conditions was *ca.* 12 hours. The oxygen NMR data for paratungstate-B were insufficient for the reliable use of curve-fitting. However, a plot of all the ^{17}O NMR shifts is shown in Figure 38. Also, the approximate shift changes between pH 7.0 (no added protons) and pH 4.5

(just over half protonated) are indicated in brackets in Table 18. The only oxygens to show a decrease in shift upon protonation of the anion are O_g and, to a lesser extent, O_e.

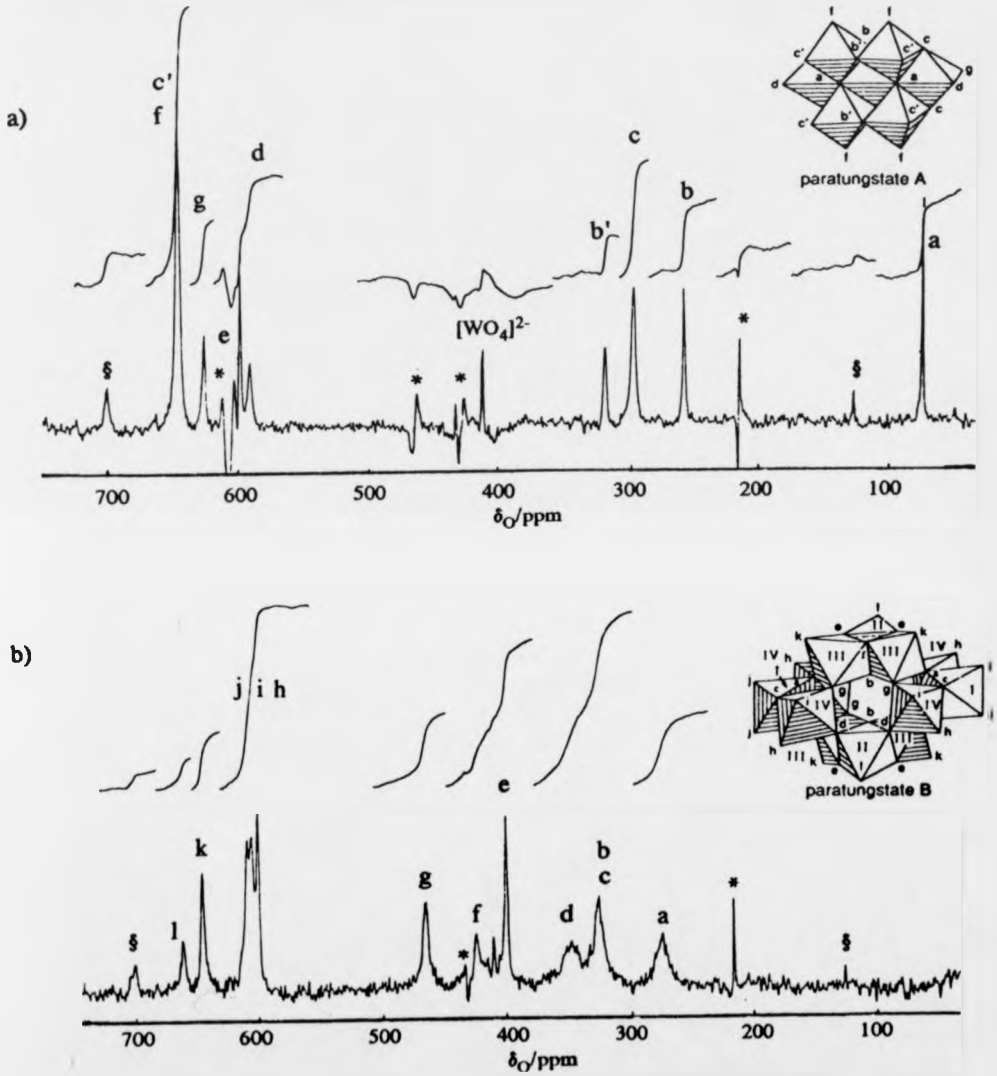

Figure 37. a) Shows the oxygen-17 NMR spectrum of a 2M WO_4^{2-} solution acidified to pH 6 and heated to 89°C for one hour, so as to maximise paratungstate-A, and cooled prior to collecting the spectrum. Then the equilibrium spectrum has been subtracted. **b)** Shows the oxygen-17 NMR spectrum of the same solution but, with the paratungstate-A rich spectrum subtracted from the equilibrium spectrum, yielding a spectrum of paratungstate-B. * Known spectrometer artefacts. § α-$[HW_{12}O_{40}]^{7-}$.

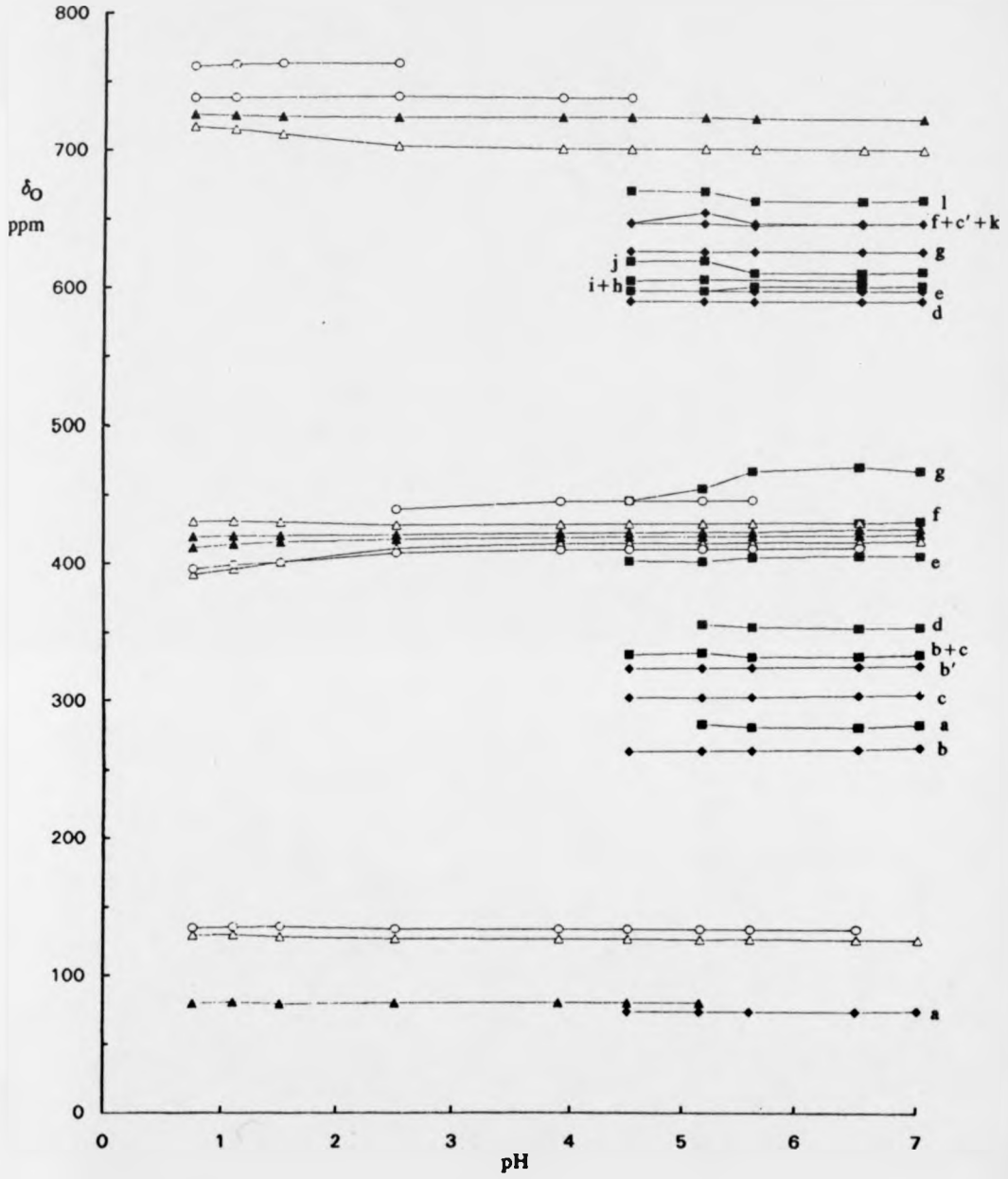

Figure 38. Oxygen chemical shifts *vs.* pH of species obtained by direct protonation of $[WO_4]^{2-}$ at 89°C. Species: ♦ = $[W_7O_{24}]^{6-}$, ■ = $[H_2W_{12}O_{42}]^{10-}$, O = β-$[H_2W_{12}O_{40}]^{6-}$, ▲ = α-$[H_2W_{12}O_{40}]^{6-}$, Δ = α-$[HW_{12}O_{40}]^{7-}$. The lines serve merely to highlight peak series.

Table 18. Oxygen chemical shifts and relative integrals for paratungstates A and B

peak label	A, $[W_7O_{24}]^{6-}$ δ_O	B, $[H_2W_{12}O_{42}]^{10-}$ δ_O	
a	74[a] (2.1 O)[b]	275 (4.1 O)	+4[c]
b	259 (2.0 O)	327 (2.1 O)	0
b'	319 (1.3 O)		
c	298 (3.8 O)	327 (4.1 O)	0
c'	648 (4.6 O)		
d	590 (1.7 O)	348 (4.1 O)	0
e	597 (1.8 O)	400 (3.6 O)	-3
f	648 (4.6 O)	424 (1.9 O)	*d*
g	626 (2.1 O)	465 (4.1 O)	-12
h		600 (4.0 O)	+4
i		605 (4.0 O)	+4
j		610 (4.0 O)	+6
k		646 (3.9 O)	+6
l		662 (2.1 O)	0

[a] ^{17}O Chemical shift (ppm) at 89°C, relative to solvent water. [b] Measured relative oxygen integral. [c] Shift upon partial protonation (see text). [d] Obscured at lower pH values.

Below pH≈ 5.5 the solutions are metastable. Upon prolonged heating they yield only the α-Keggin species (see below), and this is in any case the dominant species below pH 4. The tungsten resonances in Figure 32, that are labelled β, belong to the more minor species that appears. The two at higher shift show the same mutual coupling of 19 Hz that was reported by Lefebvre *et al.* [62]. The same solutions also show a proton resonance at 5.7 ppm, in addition to the expected α-Keggin proton resonance at 6.0 ppm [95]. The area ratio of these proton signals is the same as that of the corresponding tungsten resonances, within experimental error (See Figure 39). This independently shows that the species labelled β-Keggin has two non-exchanging protons, as does the α isomer. The proton relaxation time measurements, described below, also confirm this.

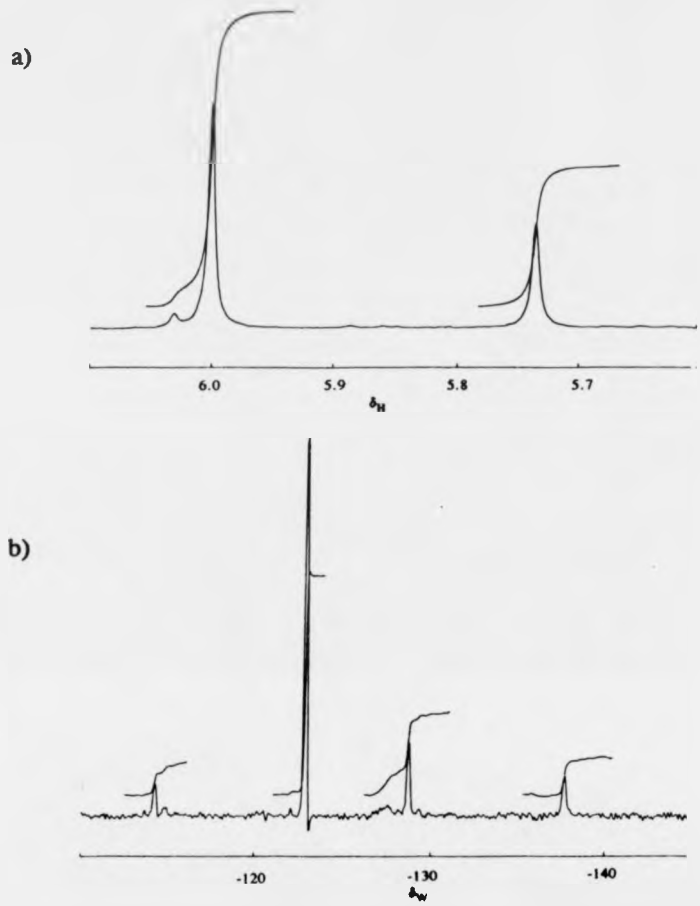

Figure 39. a) Shows the hydrogen-1 NMR spectrum of a WO_4^{2-} solution acidified to pH 2.74 at 293K yielding two resonances attributed to α-$[H_2W_{12}O_{40}]^{6-}$ at (δ_H 6 ppm) and β-$[H_2W_{12}O_{40}]^{6-}$ at (δ_H 5.7 ppm) in the area ratio 7:3. **b)** Shows the tungsten-183 NMR spectrum of the above solution with the large singlet attributed to α-$[H_2W_{12}O_{40}]^{6-}$ at (δ_W -123 ppm) and the remaining resonances assigned to β-$[H_2W_{12}O_{40}]^{6-}$ at (δ_W -112, -127 and -136 ppm). The area ratio between the large singlet and the sum of the other three is 7:3 in good agreement with the proton spectrum.

Some rather different chemistry was observed upon carrying out a series of acidifications of a concentrated tungstate solution initially at pH 7.5. The dominant species in this initial solution was paratungstate-B, along with a smaller amount of paratungstate-A. At room temperature, acidification to pH values between 4 and 3 yielded 11 new tungsten resonances of equal area (See Figure 40), in addition to the resonances from the α-Keggin and the protonated paratungstate-B species, plus

weak β-Keggin resonances (as above) between pH 3 and 4. The dependence of these new shifts upon pH is shown in Figure 41, together with the fitted titration curves that yield a pK_a of 2.65 ± 0.04, and also two other pH-independent resonances that are observed only along with the 11-resonance species. Unfortunately, no couplings could be observed, because the new 11-resonance species displays line-broadenings at all pH values, similar to those observed with protonated paratungstate-B. The linewidths were somewhat variable, and no tungsten exchange was detected in a saturation-transfer experiment in which the broadest lines were pre-irradiated using a DANTE pulse sequence [167]. (This experiment is described in Chapter 2, section 2.3). The new species showed essentially the same dependence upon metal concentration as the W_{12} species. It must therefore contain 11 tungsten atoms, rather than a multiple of this. Oxygen NMR was not attempted on this W_{11} anion because of its low concentration and high asymmetry. Further acidification gave the α-Keggin species. The two further and relatively weak resonances reported in Figure 41 could be reliably discerned in the pH range 3.4-2.0. They were independent of pH, and favoured by low ionic strength. The peaks were in approximately 4:1 area ratio, and appeared at -105.2 and -118.0 ppm respectively.

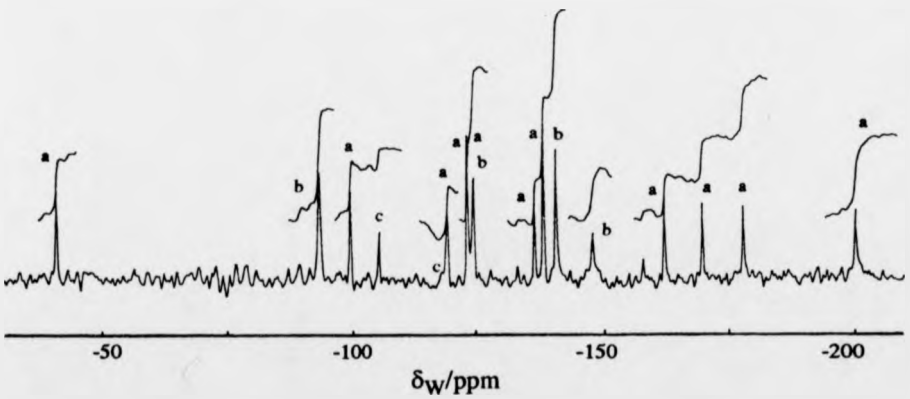

Figure 40. Tungsten-183 NMR spectrum of paratungstate-B acidified to pH 3.3 at 293K. Species: a, $[H_7W_{11}O_{40}]^{7-}$; b, $[H_3W_{12}O_{42}]^{9-}$ paratungstate-B; c, as yet unidentified.

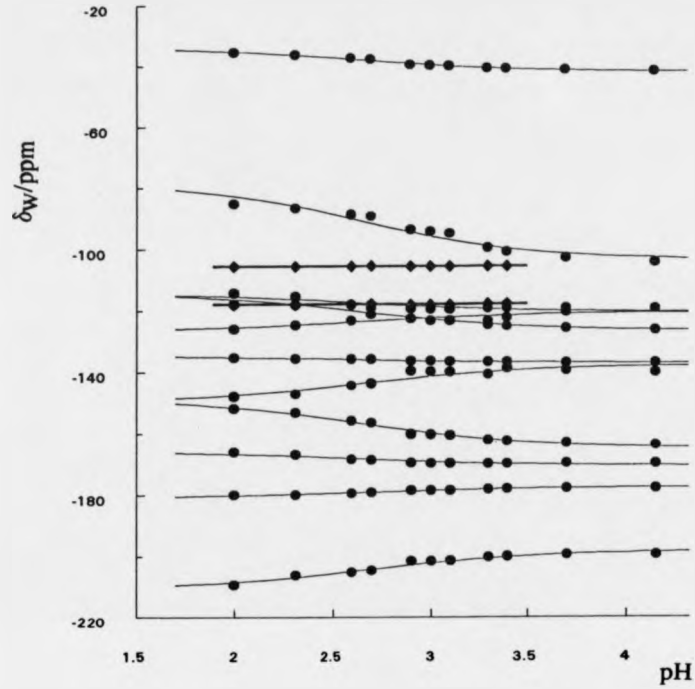

Figure 41. Tungsten chemical shifts *vs.* pH of two species that result from the metastability of protonated paratungstate-B. ● , ψ-metatungstate; ♦ , as yet unidentified.

Different chemistry again was observed when the above pH 7.5 solution was acidified stepwise, with each step being followed immediately by a raising of the temperature to 89°C. Under these conditions, also used to narrow the oxygen resonances, a single, new tungsten resonance appeared below pH 6.5, at δ_W = -143.5 ppm. Its area was somewhat greater than that of the α-Keggin species at this pH value. It yielded a set of oxygen resonances (Table 19) rather similar to those from the α-Keggin, but still clearly resolvable from these. It also gave a resonance from an internal proton at δ_H = 5.8 ppm, whose exchange with solvent D_2O was slow, the half-life being several days. Integration of this resonance alongside the α-Keggin resonance, in H_2O solution to prevent any loss of intensity, showed it to

arise from a single trapped proton, and this conclusion was supported by an approximately twentyfold increase in the proton's relaxation time (see below).

Further acidification, and also the passage of time, led to the progressive replacement of this internally monoprotonated species by the α-Keggin anion. However, its oxygen resonances could be traced down to pH 0.8. They showed some pH dependence below pH 2.5, and the α-Keggin resonances did so also, below pH 1.5, although the oxygens of lowest shift in both anions were not affected. The directions of these changes are indicated by signs, in Table 19 and this dependence is illustrated in Figure 38. It is clear that α-$[HW_{12}O_{40}]^{7-}$ exhibits a greater pH dependence than α-$[H_2W_{12}O_{40}]^{6-}$ and therefore as one would expect is more readily protonated.

Table 19. Oxygen and hydrogen chemical shifts and relative integrals for Keggin anions.

α-$[HW_{12}O_{40}]^{7-}$	α-$[H_2W_{12}O_{40}]^{6-}$	β-$[HW_{12}O_{40}]^{7-}$	β-$[H_2W_{12}O_{40}]^{6-}$
δ_O	δ_O	δ_O	δ_O
127[a](4.5O)[b][+][c]	80(2.8O)[+]	130(0.9O),133(3.3O)	61(3O),75(1O)[d]
411(13O)[-]	415(11.2O)[-]	*e*	397(6O),402(6O)[e]
425(11O)[+]	418(12.7O)[+]	*e*	442(3O),434(6O)[e]
700(11.6O)[+]	723(13.3O)[+]	765(2.7O)	725(3O),764(1O)
5.8[f](1H)[g]	6.0(2H)	*h*	5.7(2H)

[a] Oxygen shift in ppm from solvent water, 294K. [b] Measured relative oxygen integral. [c] Direction of shift change below pH 2. [d] Broad resonance. [e] Further resonances are present, but obscured by other peaks in this region. [f] Proton shift. [g] Relative proton integral per mole of anion . [h] Not resolved.

One further minor species was also detectable in the oxygen spectra only. Its proportion was about one third of the above monoprotonated species over the entire

range of pH, and its resonances had rather similar shifts. As a result, not many were clearly resolved at pH > 2. However, spectra at pH < 2 showed that further oxygen resonances from this anion lie underneath those of its more abundant congeners. Two important shifts that are resolved are listed in Table 19. No separate proton resonance was resolved for this species. Figure 42 shows a typical oxygen spectrum, in which all three resonance sets are visible.

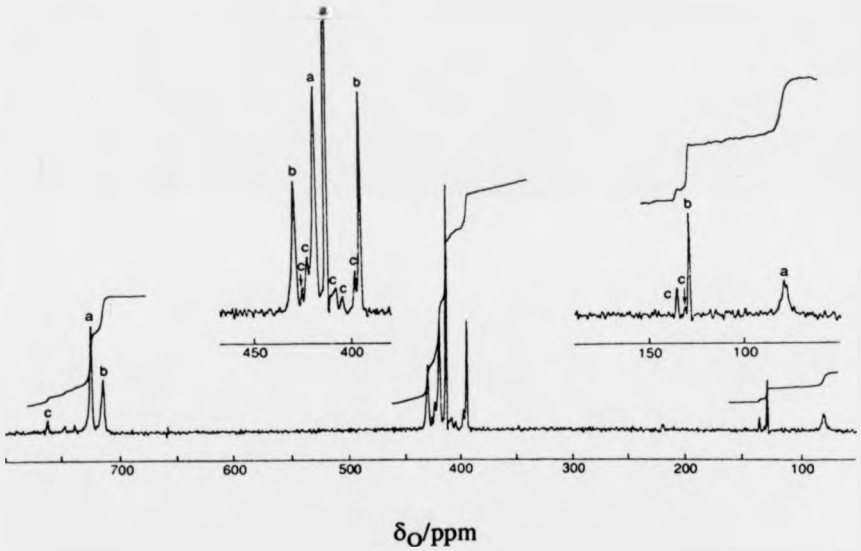

Figure 42. Oxygen-17 spectrum at 89°C, pH 1.1, with inset expansions. Species: a, α-$[H_2W_{12}O_{40}]^{6-}$, metatungstate; b, α-$[HW_{12}O_{40}]^{7-}$, ψ'-metatungstate; c, probable β-$[HW_{12}O_{40}]^{7-}$. Each of these has undergone partial further protonation at this pH. The small unlabelled resonances only appear below pH 2.5.

Proton T_1 and T_2 relaxation measurements were made over a range of temperature for the three most stable internally protonated anions. The T_1 and T_2 results are given in Tables 20 and 21 respectively. Figure 43 clearly illustrates a T_1 minimum for both species. Figure 44 shows a typical stacked T_1 plot for α- and β- Keggins at

40°C and the data fitted to equation (2.5) (see Chapter 2, section 2.1.1.) using standard software. Also the signal to noise ratio of the tungsten resonances of α-Keggin (pH 2.75), paratungstate-B (pH 7.0) and the 4W resonance (δ_W -106 ppm) of paratungstate-A (pH 7.0) were sufficient to permit tungsten spin-lattice relaxation measurements by inversion recovery. See Table 22.

Table 20. Proton T_1 spin-lattice relaxation times *vs* temperature for the Keggin anions.

Temperature/K	α-$[HW_{12}O_{40}]^{7-}$	α-$[H_2W_{12}O_{40}]^{6-}$	β-$[H_2W_{12}O_{40}]^{6-}$
337		0.590±.001[a]	0.462±.015
313		0.457±.009	0.404±.006
303		0.428±.008	0.392±.007
293	8.88±.02 [6.058±.02][b]	0.418±.004	0.407±.005
283		0.426±.003	0.426±.004
263		0.573±.009	0.628±.002

[a] T_1/s.

[b] Obtained at 250 MHz rather than 400 MHz.

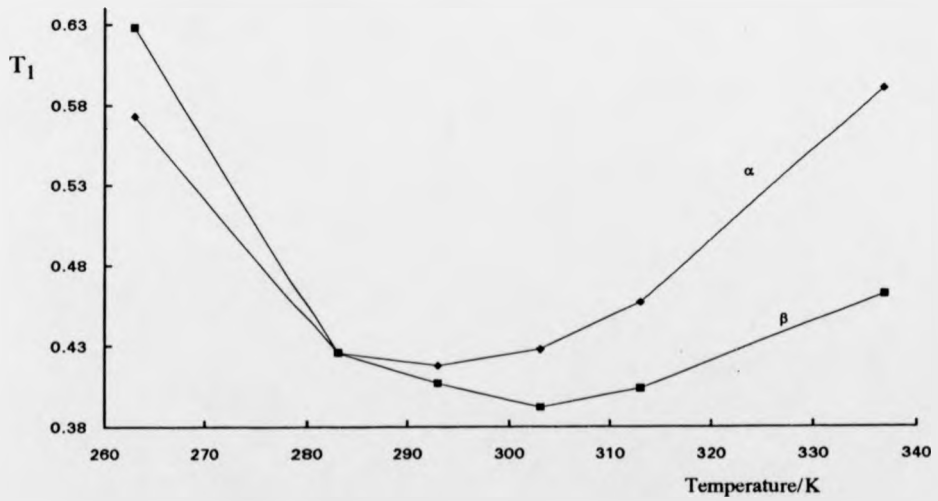

Figure 43. Proton T_1 spin-lattice relaxation times *vs* temperature illustrating T_1 minima for both α- and β- Keggin anions.

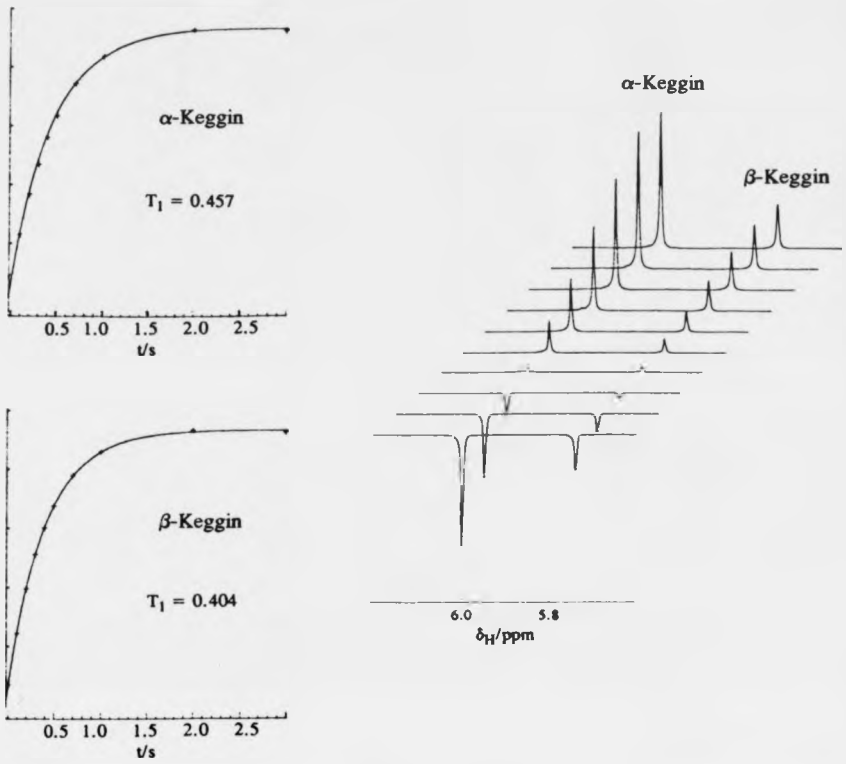

Figure 44. A typical stacked proton T_1 plot for α- and β- Keggins at 40°C. and the data fitted using standard software.

Table 21. Proton T_2 spin-spin relaxation times *vs* temperature for Keggin anions.

Temperature/K	α-$[HW_{12}O_{40}]^{7-}$	α-$[H_2W_{12}O_{40}]^{6-}$	β-$[H_2W_{12}O_{40}]^{6-}$
337		0.293±.005[a] [0.18][b]	0.241±.005[a] [0.16]
313		0.174±.006 [0.18]	0.151±.004 [0.16]
303		[0.16]	[0.14]
293	0.058 ±.01 [0.098]	0.115±.005 [0.16]	[0.15]
283		[0.15]	[0.13]
278		0.0805±.01 [0.12]	0.076±.01
263		[0.078]	[0.065]

[a] T_2/s measured using a Hahn echo experiment [170,171]
[b] T_2/s. $= 1/\pi$(linewidth) [163].

Table 22. Tungsten spin-lattice relaxation times for α-Keggin $[H_2W_{12}O_{40}]^{6-}$ and paratungstate-B, $[H_2W_{12}O_{42}]^{10-}$ and for the 4W resonance (δ_W -106 ppm) in paratungstate-A $[W_7O_{24}]^{6-}$ at 293K.

Species	Peak label	Spin-lattice relaxation time[a]	Spin-lattice relaxation time[b]
α-$[H_2W_{12}O_{40}]^{6-}$[c]		2.148±.008	0.8354±0.0126 [0.954][d]
$[W_7O_{24}]^{6-}$[e]	II	6.01 ±.014	1.94±0.0791 [2.67]
$[H_2W_{12}O_{42}]^{10-}$[e]	I	4.57 ±.006	2.38±0.0298 [2.03]
	II	0.779±.01	0.337±0.008 [0.346]
	III	1.54±.004	0.647±0.0077 [0.684]
	IV	2.81±.01	1.29±0.0090 [1.25]

[a] T_1/s measured at 16.65 MHz. [b] T_1/s measured at 24.98 MHz. [c] At pH 2.75. [d] Prediction made from the T_1 data measured at 16.65 MHz assuming that the CSA relaxation mechanism dominates, *i.e.* the T_1 measured at 24.98 MHz being smaller by the factor :- $(24.98)^2/(16.65)^2$. [e] At pH 6.5.

The majority of these isopolytungstate results have already been published [157] and a copy of the paper is shown in the Appendix.

4.2. Isopolytungstate Discussion.

4.2.1. Paratungstate species

The measurements above pH 6 essentially confirm the conclusions reached by Maximovskaya and Burtseva [64]. The increased field has, however, permitted more resolution, and the observation of one substantial W-W coupling. If one follows precedent in assigning this coupling to tungstens linked by a single oxygen [62], then all the tungsten resonances of paratungstate-B may be assigned as in Figure 45. The corresponding resonances of paratungstate-A (also in Figure 45) are simply assigned by area.

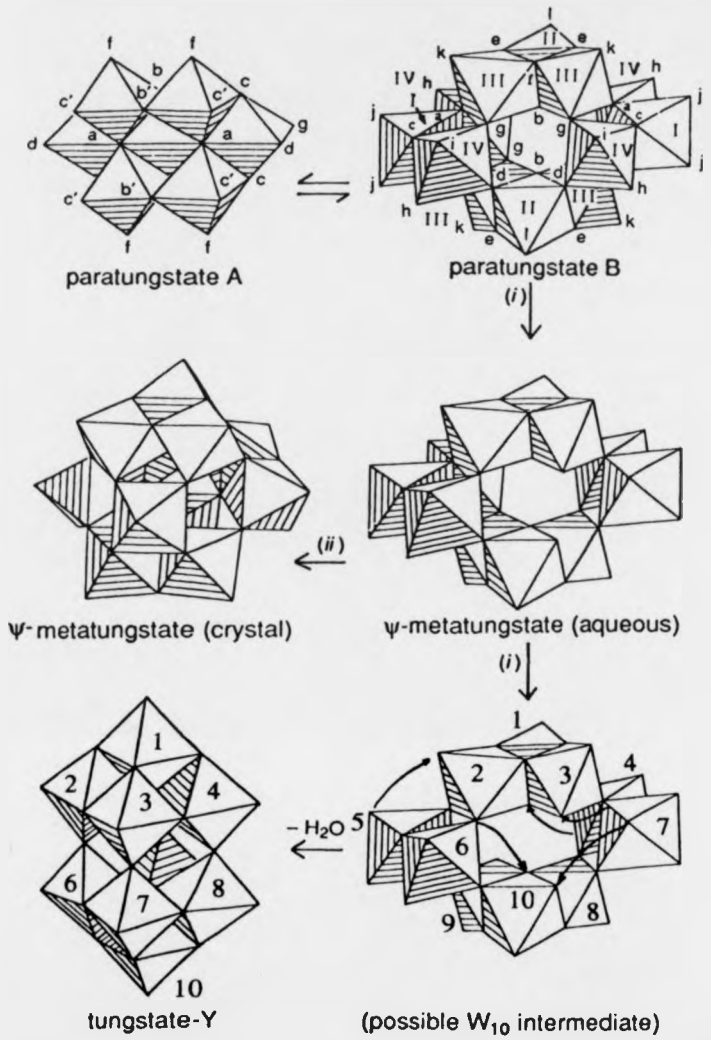

Figure 45. Atom labels in paratungstate-A and -B, together with possible links with species that result from the acidification of paratungstate-B. (*i*) H^+; (*ii*) crystallisation. The numbering of the octahedra for the tungstate-Y species and possible W_{10} intermediate serve merely to clarify the rearrangement of the species.

The oxygen assignments are more problematic, particularly in the less symmetrical B species. The proposals in Table 18 depend on the inverse correlation of oxygen shifts with the length of the shortest M-O bond (Figure 46). This has considerable approximate support [24,101], but is not reliable to high accuracy with a few deviations. In the example of paratungstate-B, O_b does not follow the general trend

of the correlation with its unusually long M-O bond length. This is because in the solid state this site is protonated [93].

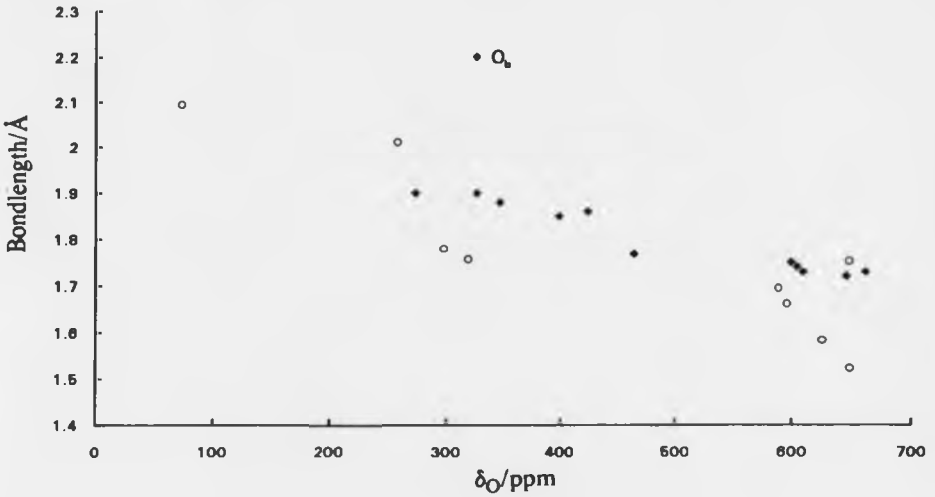

Figure 46. A correlation of Oxygen chemical shifts of paratungstates -A ∘, and -B ♦, versus the shortest M-O bond length. O_b does not follow the trend because it is bonded to hydrogen in the crystal.

If we accept these assignments at least provisionally, then the dominant protonation sites of paratungstate-B must be at O_g, because only this resonance shows a substantial reduction in its shift, upon protonation [53]. O_e may be a secondary site of protonation. Polyanions generally protonate at their most highly substituted accessible oxygens, although this pattern may be slightly perturbed in subsequent protonations [53]. The most highly substituted oxygens in paratungstate-B are O_a and O_b. These are both in the anion's central cavity. The O_a oxygens are probably inaccessible, and the two O_b oxygens are known to bind two protons in the crystal in any case [93]. This probably prevents their further protonation, along with that of some nearby oxygens, leaving O_g as the preferred site. Inspection of the structure of paratungstate-B, in Figure 45, shows that this site is internal, *i.e.* within the anion's cavity, and not readily accessible to the solvent.

Although the dependence of the tungsten shifts of paratungstate-B upon protonation is marked, it is not simply explained. The varying signs of the dependence are also unexpected. Theoretical considerations show that the chemical shift of a d^0 metal ion in polyoxoanion framework can move in either direction when the framework is protonated, depending on the details of the changes in M-O bond lengths [52]. But one finds in the decavanadate [24,53], monomolybdononavanadate [25], monotungsto-nonavanadate [156] and the tetradecaphosphovanadate [24] anions that the vanadium shifts always decrease upon protonation. In these cases, the protonation is necessarily at the exterior of the anion. The effect of interior protonation on a tungsten shift may be estimated from the data on the α-Keggin species in Table 16. It leads to an increase of 21 ppm. The change of sign probably arises because the metal atom now moves in a direction opposite to that for external protonation, within its oxygen framework. If we now regard the observed protonation at O_g as internal, then this explains the observed increases in shift of tungstens III and IV upon protonation, for O_g bridges these tungstens. This argument also implies a concomitant deprotonation near to tungstens I and, especially, II. Tungsten II is nearest to the site of protonation of $[H_2W_{12}O_{42}]^{10-}$ in the crystal. Klemperer *et al.* have already shown in the case of the decavanadate ion that its second and subsequent protonations cause a rearrangement of all the attached protons [53]. A similar rearrangement probably occurs here.

However, the protonation of paratungstate-B must be still more complex, because of the unexpected kinetic data implicit in Table 17. These clearly show that some motion involving protons is detectably slowed in the protonated (*i.e.* H_3) but not the unprotonated (H_2) anion. With some plausible assumptions regarding the shift separations and proportions of the exchanging species, one may deduce a deuteron residence time of the order of 10^{-4} s, using equation (4,2) [162];

$$k = \pi/2 \{\delta_\nu[(\delta_\nu/h)^2-(h/\delta_\nu 2)+2]^{1/2}\} \qquad (4.2)$$

where δ_v, is the shift separation of the resonances in the fully protonated anion and the unprotonated anion and h is the difference of the linewidths of the protonated anion in ^1H_2O and that of the deuterated anion measured ^2H_2O. We suspect that one of the $[H_3W_{12}O_{42}]^{9-}$ isomers bears three internal protons, with two at O_g sites, and the other has one external proton, which moves rapidly between O_e sites. The exchange of a proton between the internal and the external sites would then be the rate-determining step.

It is not surprising to find that paratungstate-A does not protonate, even though its molybdenum analogue (heptamolybdate) has a pK_a of 4.9 [116]. Polytungstates generally protonate less readily than their Mo analogues, and in any case the paratungstate resonances are not detectable below pH 5.5. We have not been able to observe the selective line broadening in the oxygen spectrum of A at high temperature, reported by Maximovskaya and Burtseva [64], and clearly observed by both these authors and ourselves in heptamolybdate [64,91]. It is less surprising to find that monotungstate does not protonate within its range of observation (pH 14 to pH 8), because its reported pK_a is 3.5 [175].

The lithium dependence of the tungsten shifts of paratungstate-A, given in Table 16, is much smaller for the central resonance, I, than for II or III, or for resonances II and IV of paratungstate-B. The latter's I and III resonances have an intermediate dependence, which may reflect a reduced local affinity for Li^+, consonant with the absence of protonation in this region. Monotungstate has the steepest dependence of all, as expected for a sterically unhindered anion. All the Li^+ shifts are in the same direction as that expected for external protonation (see above). No separate signal was observed in the ^7Li NMR spectrum. Presumably the Li^+ ion is too large to enter the cavities of either metatungstate or paratungstate-B.

Maximovskaya and Burtseva [64] also report that three of their oxygen resonances gain area in advance of the others upon addition of $H_2{}^{17}O$. There is some ambiguity

about the assignment of these resonances, because of overlap. The possibilities are b,c,h,i and j . All but one of these candidate oxygens, using the above assignment, are attached solely to tungstens I and IV. These are the tungstens that each bear two terminal oxygens, and so their relative lability is not unexpected.

4.2.2. W_{11} Species, ψ-metatungstate

This species cannot be the $[H_4W_{11}O_{38}]^{6-}$ ion whose crystal structure has been reported by Lehmann and Fuchs [10], even though it is prepared under similar conditions, because the ion observed here lacks symmetry. It is probable, however, that Lehmann and Fuchs' ion forms from the solution species by a process of oxygen elimination. We therefore give both species the identification put forward for the crystalline anion, *i.e.* ψ-metatungstate.

As the presence of protonated paratungstate-B is essential for the appearance of the species with 11 equal W resonances, one may reasonably assume that their structures are related. In any case, no fully unsymmetrical structure can be created by the simple removal of one WO_n unit from an α-Keggin anion. We propose a lacunary structure for the new species, based on the removal from paratungstate-B of one W, of type IV, and its two attached O atoms. This could yield a possible formulation $[H_7W_{11}O_{40}]^{7-}$ for the anion, along with the observed asymmetry.

All 11 W resonances of this new species alter with pH, by comparable amounts. This precludes any simple identification of a protonation site. The similarity of the W_{11} resonances to those of paratungstate-B includes selective line broadening, in both states of protonation, as well as protonation shifts in both directions. This implies that the W_{11} species bears protons in both of its states, and is similarly lacunary. This provides support for a formulation with several protons, some internal, and contrasts with the next species to be described.

Paratungstate-B has been reported to yield tungstate-Y, $[W_{10}O_{32}]^{4-}$, upon further protonation, in the presence of large cations designed to disfavour Keggin structures [176]. This reaction involves low solubilities, and is therefore difficult to investigate in solution. However, in our paper [157] we proposed that the W_{11} anion could reasonably collapse with only modest rearrangement, to give the tungstate-Y structure, upon removal of a second similar WO_2 unit. Indeed, the narrow tungsten resonances observed at δ_W -105.2 and -118.0 ppm, which appear under relatively acid conditions, have the correct area ratio to be the two tungsten resonances anticipated for tungstate-Y, $[W_{10}O_{32}]^{4-}$. A species with this relatively low charge would be favoured at lower ionic strengths, which is what we observe. The proposal for the putative relationships between these species are illustrated in Figure 45.

To corroborate this, we prepared the tetra n-butyl ammonium salt of tungstate-Y by the method of Filowitz *et al.* [101]. Our initial inspection of the tungsten NMR spectrum appeared to have two resonances in 4:1 area ratio at -98.0 and -104.8 ppm respectively. However, after more recent evidence and further refinements of the data we have concluded that these resonances were in fact resulting from a mixture of α- and β-metatungstate anions. The two additional 3W resonances expected for β-metatungstate were poorly resolved in these early spectra. However, after repeating the above preparation of decatungstate the tungsten chemical shifts observed were in fact very different, namely -27.6(8W) and -172.3 ppm (2W). So therefore there is no spectral evidence for this interconversion and consequently we have been unable assign these minor resonances.

4.2.3. Species with Keggin Structures

The strong and relatively ubiquitous tungsten resonance at -123.0 ppm must clearly arise from the α-Keggin anion $[H_2W_{12}O_{40}]^{6-}$. Its shift is equal to the -117.5 ppm reported for the Na^+ salt by Lefebvre *et al.* [62], after re-referencing to allow for the altered experimental conditions. It also has the correct proton spectrum for an

Paratungstate-B has been reported to yield tungstate-Y, $[W_{10}O_{32}]^{4-}$, upon further protonation, in the presence of large cations designed to disfavour Keggin structures [176]. This reaction involves low solubilities, and is therefore difficult to investigate in solution. However, in our paper [157] we proposed that the W_{11} anion could reasonably collapse with only modest rearrangement, to give the tungstate-Y structure, upon removal of a second similar WO_2 unit. Indeed, the narrow tungsten resonances observed at δ_W -105.2 and -118.0 ppm, which appear under relatively acid conditions, have the correct area ratio to be the two tungsten resonances anticipated for tungstate-Y, $[W_{10}O_{32}]^{4-}$. A species with this relatively low charge would be favoured at lower ionic strengths, which is what we observe. The proposal for the putative relationships between these species are illustrated in Figure 45.

To corroborate this, we prepared the tetra n-butyl ammonium salt of tungstate-Y by the method of Filowitz *et al.* [101]. Our initial inspection of the tungsten NMR spectrum appeared to have two resonances in 4:1 area ratio at -98.0 and -104.8 ppm respectively. However, after more recent evidence and further refinements of the data we have concluded that these resonances were in fact resulting from a mixture of α- and β-metatungstate anions. The two additional 3W resonances expected for β-metatungstate were poorly resolved in these early spectra. However, after repeating the above preparation of decatungstate the tungsten chemical shifts observed were in fact very different, namely -27.6(8W) and -172.3 ppm (2W). So therefore there is no spectral evidence for this interconversion and consequently we have been unable assign these minor resonances.

4.2.3. Species with Keggin Structures

The strong and relatively ubiquitous tungsten resonance at -123.0 ppm must clearly arise from the α-Keggin anion $[H_2W_{12}O_{40}]^{6-}$. Its shift is equal to the -117.5 ppm reported for the Na^+ salt by Lefebvre *et al.* [62], after re-referencing to allow for the altered experimental conditions. It also has the correct proton spectrum for an

internally diprotonated species, and its oxygen spectrum shows four resonances in the anticipated area ratio 12:12:12:4, with appropriate shifts.

The three resonances which are labelled above as β-Keggin have the same relative areas, coupling and shifts relative to the α-Keggin resonance as do the β-Keggin resonances reported by Lefebvre *et al.* [62]. The anion's proton resonance also has essentially the same shift as that reported by Launay *et al.* [95], and the associated relaxation time is in the sub-second range expected for an internally diprotonated species. Thus we may be certain that β-$[H_2W_{12}O_{40}]^{6-}$ forms spontaneously in aqueous solution, as a minor species. Because it is only minor and transient, we have not been able to identify all its oxygen resonances unambiguously. However, those we can identify (Table 19) are entirely consistent with a β-Keggin structure.

The main extra species that forms upon acidification of paratungstate, as distinct from acidification of monotungstate, gives an oxygen spectrum very similar to that of α-$[H_2W_{12}O_{40}]^{6-}$, with the same ratios of peak area. It must therefore arise from an α-Keggin structure. One may discount the possibility of an ε-Keggin because its presence would almost certainly entail the simultaneous presence of γ- and δ-Keggin species, and these are not observed. The only marked differences of shift in the new α-Keggin species are the increase of 47 ppm for the central oxygens and the concomitant decrease of 23 ppm for the terminal oxygens. Both of these shifts are the expected consequence of the loss of an internal proton. They contrast with the shifts observed at much lower pH in both species. In these cases the internal oxygens are only very weakly affected, but one of the two bridging oxygens moves to markedly lower δ_O. These latter shifts are characteristic of external protonation [53]. Even stronger evidence that the new species is internally monoprotonated comes from its rather long proton relaxation time, some twenty times that of α-$[H_2W_{12}O_{40}]^{6-}$. It also forms preferentially at somewhat higher pH. We may therefore identify this anion as α-$[HW_{12}O_{40}]^{7-}$. In previous work, this has only been made by reduction and re-oxidation [107].

We find a proton shift of 5.8 ppm for this species, which differs significantly from that of *ca.* 6.3 ppm reported previously [95]. We also noted that in D_2O solution the internal proton exchanges more slowly than that of the α-H_2 Keggin. Curiously, after repeating this exchange experiment at several pH values in collaboration with Mr. Jason Watmough, a third year project student, no exchange was observed.

The more minor species whose intensity covaries with α-$[HW_{12}O_{40}]^{7-}$ is too dilute to yield a tungsten spectrum. However, its very similar oxygen shifts and its covariance are both highly consistent with a formulation as β-$[HW_{12}O_{40}]^{7-}$. Thus we have evidence for non-electrochemical formation of both the internally monoprotonated and diprotonated Keggin species in both their α and β forms, and for the α forms also accepting external protons.

4.2.4. Relaxation Times

It is convenient that the available temperature range spans the T_1 minima for both the α and β-diprotonated Keggin species. This enables the reorientational correlation time τ_c for each species to be determined unambiguously over the range, by fitting the data to the equation (2.13) (see Chapter 2, section 2.2.1.). The fitted relaxation rates were the differences between those of the internally diprotonated species at various temperatures, and the much smaller relaxation rate of the internally monoprotonated species at room temperature. The use of a difference in this way largely eliminates uncertainties about competing relaxation mechanisms. The correlation times shown in Table 23 are reasonable values for highly charged aqueous anions with this mass.

Table 23. Variation of correlation times τ_c with temperature.

Temperature (K)	α-Keggin $[H_2W_{12}O_{40}]^{6-}$ τ_c (x 10^{-10} s)	β-Keggin $[H_2W_{12}O_{40}]^{6-}$ τ_c (x 10^{-10} s)
337	0.931 ±0.03	1.27 ±0.07
313	1.52 ±0.08	1.86 ±0.11
303	1.92 ±0.1	2.45 ±0.01
293	2.45 ±0.01	3.36 ±0.16
283	3.06 ±0.12	3.93 ±0.1
263	6.35 ±0.16	8.03 ±0.1

It requires slightly more assumptions to explain the actual values of T_1. If we assume that the difference in relaxation rates between the di- and monoprotio anions arises exclusively from the dipole-dipole interaction of the two internal protons, then we can also use the equation (2.13) (see Chapter 2, section 2.2.1.) to calculate mean interproton distances of 1.87 Å (α) and 1.85 Å (β). These are slightly shorter than the 1.92 Å deduced from solid-state proton NMR of the α-isomer [94].

It is now possible to calculate T_2 using the mean interproton distances and equation (2.15) (see Chapter 2, section 2.2.1.), a development of the above T_1 equation. Even so, it is clear in Figure 47 that the experimental T_2 values are much shorter. One possible explanation, is that the H-H vector is, in fact, experiencing two molecular motions. The first is a rapid rotation driven by exchange between internal sites and the second, a much slower rotation of the tungsten cage. However, this cannot be correct because no sharp resonance was observed in the solid. An alternative interpretation could possibly be an outer sphere Li exchange process. After all there is a linear tungsten shift dependence on the concentration of Li^+. Again with some plausible assumptions regarding the shift separations and proportions of the exchanging species, one may calculate a rate, k of 7000 s^{-1}, using equation (4.2) (see above). Where $^{\delta}\nu$ is the shift separation of the α-Keggin anion measured in a solution with 4 mol dm^{-3} in Li^+, and the theoretical shift of the

α-Keggin anion in a solution with the Li^+ concentration extrapolated to 0 mol dm^{-3} and h, is the difference of linewidth at half the height of the tungsten resonance and the natural linewidth. The slightly slower rotation of the β-isomer is probably a consequence of its lower symmetry.

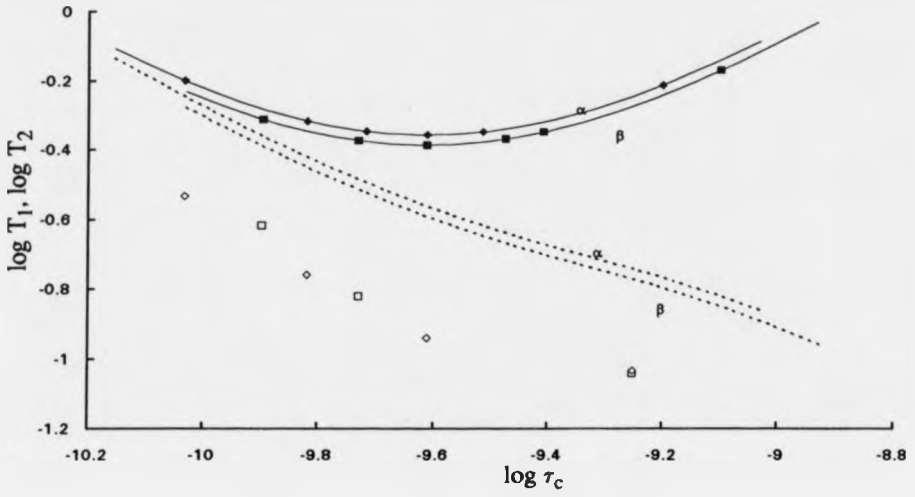

Figure 47. Proton log T_1 and log T_2 versus log τ_c for α- and β- Keggins. The solid lines are fitted using equation (2.13) whereas the dotted lines are calculated using equation (2.15) and the mean interproton distances. Experimental T_1 points: ◆ = α-Keggin and ■ = β-Keggin, and experimental T_2 points: ◊ = α-Keggin and □ = β-Keggin.

The linear relationship between log τ_c and reciprocal temperature shown in Figure 48 confirms Arrhenius behaviour and thus yields the activation energies:

α- Keggin 18.9 ± 0.6 kJ
β- Keggin 18.5 ±0.9 kJ

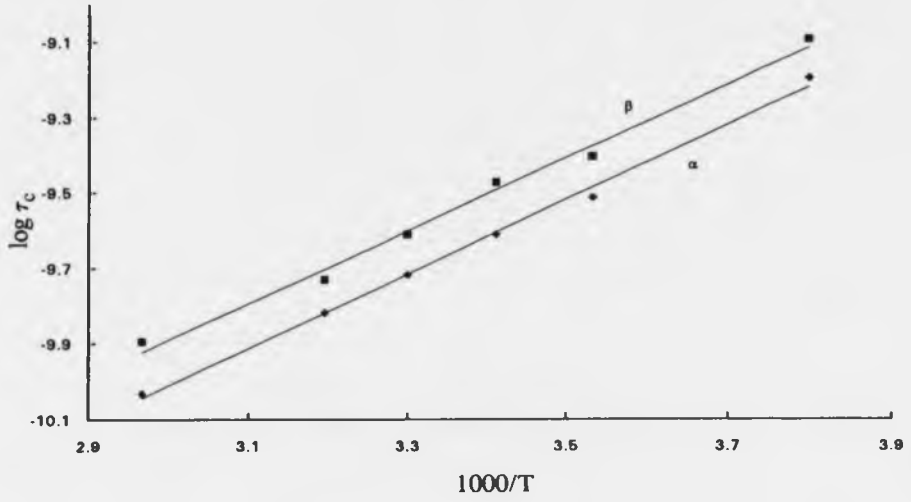

Figure 48. log τ_c values for α- and β- Keggins versus reciprocal temperature.

It is reasonable to assume that the tungsten nuclei in α-$[H_2W_{12}O_{40}]^{6-}$ relax by chemical shift anisotropy as the possibility of dipole-dipole relaxation contributing was removed by observing no enhancement of the tungsten resonance when the internal protons were irradiated. Further support for this assumption is seen in Table 21 where the tungsten T_1 values measured at 16.65 and 24.98 MHz correlate (within experimental error) to the squares of the field. Also if we have symmetric tensors *i.e.* $\sigma_{zz} \neq \sigma_{yy} = \sigma_{xx}$ and if the whole anion is tumbling at the same rate as the protons trapped in its centre, then by substitution of the tungsten T_1 and its correlation time τ_c, for α-$[H_2W_{12}O_{40}]^{6-}$ into equation (2.16) (see Chapter 2, section 2.2.2.) we calculate $\Delta\sigma$ = 1307 ppm at 293 K in ^2H_2O. This correlates very well with the CSA measurements already made from the solid state spectrum of $H_3[PW_{12}O_{40}]$ σ_{xx} = 409, σ_{yy} = 148 and σ_{zz} = -1079 which corresponds to $\Delta\sigma$ = 1357.5 ppm [177].

5. MOLYBDOTUNGSTATES

5.1. Molybdotungstate Results

The tungsten spectra for these mixed molybdotungstate solutions were very complex entailing a wide range of mixed metal species. Figure 49 shows a typical ^{183}W NMR spectrum of a solution at pH 5 with 1.143 mol dm^{-3} in Mo and 0.857 mol dm^{-3} in W. The signal to noise ratio of all but the weakest peaks permitted at least approximate integration. In fact, several measurements were made at each metal ratio, and the resulting relative integrals averaged. The tungsten chemical shifts observed were very similar to those of the isopolytungstate species already described in Chapter 4, namely, paratungstates -A and -B, and α-Keggin. We have therefore, assigned the resonances to mixed metal isomers of these anions and have no evidence for any other species with different polyoxometallate structures.

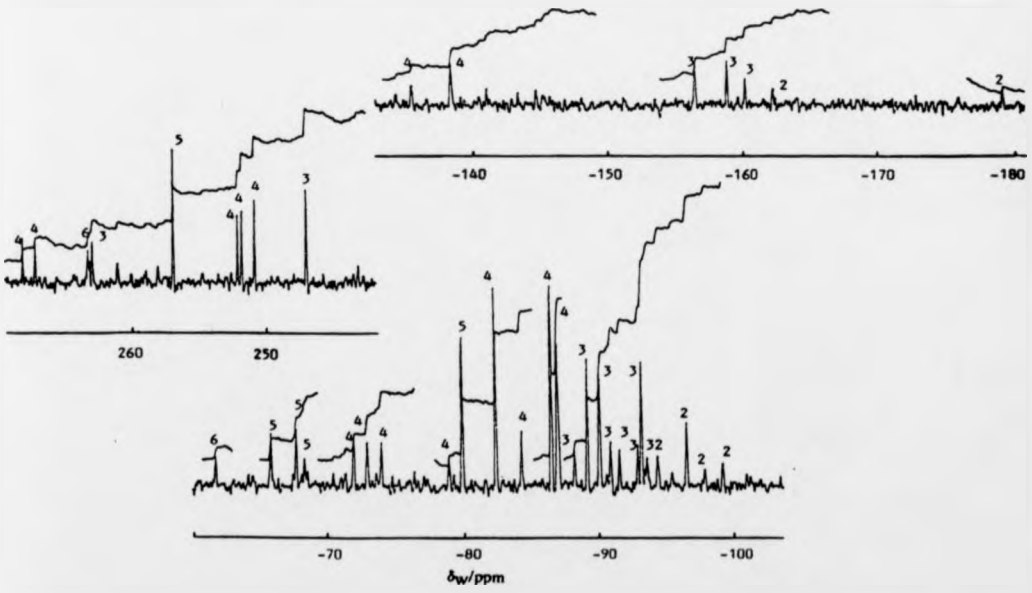

Figure 49. A typical tungsten-183 NMR spectrum of a molybdotungstate solution at pH 5, 293K with 1.143 mol dm^{-3} in Mo and 0.857 mol dm^{-3} in W. The resonances of some heptametallate species are identified by the number of molybdenum atoms they contain.

5.1.1. Substitution into the Paratungstate-A Structure

In aqueous solution, between pH 7 and 4, both W and Mo are known to form heptametallate species $[M_7O_{24}]^{6-}$ [64,91]. The four tungsten sites above and below the major symmetry plane of the heptatungstate anion correspond to the shift region -50 to -120 ppm. These are labelled II in Figure 50. The outer two in-plane tungstens, labelled III, correspond to -130 to -190 ppm shift region. The central tungsten, I, lie between 240 and 280 ppm. Assignments of these resonances are readily made from peak areas, for the more prevalent species such as $[W_7O_{24}]^{6-}$ and $[MoW_6O_{24}]^{6-}$. The other isomers are then evident from shift trends.

a) b)

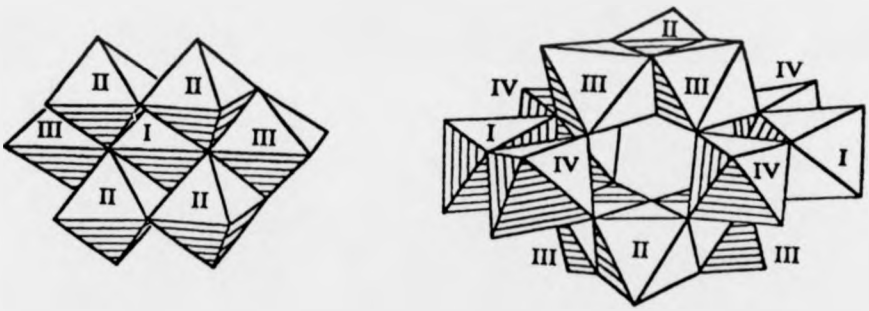

Figure 50. Structures of a) paratungstate-A, $[W_7O_{24}]^{6-}$ and b) paratungstate-B, $[H_2W_{12}O_{42}]^{10-}$, labelled as in text.

By systematically changing the metal ratio, groups of tungsten resonances were observed to alter in relative area. The metal ratio within the heptametallate species is then revealed by the order of dominance. This is illustrated by the three typical partial ^{183}W NMR spectra in Figure 51. Even though the ionic strength cannot be strictly controlled it is still possible to extract relative equilibrium constants using the LAKE [154] program since, over a limited pH range there is almost a constant species charge. This least squares fit program is able to treat pH and NMR data simultaneously, and has been found essential for establishing the speciation in highly complex systems such as aqueous molybdovanadates [26]. The dependency of each group versus metal ratio is shown in Figure 52 along with the fit of the same data obtained from LAKE [154]. This computer fit was very kindly performed by Dr. Lage Pettersson and Dr. Ingegärd Andersson of the University of Umeå, Sweden. In the main, the resonance group could then be subdivided into individual isomers simply using the necessarily integral ratios of the three tungsten types. The tungsten chemical shifts and integrals of the discernible mixed heptametallate species are reported in Table 24 and the proposed structures are presented in Figure 53. The proposed naming scheme for the isomers follows the convention for the Keggin species, where Greek letters are used to represent stability with α being the highest. Assignments of specific tungstens was not possible because the signal to noise was below that required to observe intertungsten couplings. Also, further complications in distinguishing a few isomers were experienced because the isomer ratios were close to unity.

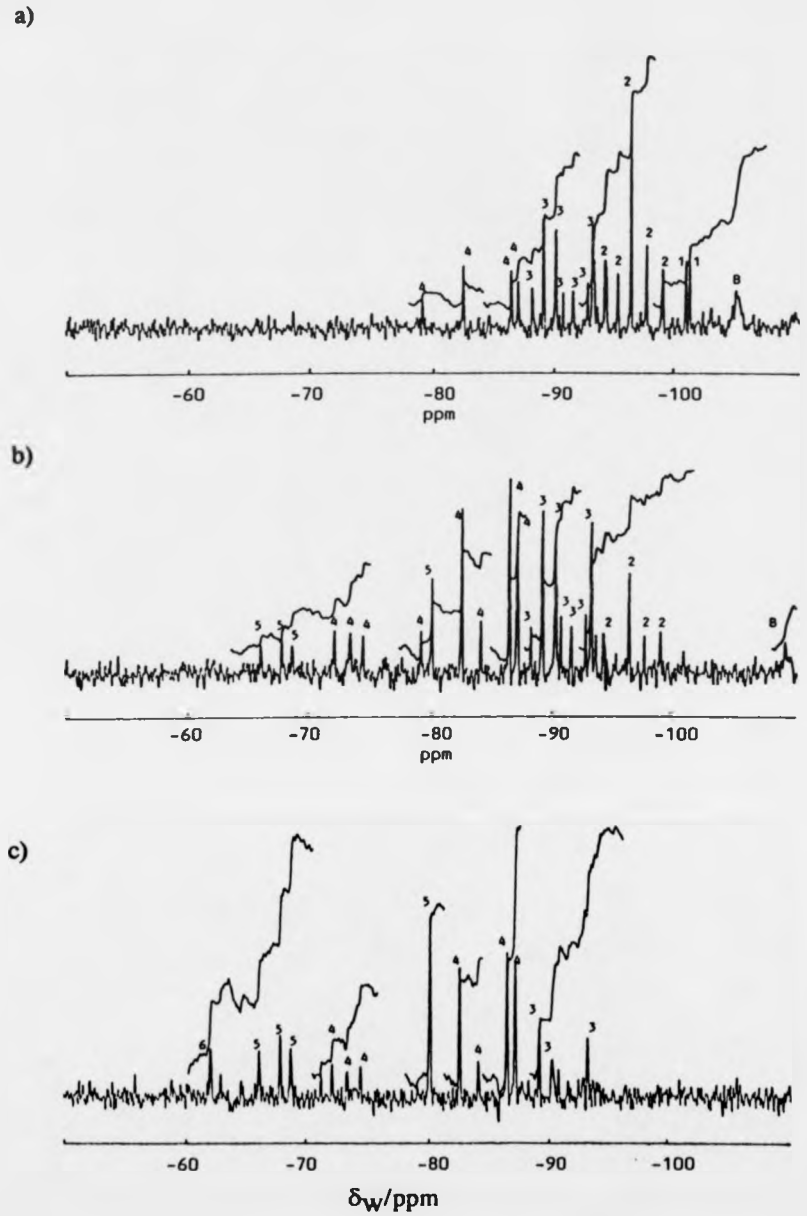

Figure 51. Typical tungsten-183 NMR spectra of mixed-metal heptametallates, showing only the capping (II) tungsten resonance region. All samples were at pH, 294K and 2 mol dm^{-3} total metal. The Mo:W ratios are **a)** 2:5, **b)** 1:1 and **c)** 5:2. The resonances of some species are identified by the number of Mo atoms they contain.

a)

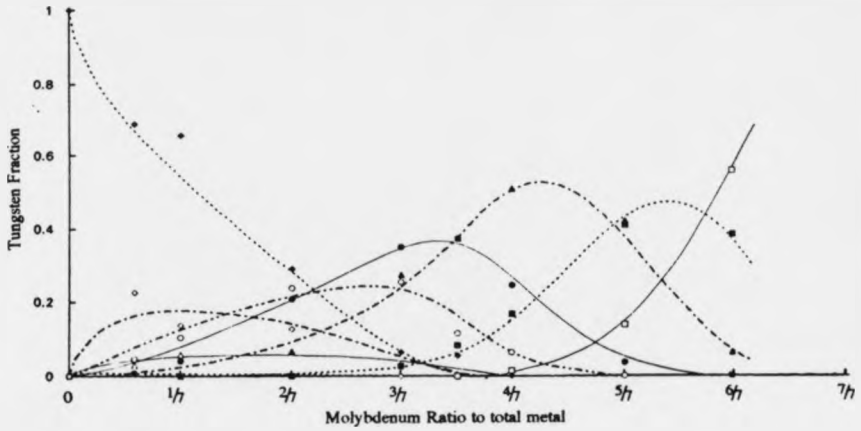

b)

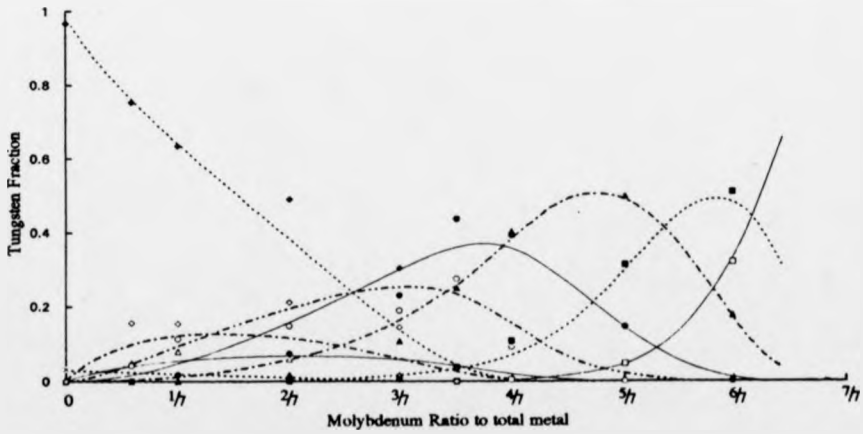

Figure 52. Dependence of the concentration of molybdotungstate species expressed as a W fraction, upon the molar concentration of Mo. [W] + [Mo] = 2 mol dm^{-3}, a) pH = 5; b) pH = 6 at 294K. Experimental plus fitted data; ♦ and · · · = (0,12), ◊ and · — = (1,11), × and · · · = (0,7), Δ and —— = (1,6), ○ and — · · = (2,5), ● and —— = (3,4), ▲ and · — = (4,3), ■ and · · · = (5,2), □ and —— = (6,1).

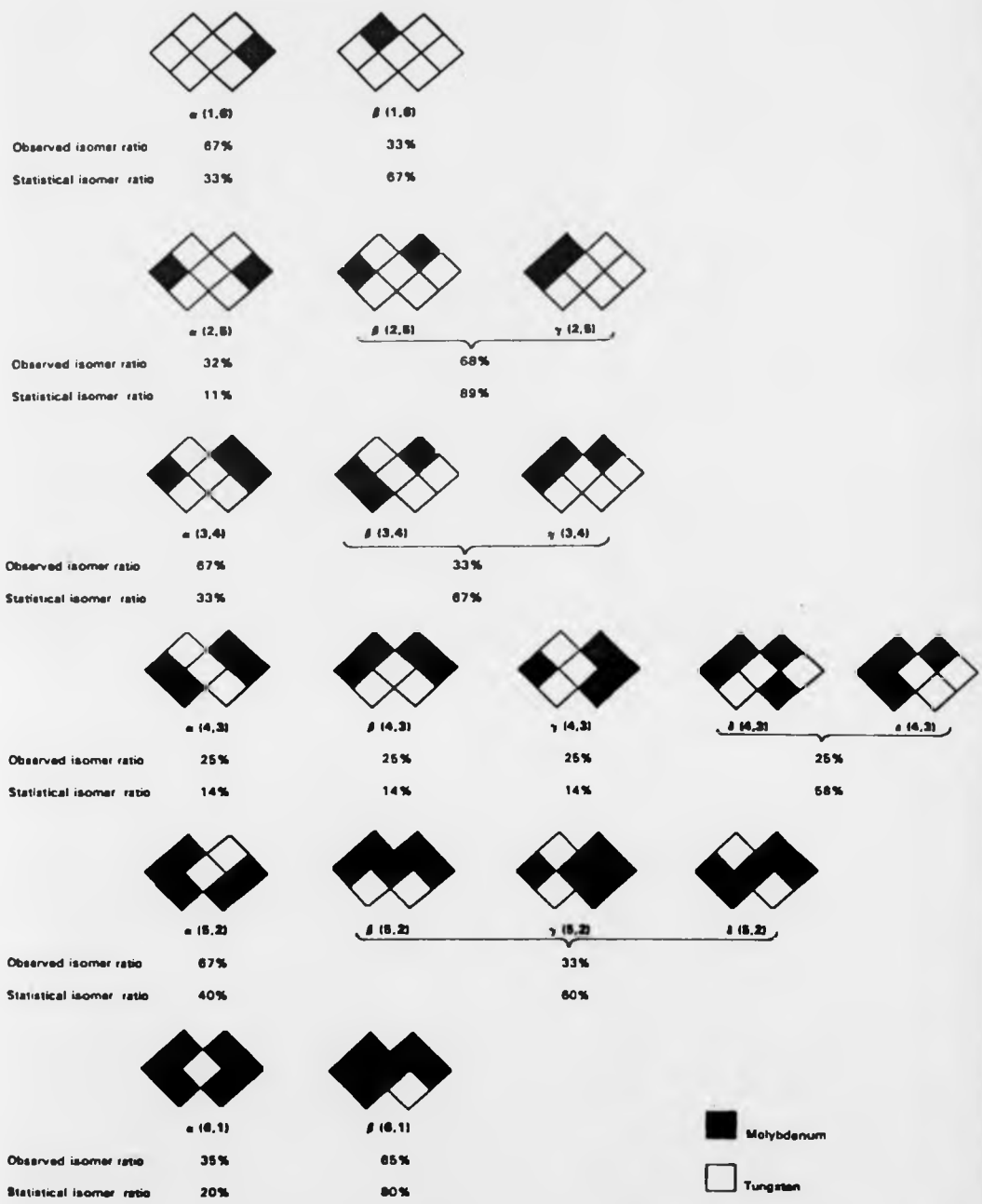

Figure 53. Proposed mixed heptametallate molybdotungstate species and their statistical and observed isomer ratios.

Table 24. Tungsten chemical shifts (ppm at 294K) and integrals of the mixed heptametallate molybdotungstate species.

species	site I	sites II	sites III	obs. ratio[a]	stat. ratio[a]
(0,7)	268	-106	-189		
α-(1,6)	255 [0.95]	-101, -101.4 [2.05], [2.05]	-182 [0.95]	0.67	0.33
β-(1,6)	272 [1.0]	-105,-112,-112.5 [1.0], [1.0], [1.0]	-168,-185 [1.0],[1.0]	0.33	0.67
α-(2,5)	259 [1.1]	-96.6 [3.9]	none	0.32	0.11
β+γ-(2,5)	258,243 [1.0],[1.0]	-94.4,-94.5,-95.2 [1.3], [1.3], [1.0] -92.8,-97.5,-99 [1.0], [2.5], [2.5] [b]	-162,-185 [1.0], [1.0]	0.68	0.89
α-(3,4)	247 [1.0]	-89,-90,-93.4 [0.9],[0.9],[1.1]	none	0.67	0.33
β+γ-(3,4)	263,264 [1.4], [1.0]	-88.6,-91.0 [1.0] , [1.0] -92.9,-93.6 [1.0], [1.4] [b]	-157,-159 [1.1], [1.4]	0.33	0.67
α+γ+δ-(4,3)	251.0,252.0, [1.0], [1.0] 252.3 [0.8]	-83,-86.5,-87.2 [1.8], [1.8], [2.0]	none	0.76	0.43
δ+ε-(4,3)	267,268 [1.1],[1.1]	-72.4,-73.5[b] [0.9], [0.9]	-136, -139[b] [0.9], [2.4]	0.24	0.57
α-(5,2)	257 [0.9]]	-80 [1.1]	none	0.67	0.60
β-(5,2)	none	-66	none	0.33	0.40
γ-(5,2)	none	-67.6	none		
δ-(5,2)	none	-69	none		
α-(6,1)	264	none	none	0.35	0.20
β-(6,1)	none	-62	none	0.65	0.80

[a] Of the listed species only. [b] Other comparable species are also present, with additional resonances which cannot be fully distinguished from these.

5.1.2. Substitution into the Paratungstate-B Structure

In the same pH range as the heptametallates, but unlike molybdenum, tungsten also forms paratungstate-B $[H_2W_{12}O_{42}]^{10-}$. In contrast to paratungstate-A, it protonates with pK_a = 4.59. Figure 54 shows the tungsten spectrum of a solution at pH 5.8, with 1.43 mol dm^{-3} in W and in 0.57 mol dm^{-3} Mo. The dominant peaks are those

from paratungstate-B, but also six new smaller peaks in the area ratio 1:2:2:2:2:2 are observed over the entire stability range. The chemical shifts along with calculated shifts for the protonated anion are shown in Table 25. Figure 55 shows the tungsten chemical shifts of $[H_2W_{12}O_{42}]^{10-}$ and $[H_2MoW_{11}O_{42}]^{10-}$ as a solution 1.43 mol dm^{-3} in W and in 0.57 mol dm^{-3} Mo solution is acidified. The new resonances all fit to the same pK_a =4.9, *i.e.* a little higher than that for paratungstate-B. Clearly they arise from the replacement of just one W by Mo in the paratungstate-B structure.

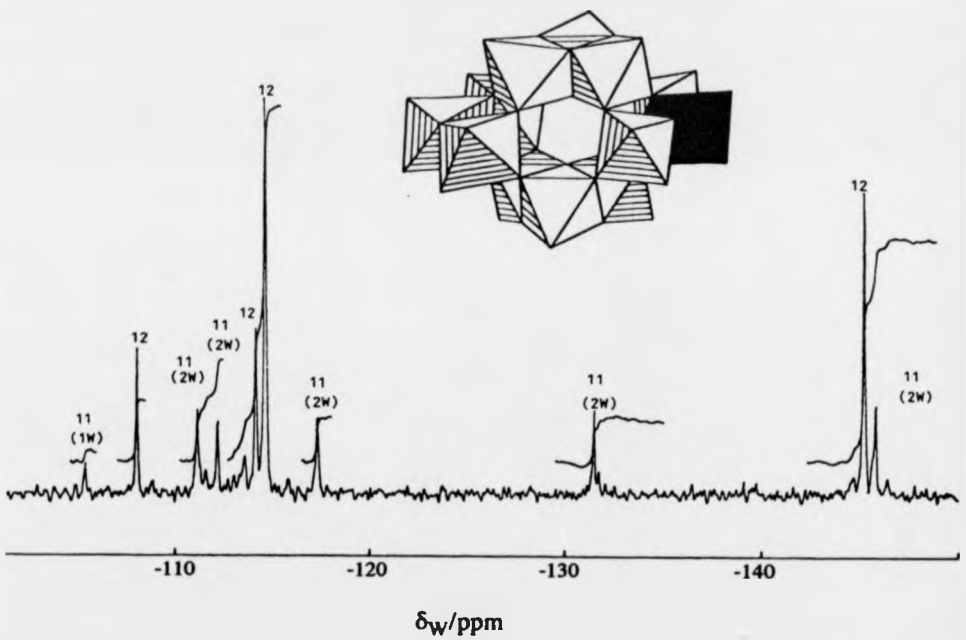

Figure 54. Proposed structure of $[H_2MoW_{11}O_{42}]^{10-}$, tungsten-183 NMR spectrum of (12), $[H_2W_{12}O_{42}]^{10-}$ and (11), $[H_2MoW_{11}O_{42}]^{10-}$, at pH 5.8, 293K with 1.43 mol dm^{-3} in W and 0.57 mol dm^{-3} in Mo.

Table 25. Tungsten chemical shifts (ppm at 293K) and relative integrals of $[H_2MoW_{11}O_{42}]^{10-}$ at pH 5.8 and the calculated chemical shifts of $[H_3MoW_{11}O_{42}]^{9-}$.

$[H_2MoW_{11}O_{42}]^{10-}$ δ_W	$[H_3MoW_{11}O_{42}]^{9-}$ δ_W	Relative integral	
-106	-117	1.2	(1)
-110	-94	1.9	(2)
-113	-132	1.8	(2)
-116	-105	1.9	(2)
-131	-131	2.1	(2)
-146	-145.7	2.1	(2)

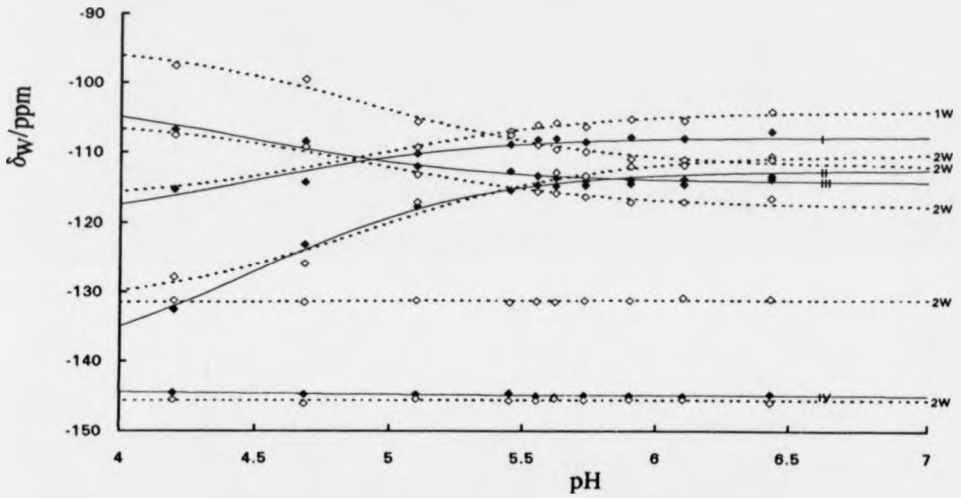

Figure 55. Tungsten chemical shifts *vs.* pH of the dodecametallates $[H_2W_{12}O_{42}]^{10-}$ (solid lines) and $[H_2MoW_{11}O_{42}]^{10-}$ (dotted lines) at 293K.

5.1.3. Substitution into the α-Keggin Structure

Below pH 4, isopolytungstate solutions form α- and β-Keggin species (see Chapter 4 section 4.2.3.), whereas molybdate solutions with Li^+ as counterion [116] form mainly octamolybdate, $[Mo_8O_{26}]^{4-}$. The tungsten NMR spectra of molybdotungstates in this pH region shows only one significant new species. Figure 56 shows a typical spectrum where 6 peaks arise, 1 from α-$[H_2W_{12}O_{40}]^{6-}$ and the

remaining 5, in the area ratio 2:2:1:2:2, from α-$[H_2MoW_{11}O_{40}]^{6-}$. The expected sixth resonance is overlapped by the unsubstituted anion. The chemical shifts of α-$[H_2MoW_{11}O_{40}]^{6-}$ are reported in Table 26.

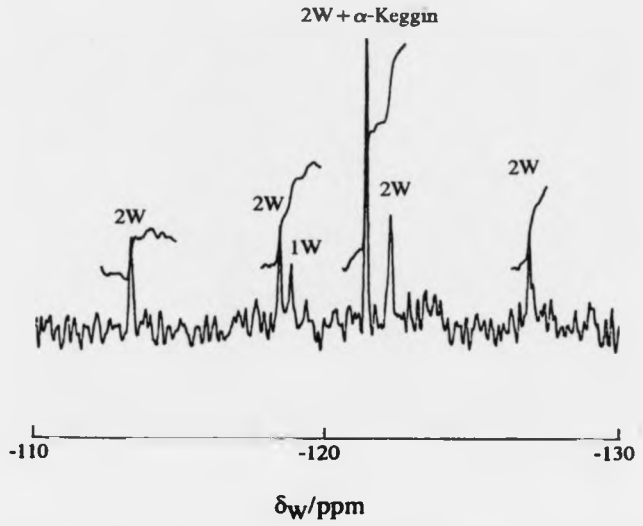

Figure 56. Tungsten-183 NMR spectrum of α-$[H_2MoW_{11}O_{40}]^{6-}$ at pH 2.2, 293K with 1.833 mol dm^{-3} in W and 0.167 mol dm^{-3} in Mo.

Table 26. Tungsten chemical shifts (ppm at 293K) and integrals for α-$[H_2MoW_{11}O_{40}]^{6-}$ at pH 2.2.

δ_W	Integral
-114.1	1.9[a] (2)[b]
-119.0	2.0 (2)
-119.5	1.0 (1)
-122.0	[c] (2)
-122.8	2.2 (2)
-127.6	1.9 (2)

[a] Measured relatiive integral, [b] notional relative integral. [c] Obscured by α-$[H_2W_{12}O_{40}]^{6-}$.

5.1.4. ^{95}Mo Chemical Shifts

As anticipated the ^{95}Mo NMR resonances of the above solutions are very broad (in excess 300 Hz) and it is also clear that exchange processes occur. Nevertheless, it is possible to gain some support for the shift trends discussed below. Figure 57 shows a typical spectrum obtained and Table 27 shows the chemical shifts and approximate integrals.

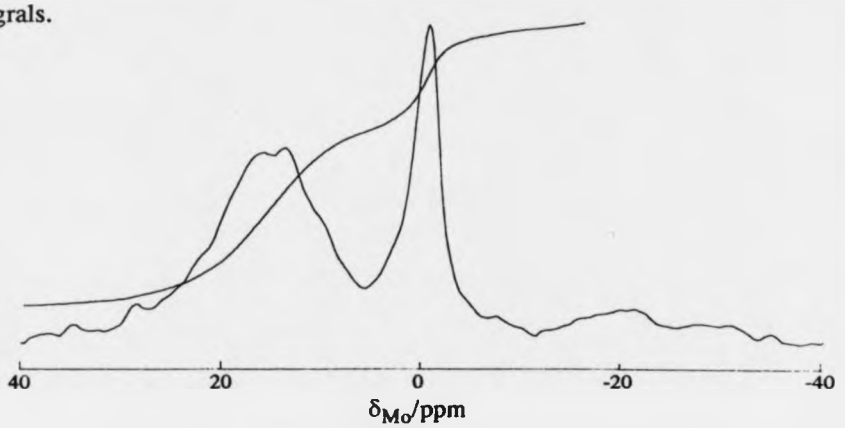

Figure 57. Molybdenum-95 NMR spectrum of a molybdotungstate solution at pH 6.2, 89°C, with 0.857 mol dm^{-3} in Mo and 1.143 mol dm^{-3} in W.

Table 27. Molybdenum chemical shifts (ppm) and integrals at 89°C

Metal Ratio Mo:W, in the solution	δ_{Mo}	Linewidth[a]	Relative Integral
all Mo (*i.e.* $[Mo_7O_{24}]^{6-}$)	28.5	320	(1.00)
5:2	21.5	500	0.98
	-9.0	170	0.02
3:4	18.3	580	0.85
	1.8	120	0.09
	-14.0	140	0.02
	-21.0	200	0.04
2:5	13.3	330	0.69
	-8.6	290	0.10
	-22.8	360	0.21

[a] Width measured at half height in Hz, after removal of broadening due to window function.

5.1.5. Equilibrium Constants

The present system of species presents unusual problems of definition and of mathematical treatment, for any equilibrium analaysis. The $[WO_4]^{2-}$ anion could not be detected in the present solutions. Even $[W_7O_{24}]^{6-}$ appears in one pH=6 solution only, as a minor species in comparison with $[H_2W_{12}O_{42}]^{10-}$. The amounts of mono and heptamolybdate also could not be measured quantitatively. ^{95}Mo NMR is insufficiently sensitive. However, an indirect assessment of Mo concentrations in all the molybdotungstate species could be obtained from the tungsten NMR data. The concentration of "free" Mo was obtained by subtracting this sum from the known total Mo. At pH=6, ["free" Mo] was found to lie between 12 and 57%, and preponderantly at >40%. At pH=5, however, most Mo was bound in the molybdotungstate anions. The "free" molybdate should be present as $[Mo_7O_{24}]^{6-}$ and $[MoO_4]^{2-}$. In the equilibrium calculations, we chose to use $[Mo_7O_{24}]^{6-}$ and $[W_7O_{24}]^{6-}$ as components. This makes possible a direct comparison of all the possible heptametallate constants. The equilibria are written as:

$$p\mathrm{H}^+ + q[\mathrm{Mo_7O_{24}}]^{6-} + r[\mathrm{W_7O_{24}}]^{6-} \leftrightarrow (\mathrm{H}^+)_p\,([\mathrm{Mo_7O_{24}}]^{6-})_q\,([\mathrm{W_7O_{24}}]^{6-})_r$$

This unusual choice of components is feasible because LAKE can treat non-integer values of the stoichiometric constants p, q and r. The species matrix used is shown in Table 28. Preliminary calculations showed that it was essential to allow not only the molybdotungstate formation constants but also that for $[MoO_4]^{2-}$ to co-vary in order to obtain self-consistent constants from the data at both pH values. The fitted curves in Figures 52(a) and 52(b) have been calculated from these constants.

Since $[W_7O_{24}]^{6-}$ is only present in very small amounts, and only then at pH=6, the (0,12) constant had to be fixed solely for the pH=6 data. For the same reason, all the constants may be in error by some fixed amount. They also have fairly large errors, which are reflected in the 3σ values in Table 28.

Table 28. Relative log formation constants[a] for molybdotungstate species at pH 5 and 6.

species	(1,6)	(2,5)	(3,4)	(4,3)	(5,2)	(6,1)	(0,12)	H(0,12)	(1,11)	H(1,11)	(1,0)
p(for H)	0	0	0	0	0	0	0.286	1.286	.286	1.286	-1.143
q(for Mo)	.143	.286	.429	.571	.714	.857	0	0	.143	.143	.143
r(for W)	.857	.714	.571	.429	.286	.143	1.714	1.714	1.571	1.571	0
log(K)obs., pH= 5 and 6	1.57	2.63	3.14	3.34	2.85	1.88	4.68	9.18[b]	4.73	9.18[b]	-6.07
$\pm 3\sigma$	0.37	0.39	0.44	0.52	0.41	0.61	0.65	(0.65)[c]	0.61	(0.62)[c]	.15[c]

[a] Relative to (0,7) and (7,0) = 0, [b] *via* the pK_a value, [c] probably an underestimate.

5.2. Molybdotungstate Discussion

5.2.1. Substitution into the Paratungstate-A Structrure

Considering the above problems, the fits of the equilibrium constants in Table 28, to the experimental variation of species concentration with metal ratio, shown in Figures 52(a) and 52(b), are surprisingly good. The trends shown by these constants are analysed below.

It is, however, clear from the data in Table 28, that there is some site preference. For example, on purely statistical grounds we would predict a ratio of 4:1 for the (6,1) species with Mo in the capping II site (Figure 50) to the isomeric species with Mo in the central I site. The experimental value is in fact 2:1. Furthermore, no isomer with W at the III sites was observed. By the same token, the substitution ratio of Mo at the sites II, III and I for the (1,6) isomers should be 4:2:1 respectively. In reality, the ratio, is 1:2:0. These ratios are, as expected, independent of pH.

The observed site preferences are all semiquantitatively consistent with a simple site-preference model. The model assumes that the preference of Mo relative to W

for site I (see Figure 50) is given by the variable *I*, and that corresponding variables *II* and *III* exist for sites II and III. These 3 variables are normalised, so that the total effect of the seven substitutions that lead from $[W_7O_{24}]^{6-}$ to $[Mo_7O_{24}]^{6-}$ lead to no net change in the normalised equilibrium constant, so that $I \times II^4 \times III^2 = 1$. However, the corresponding changes for each intermediate, mixed-metal species will not also be unity, and they will enable the isomeric proportions to be predicted algebraically for a set of species with given metal ratio. For example, the expected concentration ratio for the two main $[MoW_6O_{24}]^{6-}$ species, namely α (one Mo at site III) and β (one Mo at site II) is $(2 \times III)/(4 \times II)$, after due allowance for the number of available sites of either type.

The same three variables also predict the ratios of the equilibrium constants, listed in Table 28, because these are also normalised relative to the (0,7) and (7,0) extremes. The total relative probability for a given metal ratio is then obtained from the summation of the relative probabilities for each possible isomer, with appropriate weightings for symmetry-related species. Then by using standard software the resulting predictions can be optimised to the data given in Tables 24 and 28. Only one further variable is required at each pH, namely a fixed scaling multiplier for the constants presented as logarithms in Table 28, to compensate for the probability that the relative values for the mixed-metal species are considerably more reliable than those for the (low abundance) (0,7) and (7,0) species. The fits are shown in Table 29. It is evident that W prefers a I site (relative to a II site) by a factor of 3.0 and Mo prefers a III site, relative to a II site, by a factor of 4.3. There is no evidence, within the admittedly large experimental error, for any effects from metal substitutions at neighbouring sites.

Table 29. Fit of single-site model to pH 6 data.

species (Mo:W)	log K (obs.)[a]	log K (calc.)	isomer ratio:	(obs.)	(calc.)
(0,7)	(0)	(0)			
(1,6)	0.46	1.00	α/β	2.0	2.2
(2,5)	1.52	1.57	$\alpha/(\beta+\gamma)$	0.5	0.5
(3,4)	2.03	1.83	$\alpha/(\beta+\gamma)$	2.0	2.2
(4,3)	2.23	1.83	$(\alpha+\beta+\gamma)/(\delta+\varepsilon)$	3.0	3.2
(5,2)	1.74	1.55	$\alpha/(\beta+\gamma+\delta)$	2.0	2.0
(6,1)	0.77	0.98	α/β	0.5	0.7
(7,0)	(0)	(0)			

calculated site preferences: I = 0.26, II = 0.77, III = 3.31.
[a] Scaling parameter (See text): log K for (1,6) to (6,1) increased by 1.11.

These preferences may be explained by considering the structurally related decavanadate ion $[V_{10}O_{28}]^{6-}$, where the electron density at each atom has been calculated by Bénard *et al.* [178]. It is lowest at the central V atoms. These atoms also have the highest ^{51}V NMR shift, presumably because of the way the shift is dominated by the variation of the orbital radius term $\langle r_d^{-3} \rangle$. A low electron density implies compact d-orbitals. Therefore in the heptametallate structure we may deduce from the corresponding and well-spaced tungsten shifts that the central, I site in the heptametallate structure has the lowest electron density, and again from the chemical shifts, that the III site has the highest electron density. Clearly then, Mo prefers a site with high electron density and W, one with relatively less. It is known that tungsten [VI] forms stronger bonds to oxygen than Mo [VI] [11]. This manifests itself in lower shifts for O bound to W than for O bound to Mo, at comparable positions in comparable compounds, because of the increase in average excitation energy. Consequently because of these stronger bonds, W is less disfavoured by the generally lower availability of O electrons at sites I than is Mo. It would therefore appear that the central W atom stabilises the polyanion by resisting the tendency for negative charge to accumulate at its periphery. The

behaviour of Mo is the opposite by default. The tungsten shifts discussed below are consistent with this proposal.

Because Mo is less able to take electrons from the O atoms surrounding it, these are therefore more readily protonated. This explains our general observation that, in isostructural compounds, the polytungstates generally have lower pK_a values than the polymolybdates (see Chapters 4 and 6). The above data for (0,12) and (1,11) confirm this trend in pK_a.

5.2.2. Substitution into the Paratungstate-B Structrure

From the shift data in Figure 55 the structure of the monosubstituted dodecatungstate maybe derived with some confidence. The fact that the area ratio of its resonances is 1:2:2:2:2:2 implies a species which retains some of the symmetry. It follows therefore, that Mo substitutes at either I site or the II site, as labelled in Figure 50. Now if we assume that these two species have very similar distributions of charge, we can predict that the set of six W resonances from (1,11) will have shifts and pH dependences reasonably close to those of the four W resonances in (0,12). Figure 55 bears this out. The figure shows the fitted curves derived from a least squares fit to equation (2.22) (see Chapter 2, section 2.4). The single-W resonance of (1,11) corresponds to the I resonance of (0,12), and therefore indicates that Mo has been substituted at one of these two I sites. Also, as anticipated both III and IV resonances of (0,12) each split into equal halves. A further consequence of similar pH dependence of the resonances is that the protonation site is unaffected by the Mo substitution. It also supports the assertions made for (0,12) (see Chapter 4 section 4.2) that protonation occurred away from the I octahedron, and mainly at O_g. We may also note that the largest perturbation of shift upon substitution is at two of the four IV site tungstens, presumably those nearest to the Mo at site I.

The I site preference for Mo substitution in the paratungstate-B structure cannot be explained by a simple extension of the argument given above for paratungstate-A. This is because the tungsten shifts in paratungstate-B are much closer together than those of paratungstate-A, and thus the above argument concerning electron density is less reliable. However, the Mo site preferred is in fact in either anion the one furthest from the anionic centre, which probably means the site with the greatest negative charge.

5.2.3. Substitution into the α-Keggin Structure

Pope has already shown that V^V substitutes one of the tungsten atoms in α-$[H_2W_{12}O_{40}]^{6-}$ and he argues from both the single vanadium resonance and the proton shift of the two encapsulated protons that this yields α-$[H_2VW_{11}O_{40}]^{7-}$ [50,141]. The corresponding ^{183}W NMR spectrum of α-$[H_2MoW_{11}O_{40}]^{6-}$ yields six resonances in the area ratio (2:2:1:2:2:2). These are listed in Table 26. The area ratios favour the α-Keggin structure because the β- isomer would have to be substituted solely at just one of its two sets of 3 equivalent tungsten atoms, in order to retain a plane of symmetry and also to remain a single species. Even if this were the case, a much greater range of shifts would be expected because the unsubstituted β-Keggin anion has resonances between -112 and -136 ppm (see Chapter 4 section 4.1.) whereas the shifts for the substituted species range from -114.1 to -127.6 ppm (the unsubstituted α-Keggin resonates at -123 ppm). The relatively smaller spread of tungsten chemical shifts observed in this molybdotungstate species compared with the tungstovanadate isomer (see next chapter) is presumably because the Mo bears the same +6 charge as W. It must therefore, perturb the charge distribution less than the +5 on the vanadium atom. A further consequence of having a similar charge is that the molybdotungstate is stable in the same pH range as the unsubstituted anion.

5.2.4. Chemical Shifts

Different trends are evident from Table 24 that for shifts of the distinct tungsten sites in the heptametallates as the substitution by Mo increases. Tungstens remaining at positions II and III exhibit a general increase of shift with Mo substitution, whereas central tungsten, I, exhibits much smaller changes, in the other direction, which correlate reasonably with the asymmetry of its environment. For example, the average shifts of the II (capping) tungstens for the most stable isomer, in the series (0,7), (1,6) through to (6,1) is -106, -101.2, -96.6, -91, -85.6, -80 and -62 ppm respectively. Moreover, shifts of distinguishable II sites within one isomer do not vary much. In contrast, the averaged shifts of the central tungstens I in each metal ratio for the same series is 268, 263.5, 253, 258, 257, 264 ppm respectively.

These shifts may be interpreted as follows. The fact that ^{17}O NMR shifts of isopolymolydates are larger than those of corresponding isopolytungstates [11], implies that the W prefers to bear a higher anionic charge, and forms stronger π-bonding to the oxygen. Therefore, upon Mo substitution for W, the local bond energy at the substitution site is lowered and because of some delocalisation through the metal oxygen $d\pi$-$p\pi$ bonding network the whole anion is affected. As a result, the average excitation energy at all metal centres is reduced. Consequently, this increases all the W shifts, in approximate proportion to the degree of Mo substitution. In addition, the increase is reasonably independent of position except for the central tungsten I. Here the influences are particularly masked by slight gains of negative charge as the surrounding substitutions of Mo for W release electrons.

Assignment of the ^{95}Mo shift data in Table 27 to specific species is not possible. However, there is clearly a similar trend, in reverse of course, for the Mo shifts. The shifts of each region, where resolved, decrease with increasing W substitution.

Thus Table 27 shows the stabilising effects of W in two distinct ways, through shifts and in a reduction of lability.

Similar trends are observed for the substituted dodecametallates. All the shifts of the remaining W atoms in paratungstate (1,11) are lowered upon substitution by one Mo except the site III tungsten. The variation in lowering of the shifts may be because the extent of delocalisation, as proposed above, is restricted in such a large, open structure. A similar result is obtained when the (1,11) Keggin species is compared with the corresponding (0,12) isopolytungstate. The shifts of three of the remaining tungstens increase and only one is significantly reduced, even though in this case the Mo_6 octahedra lie in groups of 3, corner-linked by single bridging oxygens rather than edge-linked, and therefore, delocalisation is restricted even more.

5.2.5. Kinetics of Substitution

Attempts were made using both ^{183}W and ^{17}O NMR spectroscopy to determine the rate of Mo substitution into paratungstate-A, but these were severely hampered by poor signal to noise which precluded any direct reliable integral measurements of these mixed heptametallates. It was therefore only possible to follow decomposition of paratungstate-B and molybdate using ^{183}W and ^{17}O NMR spectroscopy respectively. Any calculation of the rate expressions or rate constants would necessitate accurate concentrations of all the species present. It was therefore, only feasible to approximate the rate of decomposition using zero order kinetics. Figure 58 shows the decomposition of paratungstate-B over the first 40 hrs. and also shows the simple fit to zero order kinetics reveals a rate of -0.4 %/hr.. The ^{17}O NMR spectroscopy at natural abundance was less successful and no significant change was observed.

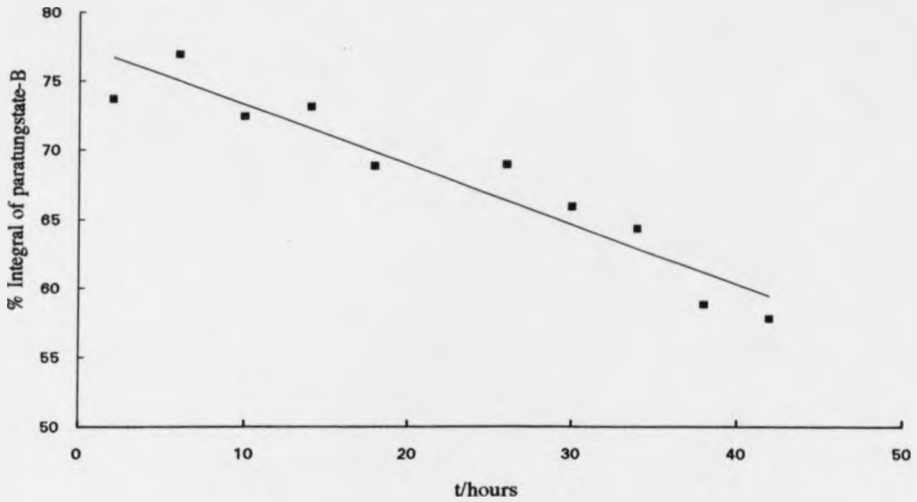

Figure 58. The decay of paratungstate-B concentration (tungsten-183 integral) *vs.* time when 1 ml of 2M molybdate solution is added to 2ml of 2M tungstate solution at pH7.

6. TUNGSTOVANADATES

6.1. Tungstovanadate Results

6.1.1. ^{51}V NMR Chemical Shifts and Assignments

Figures 59 and 60 show the vanadium chemical shifts observed at various pH values, as aqueous tungstovanadate solutions in the metal ratios, 20:80 and 50:50 mmol dm^{-3} (W:V) respectively, are acidified at 89°C. (The tetrahedral (0,n) vanadate species are not shown.) Similar pH dependences are obtained at room temperature although with generally poorer resolution and with shifts to lower frequencies. The figures show the fitted curves derived from a least squares fit to equation (2.22) (see Chapter 2, section 2.4). As with other tungstate systems previously studied [11], the equilibria are very slow and often involve metastable species. Indeed, we have followed the equilibration of acidic tungstovanadate solutions at room temperature by ^{51}V NMR and have seen changes in one case over a period of three months. Our investigation has also shown that solutions allowed two days to approach equilibrium did reach a pseudo equilibrium condition. That is to say that there was very little change observed in the ^{51}V NMR spectra recorded at 20°C, those repeated at 20°C after heating the solutions to 89°C for two hours, and those recorded up to a week later. After this period, however, changes were observed as more metastable species formed and these were beyond the scope of the present work. The proposed structures for the tungstovanadate species identified are illustrated in Figure 61. There is no evidence for any substitution into paratungstate-A or -B. The shift values for the component species, at both 89° and 20°C are reported in Tables 30 and 31 respectively. Possible ambiguities have been removed using peak intensity and two-dimensional COSY data. Typical 1D and 2D ^{51}V NMR spectra are shown in the discussion below. Some of these results have already been published [156] and a copy of this paper is shown in the Appendix.

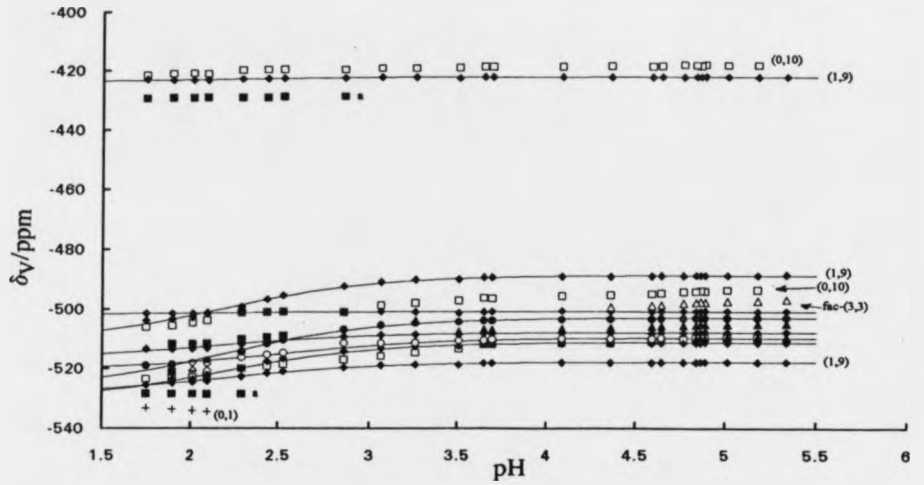

Figure 59. Dependence of vanadium-51 NMR resonances on pH 89°C, 20 mmol dm^{-3} in W and 80 mmol dm^{-3} in V. The resonances of the tetrahedral (0,n) vanadate species are not shown. The omitted labelling of the closely spaced peak series correspond with those shown in Figure 60. Experimental points: □ = (0,10), ◆ = (1,9), ■ = a (species has not been identified), Δ = *fac*-(3,3), • = *cis*-(4,2), ▲ = *mer*-(3,3), ○ = *trans*-(4,2), × = (5,1), + = (0,1).

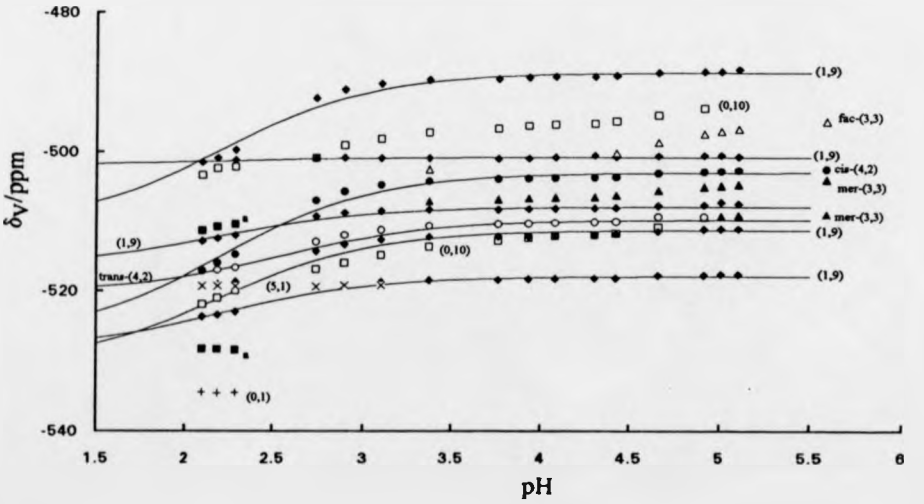

Figure 60. Dependence of vanadium-51 NMR resonances in the -540 to -430 ppm region on pH, 89°C, 50 mmol dm^{-3} in both V and W. Experimental points: □ = (0,10), ◆ = (1,9), ■ = a (species has not been identified), Δ = *fac*-(3,3), • = *cis*-(4,2), ▲ = *mer*-(3,3), ○ = *trans*-(4,2), × = (5,1), + = (0,1).

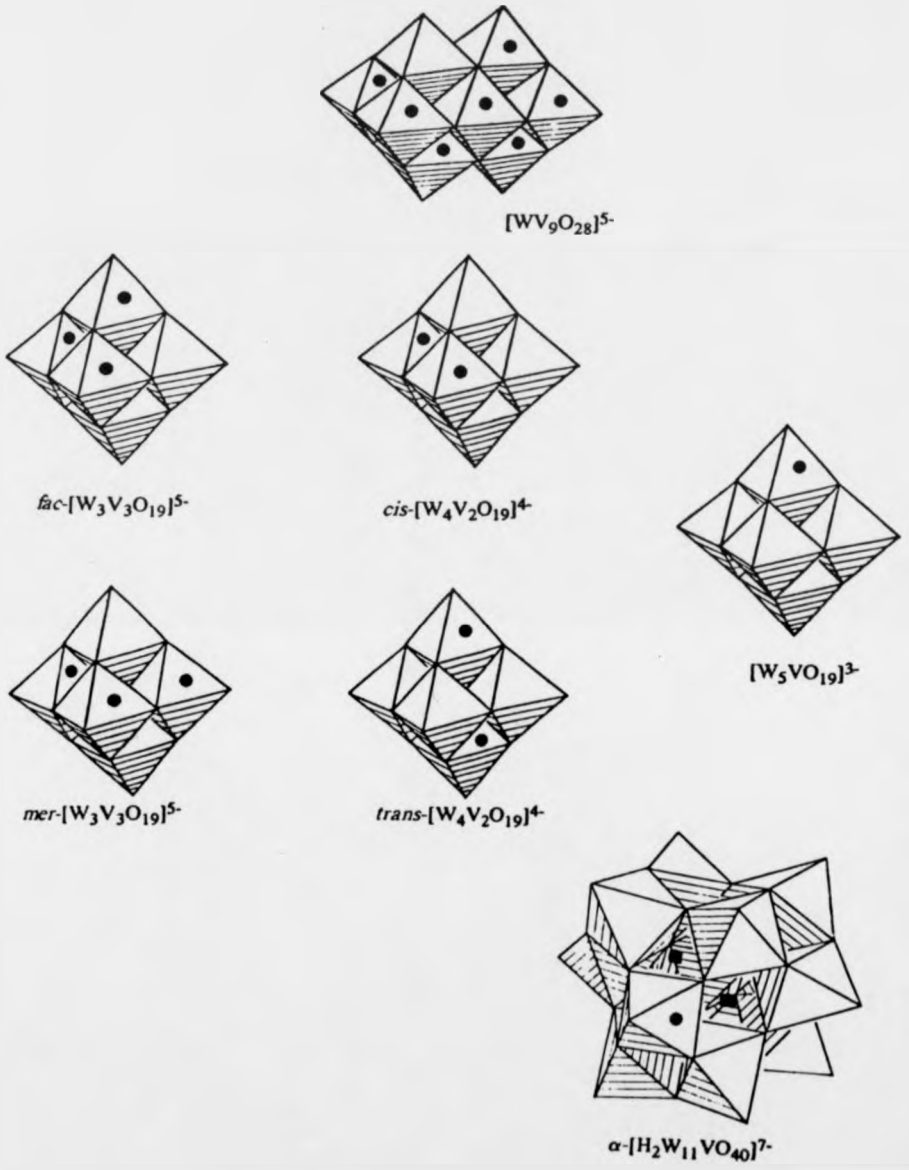

Figure 61. Proposed structures for the tungstovanadate species identified. (• = vanadium sites)

Table 30. Vanadium-51 chemical shifts (ppm) and actual relative integrals of the component species at 89°C.

Peak	$[WV_9O_{28}]^{5-}$ (15,1,9)[a]		$[HWV_9O_{28}]^{4-}$ (16,1,9)[a]
	δ_V		δ_V
(1,9)1	-421.9[b]	(1.7V)[c]	-422.9[b]
(1,9)2	-488.2	(1.9V)	-501.5
(1,9)3	-500.7	(2.1V)	-501.5
(1,9)4	-507.5	(1.1V)	-512.9
(1,9)5	-511.2	(1.1V)	-519.3
(1,9)6	-517.7	(1V)	-523.7
	$[V_{10}O_{28}]^{6-}$ (14,0,10)		$[HV_{10}O_{28}]^{5-}$ $[H_2V_{10}O_{28}]^{4-}$
(0,10)1	-418.3	(2.0V)	[d]
(0,10)2	-495.4	(3.9V)	[d]
(0,10)3	-511.6	(2.1V)	[d]
	mer-$[W_3V_3O_{19}]^{5-}$ (8,3,3)		*mer*-$[HW_3V_3O_{19}]^{4-}$ (9,3,3)
(3,3)1	-504.7	(1V)	-507.4
(3,3)2	-509.2	(2.1V)	-510.7
	fac-$[W_3V_3O_{19}]^{5-}$ (8,3,3)		*fac*-$[HW_3V_3O_{19}]^{4-}$ (9,3,3)
	-496.7	(3V)	-499.3
	cis-$[W_4V_2O_{19}]^{4-}$ (8,4,2)		*cis*-$[HW_4V_2O_{19}]^{3-}$ (9,4,2)
	-503.5	(2V)	-517.2
	trans-$[W_4V_2O_{19}]^{4-}$ (8,4,2)		*trans*-$[HW_4V_2O_{19}]^{3-}$ (9,4,2)
	-509.4	(2V)	-517.0
	$[W_5VO_{19}]^{3-}$ (9,5,1)		
	-519.4	(1V)[e]	
	α-$[H_2W_{11}VO_{40}]^{7-}$ (17,11,1)		
	-536.4	(1V)[d]	
	$[VO_2]^+$ (3,0,1)		
	-534.0	(1V)	

[a] (p,q,r) shorthand notation for H^+, $[WO_4]^{2-}$ and $[HVO_4]^{2-}$. [b] Raised to 89°C, referenced to $VOCl_3$ at 20°C. [c] Measured relative integral within each species. [d] Obscured. [e] Independent of pH.

Table 31. Vanadium-51 chemical shifts (ppm) and relative notional integrals of the component species at 20°C.

Peak	$[WV_9O_{28}]^{5-}$		$[HWV_9O_{28}]^{4-}$
	δ_V		δ_V
(1,9)1	-428[a]	(2V)[b]	-428.2[a]
(1,9)2	-496.3	(2V)	-499.1
(1,9)3	-507.8	(2V)	-507.8
(1,9)4	-513.8	(1V)	-516.5
(1,9)5	-518.6	(1V)	-525.4
(1,9)6	-525.7	(1V)	-526.6
	$[V_{10}O_{28}]^{6-}$		$[HV_{10}O_{28}]^{5-}$ $[H_2V_{10}O_{28}]^{4-}$
(0,10)1	-423.3	(2V)	[c]
(0,10)2	-497	(4V)	[c]
(0,10)3	-513.5	(4V)	[c]
	mer-$[W_3V_3O_{19}]^{5-}$		*mer*-$[HW_3V_3O_{19}]^{4-}$
(3,3)1	-513.0	(1V)	-513.7
(3,3)2	-518.0	(2V)	-518.5
	fac-$[W_3V_3O_{19}]^{5-}$		*fac*-$[HW_3V_3O_{19}]^{4-}$
	-501.4	(3V)	-505.9
	cis-$[W_4V_2O_{19}]^{4-}$		*cis*-$[HW_4V_2O_{19}]^{3-}$
	-511.4	(2V)	-522.2
	trans-$[W_4V_2O_{19}]^{4-}$		*trans*-$[HW_4V_2O_{19}]^{3-}$
	-518	(2V)	[c]
	$[W_5VO_{19}]^{3-}$		
	-526.5	(1V)	
	α-$[H_2W_{11}VO_{40}]^{7-}$		
	-542.8	(1V)	
	$[VO_2]^+$		
	-544.7	(1V)	

[a] At 20°C , referenced to $VOCl_3$ at 20°C , [b] relative notional integral, number of vanadium atoms within each species and [c] obscured. The proposed assignments are dicussed below.

6.1.2. ^{17}O NMR Chemical Shifts and Assignments

A typical ^{17}O NMR spectrum is shown in Figure 62. The peaks were mainly assigned by area and by analogy with decavanadate [136] and the molybdovanadates previously studied [25,26]. Detailed assignments are tabulated and illustrated with successive layer diagrams in the discussion below. Figure 63 shows the oxygen chemical shifts observed at various pH values, as an aqueous tungstovanadate solution with 250 mmol dm^{-3} in both V and W is acidified. The only oxygen resonances to show a significant decrease in shift upon protonation are O_h for *cis*-(4,2) and, $O_c + O_{c'}$ for (1,9).

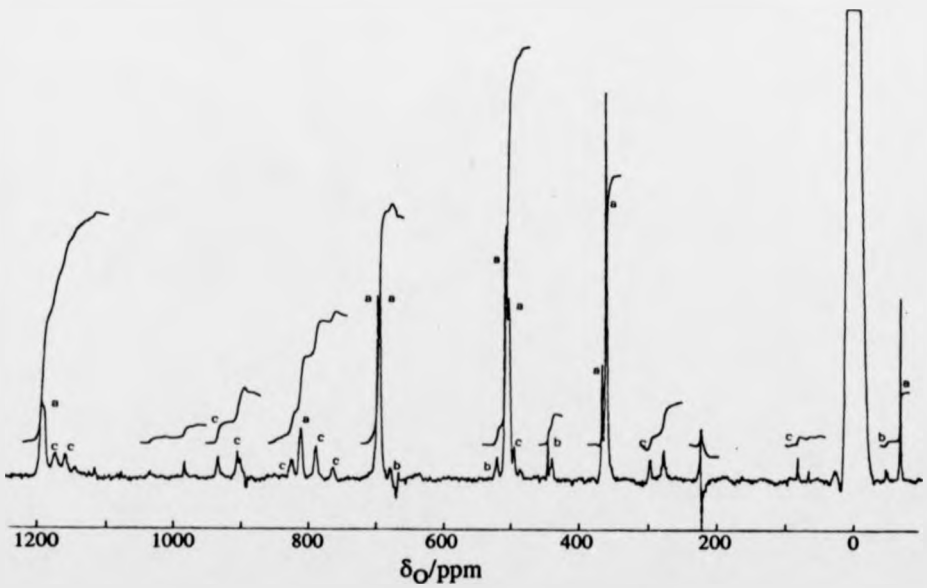

Figure 62. A typical oxygen-17 NMR spectrum of a solution at 20°C with 250 mmol dm^{-3} in both W and V. Species: a, *cis*-(4,2); b, *fac*- and *mer*-(3,3); c, (1,9).

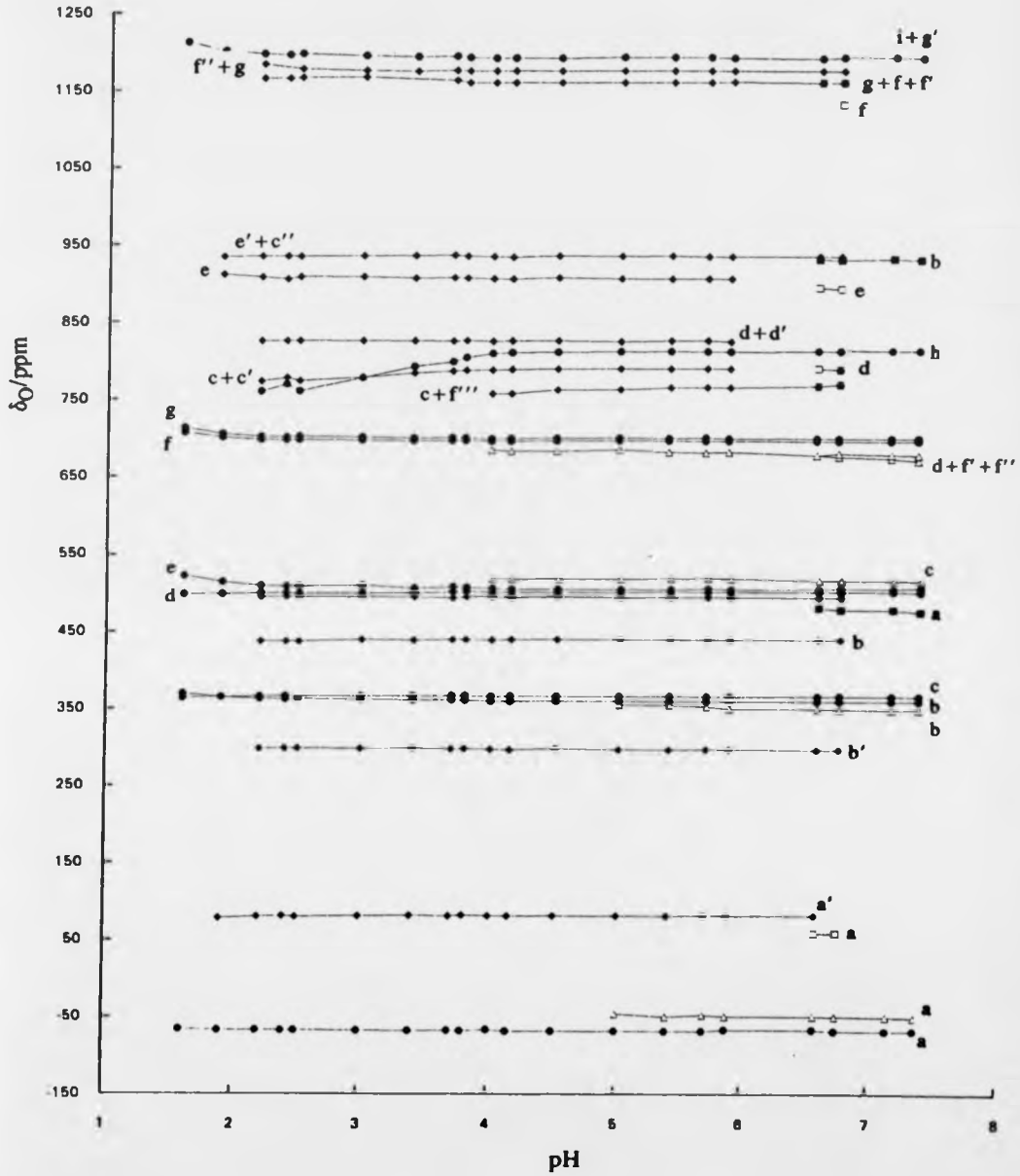

Figure 63. Dependence of oxygen-17 NMR resonances on pH at 20°C with 250 mmol dm^{-3} in both W and V. The lines serve merely to highlight peak series. Experimental points: • = *cis*-(4,2), □ = (0,10), ◆ = (1,9), ■ = (0,4) and (0,5), Δ = *fac*-(3,3) and *mer*-(3,3).

6.1.3. ^{183}W NMR Chemical Shifts and Assignments

The tungsten NMR data in Table 32 are restricted to the major species because of the low receptivity of the ^{183}W nucleus and the couplings to vanadium which broaden the resonances. Assignments were confirmed by the integrals of the vanadium resonances of the same species.

Table 32. Tungsten chemical shifts at 294K/ppm

Species	Linewidth[a]	δ_W	Relative Integral
$[WV_9O_{28}]^{5-}$	4.54	74.5	
cis-$[W_4V_2O_{19}]^{4-}$	46.3	69.0	
α-$[H_2W_{11}VO_{40}]^{7-}$	2.9	-111.6	2.34 (2W)
	1.4	-119.8	1.87 (2W)
	b	-121.3	1.87 (2W)
	b	-121.5	1.17 (1W)
	1.5	-124.0	1.87 (2W)
	2.2	-132.7	1.87 (2W)

[a] Width measured at half height in Hz, after removal of broadening due to window function.
[b] Partially overlapped

6.2. Tungstovanadate Discussion

It is first easiest to discuss each species in turn.

6.2.1. *cis*-$[W_4V_2O_{19}]^{4-}$ and $[HW_4V_2O_{19}]^{3-}$

This anion has previously been characterised by Pope and Leparulo-Loftus [143]. The *cis*-(4,2) species [(n,m) is shorthand for the species $[W_nV_mO_x]^{(2x-6n-5m)-}$] exhibits a single, sharp, vanadium resonance at δ_V = -511.4, and on raising the temperature to 89°C, there is a small shift to higher frequency δ_V = -503.5 ppm. At lower pH the species protonates with a pK_a of *ca.* 2.1 (20°C) and 2.2 at (89°C) (see Figure 60). The comparatively large effect of protonation upon the vanadium

chemical shift (-13.7 ppm) is consistent with protonation at the unique V-O-V oxygen atom as originally suggested by Kazanskii [47]. The unprotonated *cis*-(4,2) species dominated the ^{51}V NMR spectra at fairly high W:V metal ratios. It typically accounted for 45% of the vanadium present in solutions with (W:V, 50:50 mmol dm^{-3}, pH 3-7) or 9% in (W:V, 20:80 mmol dm^{-3}, pH 3-7).

The somewhat sharper ^{51}V NMR resonance of *cis*-(4,2) compared with those of (1,9) and the (11,1) species implies a longer relaxation time for the vanadium nucleus in *cis*-(4,2). Consequently, the ^{51}V quadrupolar couplings to other nuclei in the *cis*-(4,2) species are less strongly decoupled by relaxation and thus broad ^{17}O and ^{183}W NMR resonances are observed. In fact, in our ^{17}O NMR spectra $^{1}J_{VO}$ = 120 Hz couplings were measured.

The ^{17}O NMR spectrum of this anion is readily assigned because of its high concentration, symmetry, integrals and visible vanadium couplings. The assignments shown in Table 33 and Figure 64 confirm the conclusions made by Maksimovskaya and Chumachenko [145]. The protonation site indicated above is further supported by the V-O-V bridging oxygen resonance, O_h at δ_O = 811 ppm shifting substantially to lower frequency, δ_O =762 ppm upon acidification.

Table 33. Oxygen-17 chemical shifts at 294K /ppm and relative integrals of *cis*-$[W_4V_2O_{19}]^{4-}$.

Peak label	*cis*-$[W_4V_2O_{19}]^{4-}$ δ_O	Relative Integral		*cis*-$[W_4V_2O_{19}]^{4-}$ δ_O
a[a]	-68.2	1	(1)	-67[b]
b	360.0	4	(4)	361
c	366.3	1.29	(1)	368
d	502.3	2.12	(2)	510
e	507.8	4.23	(4)	510
f	693.9 or 697.4	2.29	(2)	695
g	693.9 or 697.4	2.29	(2)	698
h	810.9	1.06	(1)	814
i	1191	2.12	(2)	1190

[a] Labelling as per Figure 14 (b). [b] Oxygen-17 NMR chemical shifts from [148].

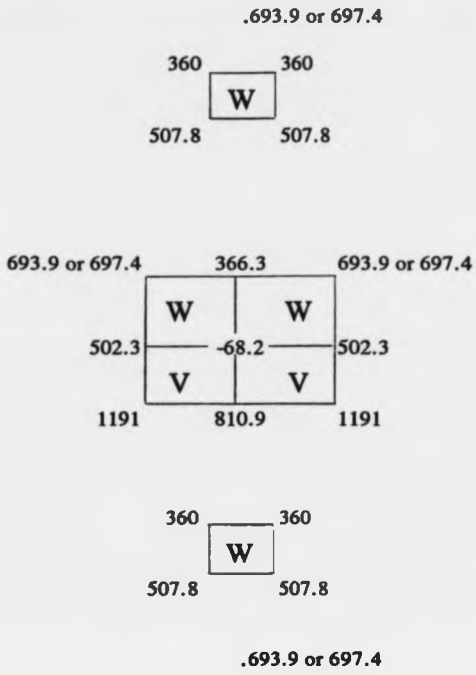

Figure 64. Successive layer diagram structure of species *cis*-(4,2) with oxygen chemical shifts at 294K assigned as in the text.

6.2.2. *trans*-$[W_4V_2O_{19}]^{4-}$ and $[HW_4V_2O_{19}]^{3-}$

This anion was assigned to a small, sharp, single resonance (peak series labelled *trans*-(4,2) in Figure 60) because it exhibits the same dependence on concentration and metal ratio, and has a similar pK_a *ca.* 2.5 (89°C) to *cis*-(4,2). The vanadium shift for the anion is δ_V = -517.2 ppm at 20°C. On raising the temperature to 89°C, this becomes δ_V = -509.4 and on protonation at this temperature δ_V moves to -518 ppm. The *trans*- geometry of the vanadium atoms is supported by the relatively smaller difference in the vanadium chemical shift upon protonation -8.6 ppm, compared with -13.7 ppm for the *cis*-(4,2) isomer. This is because protonation is no longer taking place at a single V-O-V site as it would with a *cis*- arrangement.

Furthermore, the chemical shift is commensurate with isolated VO_6 octahedra [143]. The *trans*-(4,2) species only represented 1% of the total vanadium present in solutions with (W:V, 50:50 mmol dm^{-3}) over the pH 3 to 7 range. Consequently we were unable substantiate this proposal with ^{17}O NMR data. However, the simple ^{51}V NMR spectrum in Figure 65, only has two peaks in the shift region for octahedral V [143], the major resonance being *cis*-(4,2) and the other *trans*-(4,2). This at least rules out the possibility of any other resonance being involved unless of course this resonance were under the *cis*-(4,2), but this is unlikely since no cross peaks were observed in the COSY spectrum.

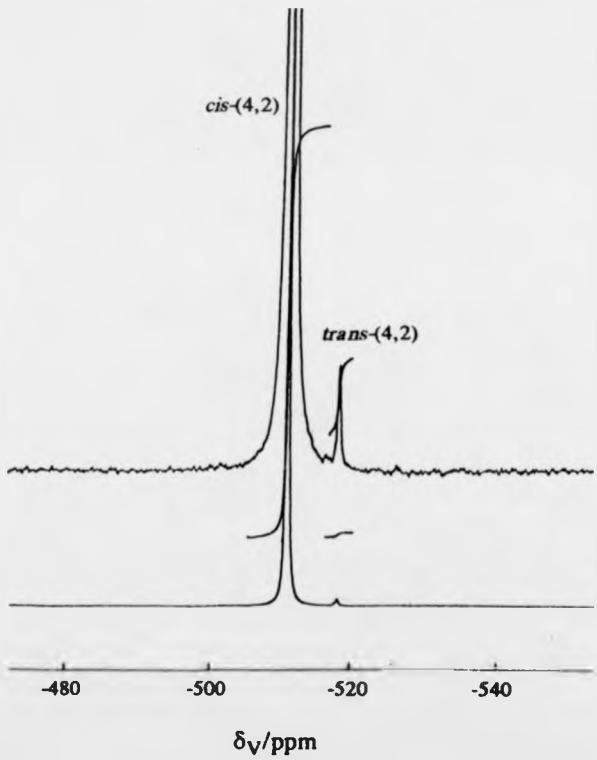

Figure 65. Vanadium-51 NMR spectrum of a solution at pH 7.0, showing species *cis*- and *trans*-(4,2), 80 mmol dm^{-3} in tungsten and 20 mmol dm^{-3} in vanadium at 20°C.

6.2.3. $[W_5VO_{19}]^{3-}$

This ion has already been identified in both acetonitrile by Klemperer and Shum [41] and in aqueous solutions by Pope and Leparulo-Loftus [143]. We confirm these earlier results, that this anion yields a narrow, pH independent resonance at δ_V = -526.5 at 20°C and -519.4 ppm at 89°C (see Figure 60). The resonance appears below pH 3, and its narrowness must be due to the near-zero field gradient at V, which arises because this atom is confined to an internal diagonal of the double octahedron structure.

The ^{17}O NMR assignments and integrals shown in Table 34 and Figure 66 are in good agreement with those reported by Klemperer and Shum [41].

Table 34. Oxygen chemical shifts at 294K /ppm and relative integrals of $[W_5VO_{19}]^{3-}$.

Peak label	$[W_5VO_{19}]^{3-}$ δ_O	Relative Integral	$[W_5VO_{19}]^{3-}$ δ_O
a[a]	-76.2	0.67 (1)	-75[b]
b	385	4.67 (4)	389
c	403	4.44 (4)	395
d	544.4	3.78 (4)	562
e	739.3	(1)	731
f	739.3	4.66 (4)	731
g	1235	0.67 (1)	1217

[a] Labelling as per Figure 14 (a). [b] Oxygen-17 NMR chemical shifts from [41].

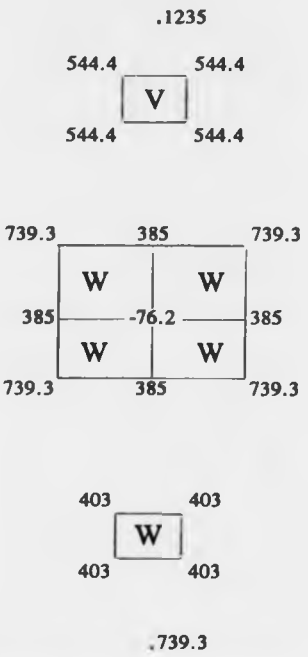

Figure 66. Successive layer diagram structure of species (5,1) with oxygen chemical shifts at 294K assigned as in the text.

6.2.4. *fac*- $[W_3V_3O_{19}]^{5-}$ and *mer*- $[W_3V_3O_{19}]^{5-}$

Figure 67 shows the ^{51}V NMR spectrum of a solution at pH 6.5, raised to 89°C, with 50 mmol dm^{-3} in both tungsten and vanadium. The dominant peaks are those from *cis*-(4,2) (truncated in figure) and tetrahedral (0,n) species. The weak peaks from (1,9) are also apparent. There is also a peak at δ_V = -496.7 ppm arising from *fac*-(3,3), previously reported by Pope and Leparulo-Loftus [143]. The remaining resonances at δ_V = -504.7 and -509.2 ppm have the area ratio (1:2) and also have the same dependence on concentration and metal ratio as the *fac*-(3,3) peak. Furthermore, they exhibit a strong ^{51}V-^{51}V coupling in COSY spectra (see Figure 68). We therefore propose that they arise from *mer*-(3,3). Overlap of other resonances precluded any pK_a measurements.

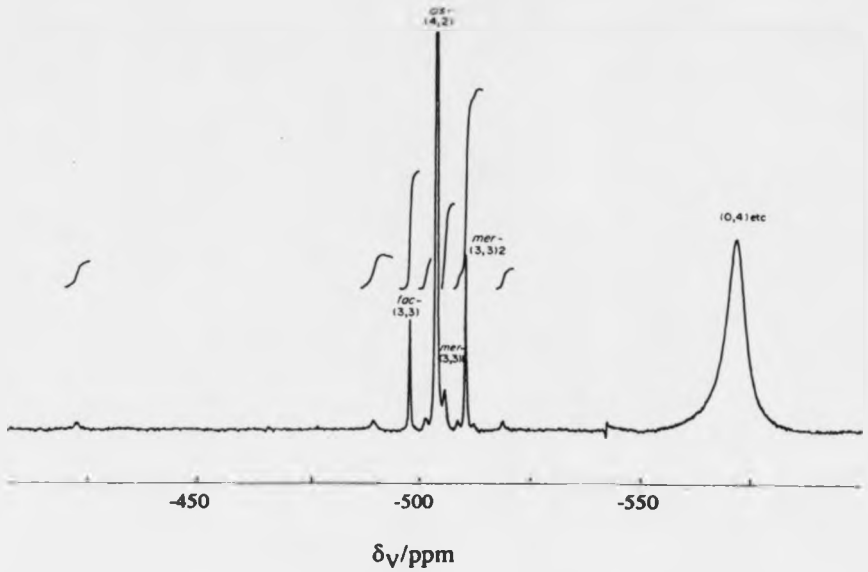

Figure 67. Vanadium-51 NMR spectrum at pH 6.5, 89°C, 50 mmol dm^{-3} in both tungsten and vanadium, showing predominantly *cis*-$[W_4V_2O_{19}]^{4-}$, tetrahedral vanadates and *fac*- and *mer*-$[W_3V_3O_{19}]^{5-}$

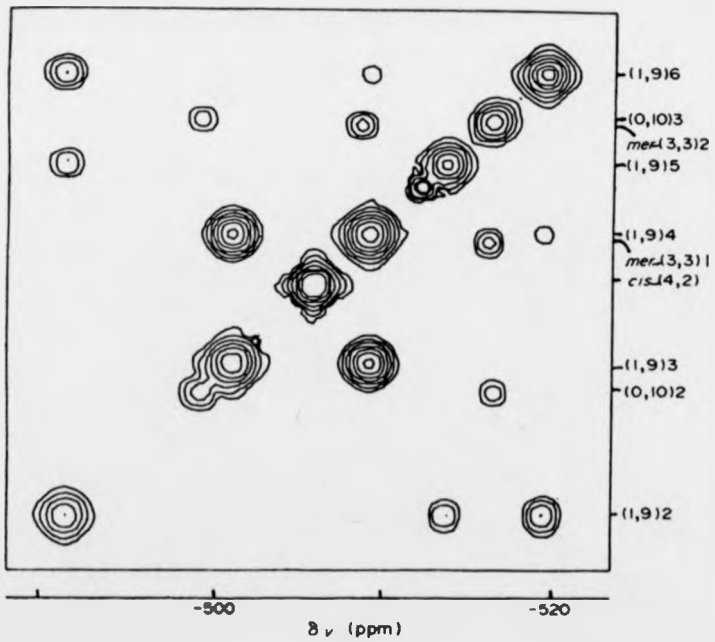

Figure 68. 89°C ^{51}V-^{51}V COSY-90 spectrum of $[WV_9O_{28}]^{5-}$, together with some $[W_5VO_{19}]^{3-}$, *cis*-$[W_4V_2O_{19}]^{4-}$ and *fac*- and *mer*-$[HW_3V_3O_{19}]^{4-}$. 400 mmol dm^{-3} in vanadium, 125 mmol dm^{-3} in tungsten; pH 3.56.

Due to the low concentration of these (3,3) species and overlap from *cis*-(4,2), the ^{17}O NMR assignments are rather tentative, although those of *fac*-(3,3) are reasonably consistent with the findings of Maksimovskaya *et al.* [148]. The assignments of *fac*-(3,3) and *mer*-(3,3) are tabulated in Tables 35 and 36 and illustrated, in Figures 69 and 70 respectively.

Table 35. Oxygen-17 chemical shifts at 294K /ppm and relative integrals of *fac*- $[W_3V_3O_{19}]^{5-}$.

Peak label	*fac*-$[W_3V_3O_{19}]^{5-}$ δ_O	Relative Integral		*fac*-$[W_3V_3O_{19}]^{5-}$ δ_O
a[a]	-51	1	(1)	-67[b]
b	349	2.75	(3)	345
c	502[c]	[c]	(6)	467
d	669 or 676[d]	[d]	(3)	668,656
e	811[c]	[c]	(3)	764
f	1190[c]	[c]	(3)	1132

[a] Labelling as per Figure 16 (a). [b] From [148]. [c] Under (4,2). [d] Not certain.

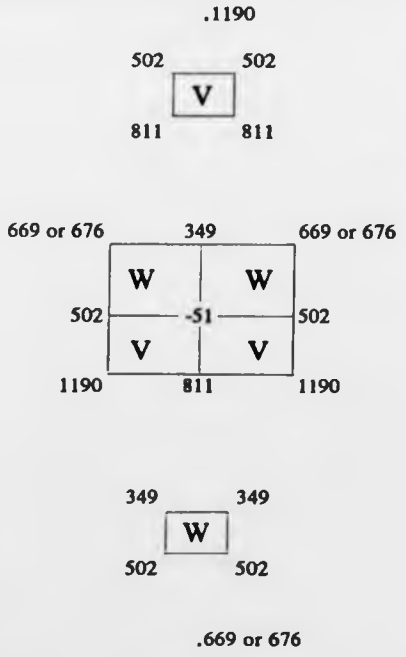

Figure 69. Successive layer diagram structure of species *fac*-(3,3) with oxygen chemical shifts at 294K/ppm assigned as in the text.

Table 36. Oxygen-17 chemical shifts at 294K /ppm and relative integrals of *mer*-$[W_3V_3O_{19}]^{5-}$ at 294K /ppm.

Peak label	*mer*-$[W_3V_3O_{19}]^{5-}$ δ_O	Relative Integral	
a[a]	-51	1	(1)
b	355	2	(2)
c	480[b]		(2)
d	506[c]		(2)
e	517.5	4.5	(4)
f	669 or 676[d]		(2)
f'	669 or 676[d]		(1)
g	811[c]		(2)
h	1190[c]		(2)
h'	1190[c]		(1)

[a] Labelling as per Figure 16 (b). [b] Under (0,n). [c] Under (4,2). [d] Not certain.

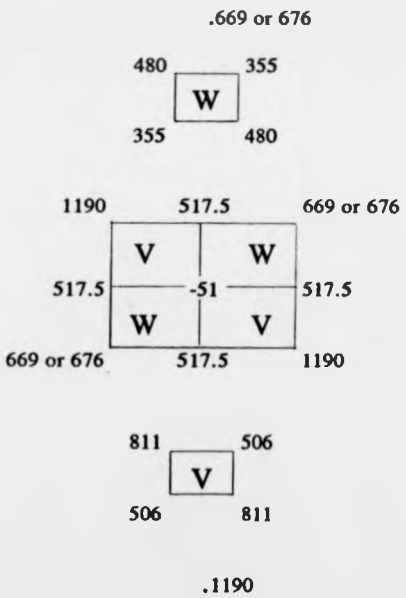

Figure 70. Successive layer diagram structure of species *mer*-(3,3) with oxygen chemical shifts at 294K assigned as in the text.

6.2.5. $[WV_9O_{28}]^{5-}$ and $[HWV_9O_{28}]^{4-}$

Maximovskaya and Chumachenko [145] have proposed the existence of this species on the basis of their ^{51}V and ^{17}O NMR data. They also suggested that the decavanadate framework is retained with a tungsten atom replacing one of the "capping" vanadium atoms (see Chapter 1. section 1.9.2.).

The increased field has, however, permitted more resolution. The ^{51}V NMR spectrum of (1,9) does in fact have six peaks in the area ratio 2:2:2:1:1:1, and not five as previously reported [145]. We confirm that the "capping" position is replaced. Presumably the more electropositive tungsten [VI] atom substitutes the apical vanadium sites partly because there is more room for the larger tungsten atom and partly because these sites have the greatest electron density in the decavanadate anion. This analysis receives confirmation from the Bénard *et al.*'s [178] calculation of the electron density at each vanadium site in decavanadate. Furthermore, there is no evidence for the *cis*- or *trans*-(2,8) species as found with molybdovanadate analogues already studied by Howarth *et al.* [25] (see Chapter 1. section 1.10.1.2).

In Figure 71, the sharp peak at δ_V = -503.5 ppm arises from *cis*-(4,2), with weaker peaks arising from decavanadate (0,10) at δ_V = -418.3, -495.4 and (in part) -511.6 ppm. The broad resonance at δ_V = -564 ppm arises from exchange-averaged tetrahedral vanadate species. The remaining peaks are in the area ratios 2:2:2:1:1:1, and their shifts are close to those of $[MoV_9O_{28}]^{5-}$ [25] as shown in Table 37. Peaks assigned to (1,9) and its protonated form are labelled (1,9)x, where x increases with decreasing δ_V. Figure 68, part of a ^{51}V-^{51}V COSY spectrum at pH 3.56, reveals the connectivities of the vanadium atoms in this species. The full spectrum also shows the connectivities (1,9)1-2, 1-3 and 5-6, albeit more weakly. However, in contrast to the molybdo analogue, the assignments of (1,9)4 and (1,9)5 are reversed.

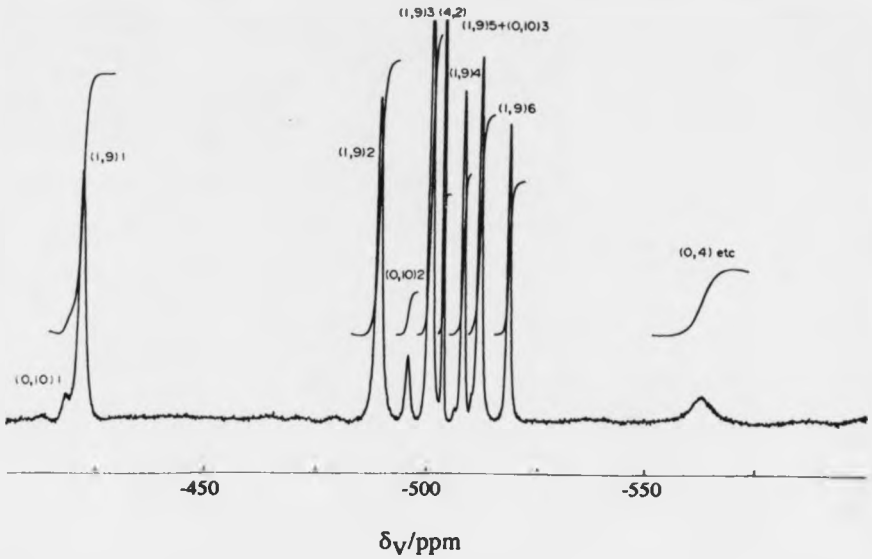

Figure 71. Vanadium-51 NMR spectrum at pH 5, 89°C, 20 and 80 mmol dm^{-3} in tungsten and vanadium, respectively, showing predominantly $[WV_9O_{28}]^{5-}$.

Table 37. A comparison of vanadium chemical shifts for $[WV_9O_{28}]^{5-}$ and $[MoV_9O_{28}]^{5-}$ [25].

Peak[a]	$[WV_9O_{28}]^{5-}$	$[MoV_9O_{28}]^{5-}$
	δ_V	δ_V
1[b]	-428[c]	-425[c]
2[b]	-496.3	-495.5
3[b]	-507.8	-505
4	-513.8	-514.9
5	-518.6	-516.2
6	-525.7	-525.3

[a] Labelling as per Figure 19.[b] Two vanadium atoms per molecule. [c] δ_V (ppm), referred to $VOCl_3$ capillary, 20°C.

The ^{17}O NMR resonances are mostly assigned by area and by analogy with the molybdo analogue. These assignments (shown in Table 38 and Figure 72) confirm those of Maksimovskaya and Chumachenko [145] except in our spectra the water resonance obscured O_a; our integrals favoured a different assignment for O_c'' and O_d; and we report an assignment for O_f''.

At lower pH the species protonates, and although decomposition occurs before protonation is complete the pK_a is *ca.* 2.1(20°C) and 2.2 (89°C) (see Figure 60). Howarth *et al.* [25] have reported that monomolybdononavanadate protonates at both O_b and O_c, although preferentially at the O_c site which is further from the added positive charge of the Mo^{VI}. Similarly in the tungsto case, peaks (1,9)2 and (1,9)5 exhibit the largest ^{51}V protonation shifts, 15.5 and 12.5 ppm respectively, and the only oxygen peaks whose shifts are lowered upon protonation are $O_{a'}$ (-3), O_b (-2) and $O_c + O_{c'}$ (-12.1 ppm). Unfortunately, we were unable to distinguish between O_c and $O_{c'}$, and therefore assume that the two sites are equally favoured.

Table 38. Oxygen chemical shifts at 294K/ppm and relative integrals for $[WV_9O_{28}]^{5-}$.

Peak label	$[WV_9O_{28}]^{5-}$ δ_O	Relative Integral		$[WV_9O_{28}]^{5-}$ δ_O		$[MoV_9O_{28}]^{5-}$ δ_O	
a[a]	[b]	[b]	(1)[c]	14[d]	(1)[c]	-27.6[e]	(1)[c]
a'	81.8	1[f]	(1)	82	(1)	80.2	(1)
b'	297.5	1.75	(2)	298	(2)	337.2	(2)
b	440.0	2	(2)	439	(2)	438.7	(2)
c'''	495	2.25	(2)	495	(2)	604.4	(2)
c'	788	1.88	(2)	788	(2)	786	(2)
c	788	1.88	(2)	788	(1)	786	(2)
c''	905	2	(2)	825	(2)	825	(2)
d	824	0.88	(1)	807	(1)	806	(1)
d'	824	0.88	(1)	825	(1)	806	(1)
e	905	2	(2)	904	(2)	896.8	(2)
e'	934	2	(2)	933	(2)	930.1	(2)
f'''	762.1	1	(1)	[g]		881.4	(1)
f	1160	1.13	(1)	1143	(2)	1143	(1)
f''	1175	1.08	(1)	1174	(2)	1180	(1)
g	1175	2.16	(2)	1195	(3)	1170.8	(2)
g'	1191	[h]	(2)	1191	(2)		

[a] Labelling as per Figure 19. [b] under water resonance, [c] notional integrals, [d] from [145], [e] from [25]. [f] measured integrals, [g] omitted, [h] under *cis*-(4,2).

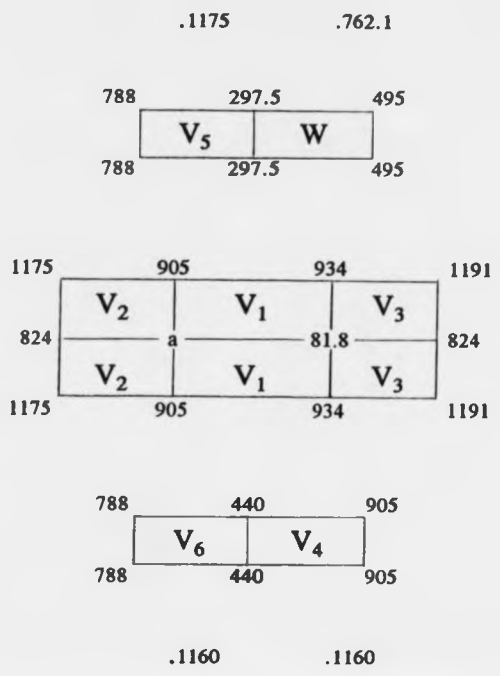

Figure 72. Successive layer diagram structure of species (1,9) with oxygen chemical shifts at 294K assigned as in the text.

6.2.6. α-$[H_2W_{11}VO_{40}]^{7-}$

Previously characterised by Pope [51,141], this species exhibits a single ^1H NMR signal δ_H = 6.0 and a ^{51}V NMR resonance at δ_V = -542.8 and on raising the temperature to 89°C, shifts to a slightly higher frequency, -536.4 ppm. The proposed 7- anionic charge is with observation that this anion has its maximum stability at somewhat higher pH than α-Keggin species (see Chapter 4). No significant pH dependence was observed. The ^{183}W NMR spectrum (Figure 73) is similar to that of α-$[H_2W_{11}MoO_{40}]^{6-}$ (see Chapter 5. section 5.1.3.) in that it has six resonances in area ratio 2:2:2:1:2:2, and therefore it must have the symmetrical α-Keggin structure. Also, the internally diprotonated anion is further supported by

the fact that the tungsten shifts centre around the resonance of α-$[H_2W_{12}O_{40}]^{6-}$. It is surprising that the range of shifts is small in comparison with those reported by Domaille [144] for the corresponding monosubstituted heteropolytungstates with the α-Keggin structure. These typically spread from -70 to -140 ppm, with the W nearest to V often having the highest shift. This may be because the present species has two internal protons. Perhaps the protons move so as to minimise the difference in charge distribution caused by the substitution. Internal protonation certainly affects the tungsten shifts. Removal of just one internal proton decreases the isopolytungstate shift by 21 ppm (see Chapter 4). In the ^{51}V NMR spectrum of a solution 1.67 mol dm^{-3} in V and 0.33 mol dm^{-3} in W at pH 2.65, 20°C, α-(11,1) accounts for 1% of the vanadium present, however, upon ageing three months the acidity of the solution decreases to pH 5 and the anion represents some 12%. (See below).

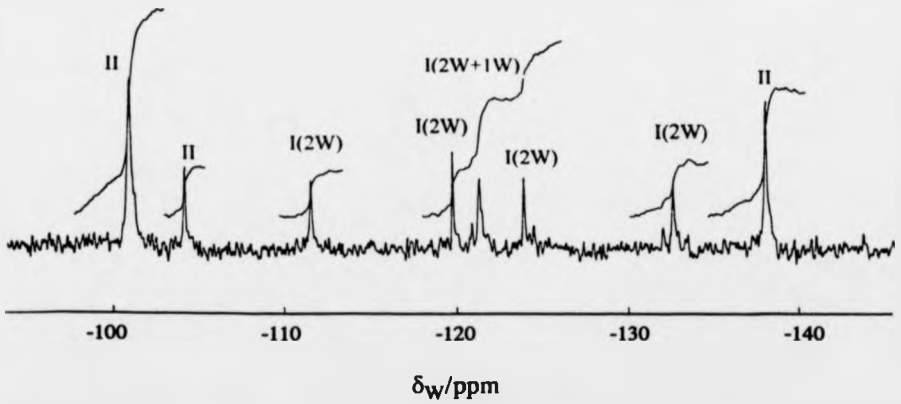

Figure 73. Tungsten-183 NMR spectrum of 0.333 mol dm^{-3} [V], 1.667 mol dm^{-3} [W] aqueous solution at 295K, pH 4.9. Species I α-$[H_2W_{11}VO_{40}]^{7-}$ and II paratungstate-B $[H_2W_{12}O_{42}]^{10-}$.

6.2.7. Other Minor Tungstovanadate Species

As a solution with 20 mmol dm^{-3} in W and 80 mmol dm^{-3} in V is acidified to pH ≈ 2.5 (measured at 20°C) four small, as yet unidentified resonances start to appear.

Unfortunately, these resonances are very small and only observable at elevated temperatures and COSY spectra could not reveal their connectivities. Figure 74 illustrates these resonances and Table 39 shows the ^{51}V NMR chemical shifts at their observable pH extrema.

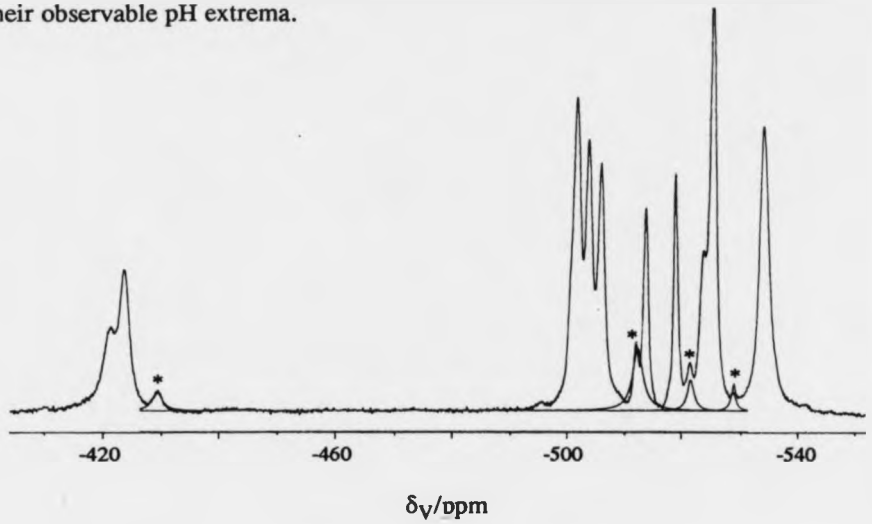

Figure 74. Vanadium-51 NMR spectrum at pH 1.6, 89°C, 20 mmol dm^{-3} in W and 80 mmol dm^{-3} in V showing the four minor resonances deconvoluted (indicated by *).

Table 39. Vanadium chemical shifts (ppm) of minor tungstovanadate species at 89°C.

pH 2.6 δ_V	pH 1.6 δ_V	Integral
-428.7	-429.6	1024
-509.2	-511.9	2434
-520.1	-521.9	1725
-528.6	-528.6	1512

The fact that their chemical shifts are close to those of the (1,9) species and that the peaks maximise at low tungsten metal ratios, suggests a substituted decavanadate species. Similarly in the molybdovanadate system Howarth *et al.* [25] observed additional resonances close to those of the (1,9) species below pH 3 and assigned them to *cis*- and *trans*- dimolybdo-octavanadate (2,8). See Table 40.

Table 40. Vanadium chemical shifts (ppm) of *cis*- and *trans*- dimolybdo-octavanadate at 353K [25].

trans-$[Mo_2V_8O_{28}]^{4-}$ δ_V	*cis*-$[Mo_2V_8O_{28}]^{4-}$ δ_V
-427 (2V)	-424 (2V)
-505 (4V)	-505 (4V)
-516.2 (2V)	-525.5 (2V)

Initial inspection of this molybdovanadate data would imply that the four resonances observed in the tungstovanadate system might be a mixture of *cis*- and *trans*- ditungsto- octavanadate with the remaining resonances obscured. However, the act of substituting a further V^V atom with Mo^{VI} or W^{VI} reduces the negative charge on the anion, and therefore decreases the anion's pK_a. In the molybdovanadate case, the (1,9) species exhibits a $pK_a = 2.77$ [25], higher than the tungsto- analogue (see above) and the resonances of the (2,8) anions are independent of pH, as low as pH 2. In contrast the minor tungstovanadate resonances exhibit pH dependences (see Table 39) which approximately parallel those of the (1,9) species. Consequently because of this they cannot be attributed to the *cis*- and *trans*- (2,8) species, but rather another protonated (1,9) isomer or a structurally similar species.

Further minor resonances are observed in aged solutions with high tungsten ratios initially at pH < 3. Assignment of these is hampered by the lack of cross peaks in the COSY spectra, overlap and a number of the resonances having a similar intensity. Figure 75 shows the ^{51}V NMR spectrum of a solution initially at pH 2.8, aged three months, raised to 89°C, with 400 mmol dm^{-3} in tungsten and 100 mmol dm^{-3} in vanadium. The two dominant resonances are from *cis*-(4,2) and (5,1), then the next four intense signals may possibly be attributed to two species with two remote distinct vanadium atoms. The assignment to two species becomes more apparent when the equilibration of a similar solution is followed by ^{51}V NMR and the peak intensities of these four signals are seen to covary as two pairs. (See below.) The remaining smaller resonances fall into two chemical shift regions. The

first, δ_V =-520 to -535 ppm corresponding to isolated VO_6 octahedra [143] and the second, δ_V = -550 to -560 ppm region, corresponding to tetrahedral vanadium atoms [143]. So perhaps these originate from a series of substituted Keggin structures with the internal protons replaced by a tetrahedral vanadium atom as previously described by Pope [143]. (See Chapter 1 section 1.9.3.).

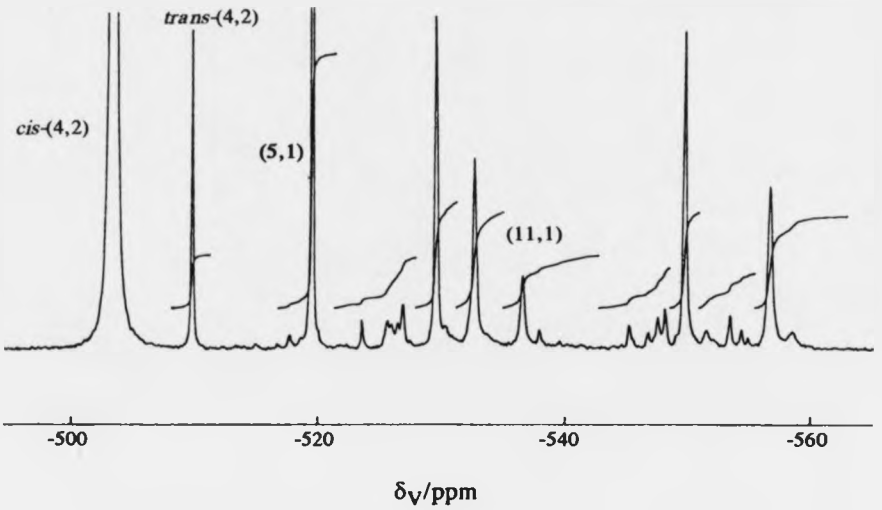

Figure 75. Vanadium-51 NMR spectrum of a solution initially at pH 2.8, aged three months, raised to 89°C, with 400 mmol dm^{-3} in tungsten and 100 mmol dm^{-3} in vanadium.

Any further insight to the possible structures of these two species is very tentative and can only be ascertained from the vanadium chemical shifts and linewidths. It is clear that the two signals δ_V = -529.4 and -532.6 ppm are in the region characteristic of isolated VO_6 octahedra [143]. It is also evident from Table 41 that the linewidths of these resonances are comparable to those of *cis*-(4,2) and the (5,1) species, and therefore, these vanadium atoms too, must also have similar symmetrical environments. The chemical shifts of the other two resonances δ_V = -549.7 and -556.2 ppm appear to imply tetrahedral vanadium atoms, however it is

apparent from Table 41 that these linewidths are rather broad, and therefore these vanadium atoms are more likely to have octahedral symmetry.

Table 41. Vanadium NMR data for the four unknown resonances compared with data of known species with a range vanadium sites.

Species Peak	δ_V at 89°C	Relative[a] Integral	Linewidth[b] at 89°C	δ_V at 20°C	Linewidth[b] at 20°C
(a)	-532.6	1.02	38	-534.6	103
(b)	-556.7	0.98	42	-561.1	113
(c)	-529.4	1.08	28	-530.4	70
(d)	-549.7	0.92	29	-555.9	141
cis-(4,2)	-503.36		27	-512.6	46
(5,1)	-519.45		14	-527.1	33
(11,1)	-536.6		58	-543.3	132
"tetrahedral vanadiums"[c]			17-20		39-46

[a] Relative integrals measured at 89°C. [b] Linewidth measured at half height in Hz, after removal of broadening due to window function. [c] These are the sharpest resonances in the region δ_V -550 to -560 and presumably arise from tetrahedral vanadium atoms.

It is already known that under these conditions tungstate forms the metastable decatungstate structure $[W_{10}O_{32}]^{4-}$ [8]. So perhaps two vanadium atoms with their lower ionic charge can stabilise this condensed species. However, there is only one possible structure (see Figure 76) that has two distinct uncoupled vanadium atoms. Therefore, if the other two resonances were also attributed to substituted decatungstate species they would have to represent two further species with either mono- or di-substitution (vanadium occupying equivalent sites) and which by coincidence have similar intensities. Evidence for a possible assignment is provided by the ^{183}W NMR spectrum isopolytungstate anion. The eight corner tungstens resonate at δ_W = -27.6 ppm and the other two resonate at much higher field δ_W = -172.3 ppm (see Chapter 4). Therefore the two vanadium signals with shifts similar to the (5,1) resonance, namely, δ_V = -529.4 and -532.6 ppm would be assigned to

the vanadium atoms occupying the corner sites and the other two resonances, δ_V = -549.7 and -556.2 ppm, end sites.

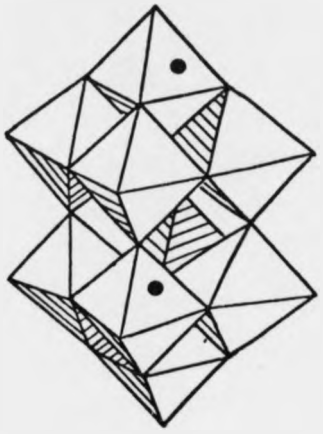

Figure 76. Structure of $[W_8V_2O_{32}]^{6-}$ (• = vanadium sites).

Alternatively these four vanadium resonances could also be assigned either to two di-substituted β-Keggin isomers; or a mixture of one di-substituted β-Keggin and the above di-substituted decatungstate species; or some other related species. Assignment of the resonances for the β-Keggin species would be as follows. The two resonances at δ_V = -529.4 and -532.6 ppm are again as discussed above consistent shift-wise with the assignment to the vanadium atoms replacing the octahedral tungsten atoms. However, the linewidths of these seem rather narrow for these distorted octahedra. The other two resonances at δ_V = -549.7 and -556.2 ppm are again shift-wise consistent with tetrahedral vanadium atoms but, their linewidths are rather broad. This may be possibly because of the asymmetrical nature of the β-Keggin central site.

6.2.8. Vanadate Species

Above pH 5.5, just before the formation of decavanadate, vanadium mainly forms a series of meta-vanadates based on $[H_2VO_4]^-$, $[H_2V_2O_7]^{2-}$, $[V_4O_{12}]^{4-}$ and $[V_5O_{15}]^{5-}$

as described by Heath and Howarth [51] in these tungstovanadate solutions. This region of vanadium chemistry is very complicated and indeed Heath and Howarth [51] have identified 15 species over the pH 4-11 range and it is still believed that further oligomers are in fact present.

At 20°C four metavanadate resonances are observed as described in Table 42, however, on raising the temperature to 89°C, fast exchange processes reduce these to a single broad resonance at δ_V = -571.6 ppm. Below *ca.* pH 5 the concentration of these metavanadate species falls sharply to *ca.* 10% of the vanadium present in solutions with metal ratio W:V, 20:80 mmol dm^{-3}. In the same solutions below pH 2 the concentration of VO_2^+ rises sharply to *ca.* 60% of the vanadium present.

Table 42. Vanadium chemical shifts (ppm), relative integrals and linewidths of vanadate species at pH 6.9, 20°C.

δ_V	Relative Integral	Linewidths[a]	Assignment[b]
-559.2	3	232	$[H_2VO_4]^-$
-572.2	5	65	$[H_2V_2O_7]^{2-}$
-576.1	100	70	$[V_4O_{12}]^{4-}$
-584.2	29	134	$[V_5O_{15}]^{5-}$

[a] Linewidth measured at half height in Hz, after removal of broadening due to window function.
[b] Assignments made as per Heath and Howarth [51].

6.2.9 Speciation and Linewidth Analysis

Measuring the vanadium integrals and using standard deconvolution software (for crowded regions) distributions of these anions versus pH have been calculated. In general deconvolutions of the spectra were very effective for calculating areas and linewidths. Figure 77 shows a typical example. The deconvolution report and the integrals measured are shown in Table 43. Distribution diagrams for these

complexes for both metal ratios 20:80 and 50:50 mmol dm^{-3} (W:V) at 89°C are shown in Figures 78 and 79 respectively.

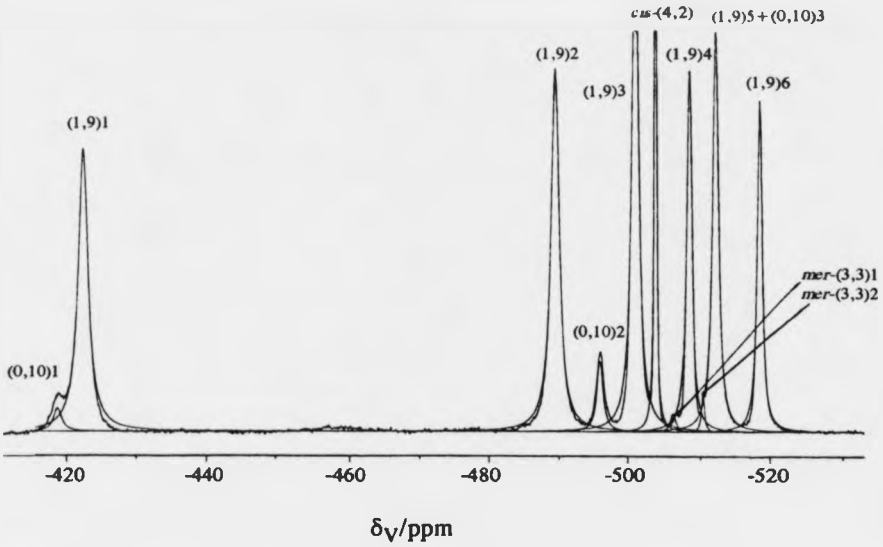

Figure 77. Vanadium-51 NMR spectrum of a solution at pH 5.0, 20 mmol dm^{-3} in tungsten and 80 mmol dm^{-3} in vanadium raised to 89°C deconvoluted.

Table 43. A typical deconvolution report for a vanadium-51 NMR spectrum. The solution being at pH 5.0, 20 mmol dm^{-3} in tungsten and 80 mmol dm^{-3} in vanadium raised to 89°C.

Peaks	Linewidths[a]	Area
(0,10)1	145.98	862.45
(0,10)2	111.79	2030.08
(0,10)3		*b*
(1,9)1	172.79	12920.92
(1,9)2	145.33	13956.84
(1,9)3	113.34	15587.39
(1,9)4	87.06	8315.37
(1,9)5	99.58	10578.45[b]
(1,9)6	85.66	7516.09
cis-(4,2)	35.02	6457.60
mer-(3,3)1	86.81	416.86
mer-(3,3)2	51.54	548.80

[a] Linewidth measured at half height in Hz, after removal of broadening due to window function.
[b] (0,10)3 and (1,9)5 overlapped.

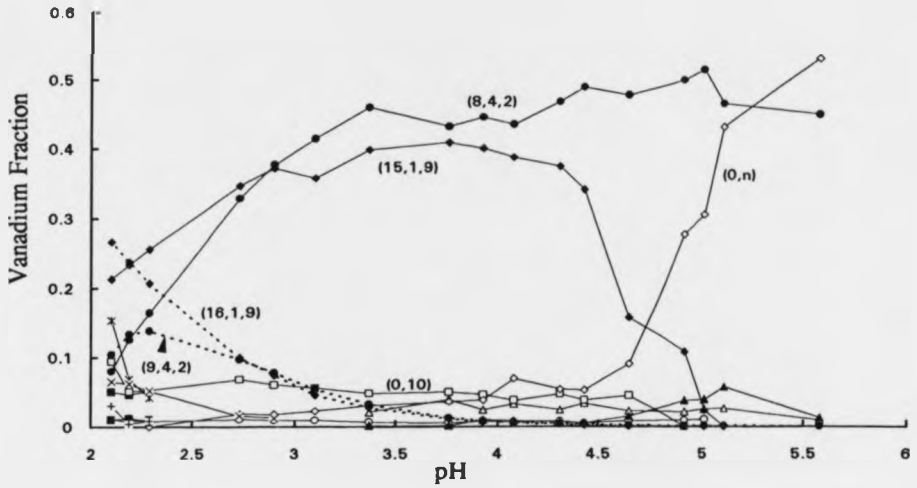

Figure 78. Distribution of component species in solutions with 50 mmol dm^{-3} in both V and W at 89°C. The lines serve merely to highlight peak series. Experimental points: □ = (0,10), ◆ = (1,9), ■ = a (species has not been identified), Δ = *fac*-(3,3), • = *cis*-(4,2), ▲ = *mer*-(3,3), ○ = *trans*-(4,2), × = (5,1), + = (0,1).

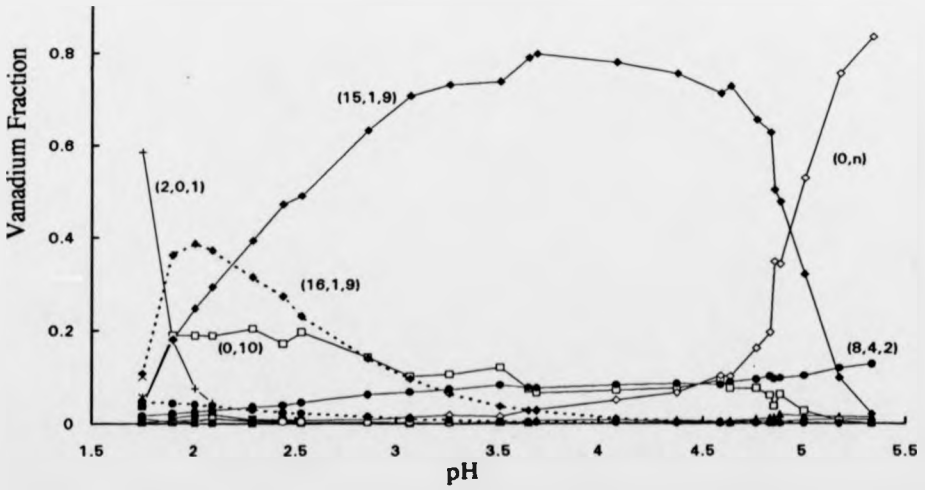

Figure 79. Distribution of component species in solutions with 20 mmol dm^{-3} in W and 80 mmol dm^{-3} in V at 89°C. The lines serve merely to highlight peak series. Experimental points: □ = (0,10), ◆ = (1,9), ■ = a (species has not been identified), Δ = *fac*-(3,3), • = *cis*-(4,2), ▲ = *mer*-(3,3), ○ = *trans*-(4,2), × = (5,1), + = (0,1).

On raising the temperature of a solution with 20 mmol dm^{-3} in W and 80 mmol dm^{-3} in V to 89°C, the pH changed. Some representative measurements are shown in Table 44. Figure 80, shows the changes in concentration of the major species when a series of solutions are heated versus pH. The increase in concentration of the (1,9) species, metavanadate species and the decrease of *cis*-(4,2) and (0,10) species may be expressed by the following equilibria.

$$8[W_4V_2O_{19}]^{4-} + 6[HV_{10}O_{28}]^{5-} = 8[WV_9O_{28}]^{5-} + [H_2W_{12}O_{42}]^{10-} + [V_4O_{12}]^{4-} + 2H^+ \quad (6.1)$$

$$4[HW_4V_2O_{19}]^{3-} + 3[H_2V_{10}O_{28}]^{4-} = 4[HWV_9O_{28}]^{4-} + [H_2W_{12}O_{40}]^{6-} + 2[VO_2]^+ + 2[OH]^- \quad (6.2)$$

The first proposal could account for the increase in acidity for solutions with higher pH values, and the second possibly explains why the solutions below pH 3 become more alkaline.

Table 44. Representative pH measurements made on a solution with 20 mmol dm^{-3} in W and 80 mmol dm^{-3} in V at 20 and 89°C.

pH at 20°C	pH at 89°C	Difference
6.01	4.77	-1.24
5.86	4.67	-1.19
5.34	4.34	-1.00
5.19	4.24	-0.95
4.36	3.69	-0.67
3.70	3.26	-0.44
3.09	2.86	-0.23
2.04	2.18	0.14

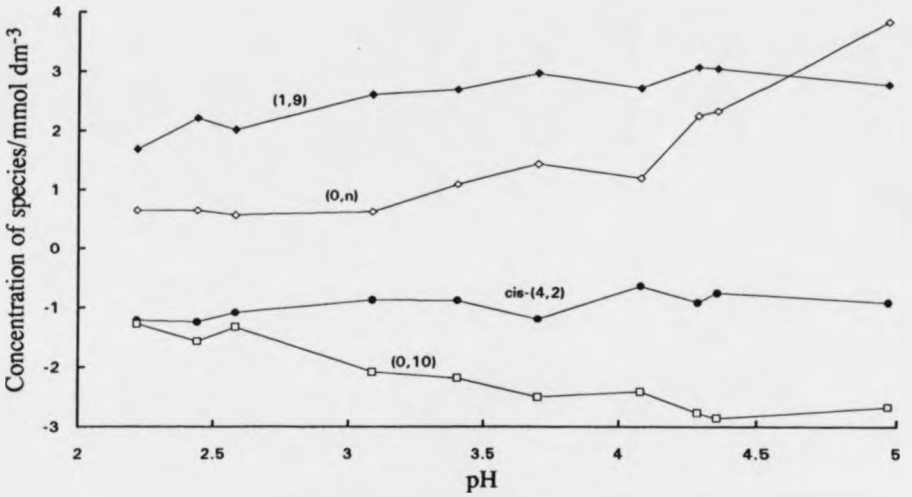

Figure 80. Variation of concentration of the major species when solutions with 20 and 80 mmol dm^{-3} in tungsten and vanadium, respectively, are heated from 20 to 89°C.

The solutions containing 50 mmol dm^{-3} in both W and V exhibit a similar pH trend on heating (see Table 45) except that the variations in concentration of these species are much more erratic and therefore no rationale was attempted.

Table 45. Representative pH measurements made on a solution with 50 mmol dm^{-3} in both W and V at 20 and 89°C.

pH at 20°C	pH at 89°C	Difference
6.02	4.82	-1.2
5.96	4.76	-1.2
5.59	4.41	-1.18
4.70	4.16	-0.54
3.23	3.10	-0.13
2.09	2.37	0.28

Distributions at 20°C were rather more difficult to determine very precisely because of severely overlapped broader peaks, however, it was possible to obtain reasonable integrals for the major species. Furthermore, at this temperature, the formation constants of the vanadate species are known [44], thus it is possible using the LAKE [154] computer program, to fit the integrals and chemical shifts for the main tungstovanadate species and obtain formation constants for *cis*-(4,2), (1,9) and for their corresponding protonated forms. This computer fit was very kindly performed by Dr. Lage Pettersson and Dr. Ingegärd Andersson of the University of Umeå, Sweden. The data fitted was restricted to the pH 5.4 to 3 range because in this region these major species represented at least 96% of the vanadium present and other minor species could be ignored. As a result of this approximation the LAKE fit shown in Figure 81 overestimates the concentration of the (0,10) species beyond these pH limits as the ignored minor species become more significant. Improving this approximation is very difficult indeed and would necessitate reliable integrals of overlapped resonances, pK_a values and a full assignment of these minor species. However, the fit to (1,9), *cis*-(4,2) and their protonated forms are within tolerable limits. The formation constants extracted are shown in Table 46. Also shown in Table 46 are the formation constants for the molybdo analogues. It is clear from their greater magnitudes that these molybdo analogues are more stable, especially the $[MoV_9O_{28}]^{5-}$ anion and its protonated form. This presumably explains the absence of any ditungsto-octavanadate species and implies that tungsten is less suited to this compact structure than molybdenum.

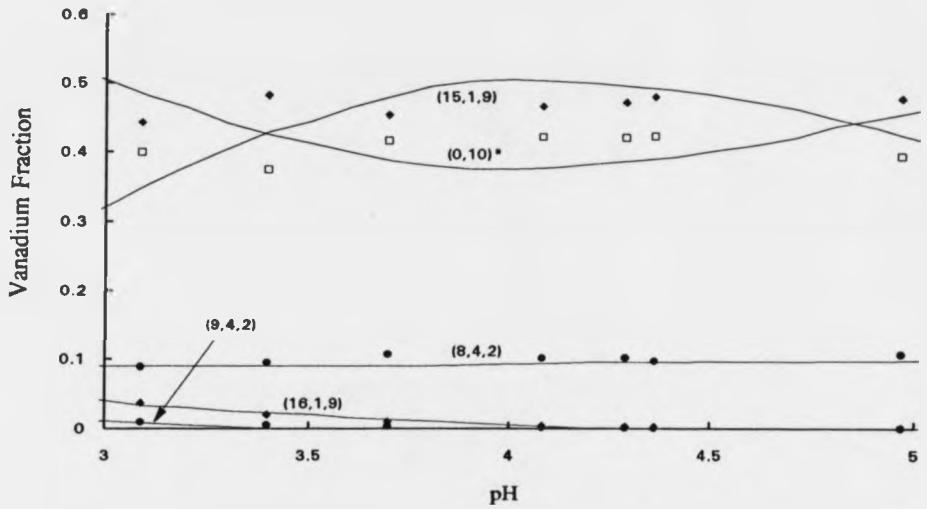

Figure 81. A LAKE fit to the integrals and shifts measured for the major species in a solution with 20 mmol dm^{-3} in W and 80 mmol dm^{-3} in V at 20°C. (0,10)* represents the sum of (14,0,10), (15,0,10), (16,0,10), (17,0,10).

Table 46. Species and formation constants calculated using the LAKE program [154].

Species	(p,q,r)	$\log\beta_{p,q,r}$	Species	(p,q,r)	$\log\beta_{p,q,r}$
cis-$[W_4V_2O_{19}]^{4-}$	(8,4,2)	50.15	*cis*-$[Mo_4V_2O_{19}]^{4-}$	(8,4,2)	60.37[a]
cis-$[HW_4V_2O_{19}]^{3-}$	(9,4,2)	52.25	*cis*-$[HMo_4V_2O_{19}]^{3-}$	(9,4,2)	64.11
$[WV_9O_{28}]^{5-}$	(15,1,9)	63.503	$[MoV_9O_{28}]^{5-}$	(15,1,9)	134.56
$[HWV_9O_{28}]^{4-}$	(16,1,9)	65.600	$[HMoV_9O_{28}]^{4-}$	(16,1,9)	137.33
$[V_{10}O_{28}]^{6-}$	(14,0,10)	52.130			
$[HV_{10}O_{28}]^{5-}$	(15,0,10)	58.13			
$[H_2V_{10}O_{28}]^{4-}$	(16,0,10)	61.87			
$[H_3V_{10}O_{28}]^{3-}$	(17,0,10)	63.5			

[a] From ref. [26].

The importance of recording vanadium linewidths is that it can reveal the site symmetry of the vanadium atoms, but it must be remembered that these very often

include substantial vanadium couplings. However, it is worth noting that in the near future these linewidths will become calculable by the methods of Bénard *et al.* [178]. Figure 82 shows the linewidths for the *cis*-(4,2) and (1,9) anions versus pH at 89°C and Table 47 summarises the linewidths calculated (where possible) using deconvolution software of unprotonated and most protonated component species at both 20° and 89°C. Upon protonation all the peaks broaden. As expected the linewidths controlled by quadrupolar relaxation, sharpen on raising the temperature to 89°C (see Chapter 2). The linewidths for the (1,9) vary from 83 Hz ("capping" vanadiums) to 170 Hz (central vanadiums) in the unprotonated state. The "capping" vanadiums, (1,9)4 and (1,9)6 have very similar linewidths to decavanadate whereas (1,9)5, *cis*- to the tungsten atom is 12% broader and the effect is even more marked between (1,9)2 and (1,9)3, with (1,9)2 being 25% wider.

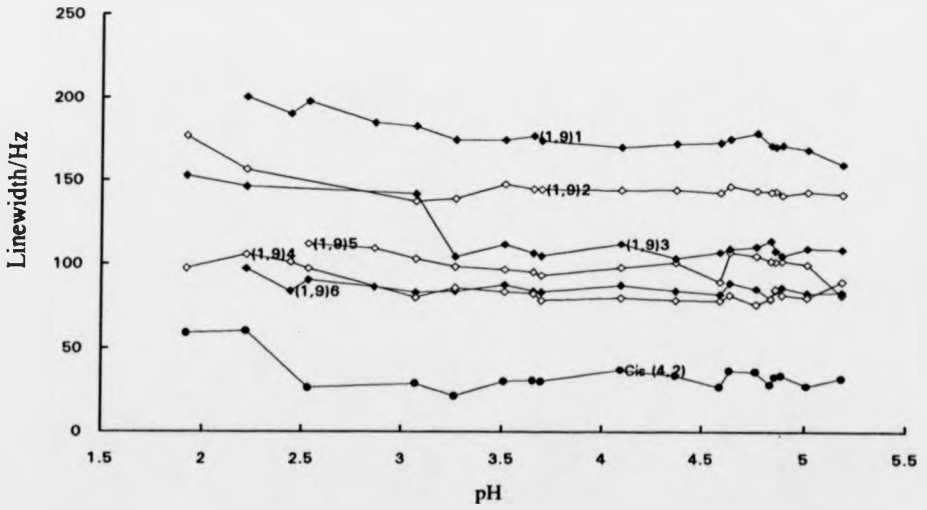

Figure 82. Vanadium linewidths of $[WV_9O_{28}]^{5-}$ and $[W_4V_2O_{19}]^{4-}$ measured at half the peak height at 89°C *vs.* pH.

Table 47. Vanadium linewidths (Hz) of the component species at both 89° and 20°C.

peak	$[V_{10}O_{28}]^{6-}$		$[HV_{10}O_{28}]^{5-}$	
(0,10)1	164[a]	434[b]	246[a]	*c*
(0,10)2	103	335	130	*c*
(0,10)3	82	146	105	*c*
	$[WV_9O_{28}]^{5-}$		$[HWV_9O_{28}]^{4-}$	
(1,9)1	168	543	194	*c*
(1,9)2	143	432	174	*c*
(1,9)3	109	197	113	*c*
(1,9)4	80	168	105	136[b]
(1,9)5	100	167	109	*c*
(1,9)6	82	153	97	194
	mer-$[W_3V_3O_{19}]^{5-}$		*mer*-$[HW_3V_3O_{19}]^{4-}$	
(3,3)1	44	124	*c*	*c*
(3,3)2	40	120	*c*	*c*
	fac-$[W_3V_3O_{19}]^{5-}$		*fac*-$[HW_3V_3O_{19}]^{4-}$	
	40	121	48	*c*
	cis-$[W_4V_2O_{19}]^{4-}$		*cis*-$[HW_4V_2O_{19}]^{3-}$	
	27	46	52	69
	trans-$[W_4V_2O_{19}]^{4-}$		*trans*-$[HW_4V_2O_{19}]^{3-}$	
	22	36	28	*c*
	$[W_5VO_{19}]^{3-}$			
	14	33		
	α-$[H_2W_{11}VO_{40}]^{7-}$			
	58	132		
	$[VO_2]^{+}$			
	193	436		

[a] Width at half height in Hz, after removal of broadening due to window function. raised to 89°C , [b] and similarly at 20°C. [c] Obscured.

6.2.10. Kinetics of Formation

It is already known that tungsten equilibria are slow [11]. We were interested to discover how our high tungsten ratio solutions below pH 3, changed to about pH 5 on ageing two or three months.

Figures 83 and 84 show the fraction of vanadium present for each ^{51}V NMR resonance versus time in two tungstovanadate solutions. These were both initially at pH 2.65 and finally pH 5, with 1.67 mol dm^{-3} in W and 0.33 mol dm^{-3} in V, except that the sample represented in Figure 83 was initially heated for 20 min. prior to the first spectrum.

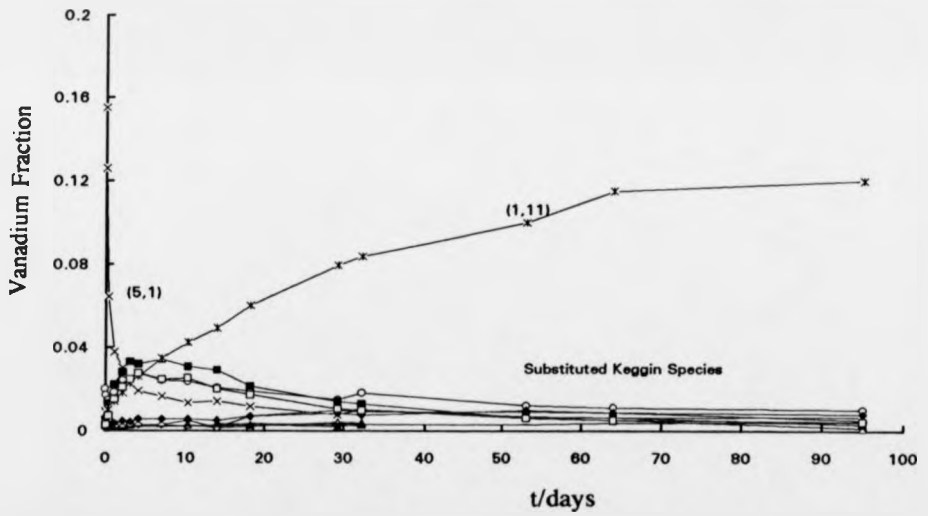

Figure 83. Equilibration of a tungstovanadate solution with 1.67 mol dm^{-3} in W and 0.33 mol dm^{-3} in V was followed by ^{51}V NMR. The solution was initially at pH 2.65, heated to 60°C for 20 min., quenched to 20°C prior to collecting the spectra and finally at pH 5 after 100 days. For clarity the fraction of the *cis*-(4,2) species (≈ 80% of the vanadium present) is off this scale.

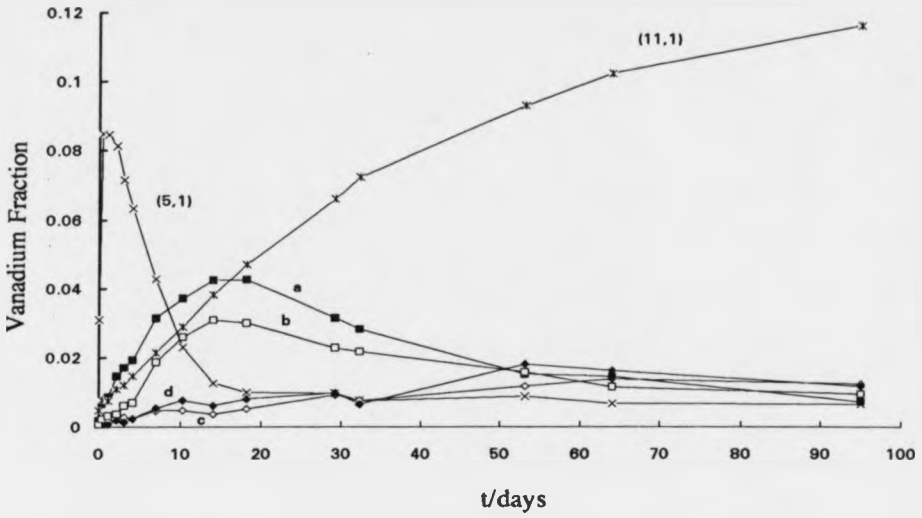

Figure 84. Equilibration of a tungstovanadate solution with 1.67 mol dm^{-3} in W and 0.33 mol dm^{-3} in V was followed by ^{51}V NMR. The solution was initially at pH 2.65, and finally at pH 5 after 100 days. It shows the two proposed pairs of resonances a,b and c,d discussed in text. For clarity the fraction of the *cis*-(4,2) species (≈ 80% of the vanadium present) is off this scale and minor resonances have been edited.

Heating the sample not only increases the rate of equilibration but, also transiently increases the concentration of (5,1) by a concomitant loss of *cis*-(4,2).

$$2[W_4V_2O_{19}]^{4-} + [H_2W_{12}O_{40}]^{6-} + 2[OH]^- = 4[W_5VO_{19}]^{3-} + H_2O \qquad (6.3)$$

However, within 8 hrs. the concentration of (5,1) is comparable to that of the other solution after 4 days. This shows that (5,1) is kinetically favoured whereas *cis*-(4,2) is the more thermodynamically stable product. This contention is further supported by the fact that in the unheated sample *cis*-(4,2) is slow to decompose to (5,1). The next feature of this equilibrium process is the slow formation of α-(11,1) at the expense of *cis*-(4,2) and possibly (5,1). The equilibria below also account for the increase in pH.

$$2H^+ + 2[W_5VO_{19}]^{3-} + [H_2W_{12}O_{42}]^{10-} = 2\alpha\text{-}[H_2W_{11}VO_{40}]^{7-} \qquad (6.4)$$

$$2H^+ + [W_4V_2O_{19}]^{4-} + [H_2W_{12}O_{42}]^{10-} = [W_5VO_{19}]^{3-} + \alpha\text{-}[H_2W_{11}VO_{40}]^{7-} + 2H_2O \quad (6.5)$$

As discussed above, the remaining resonances are difficult to assign. However, it is evident from Figure 84 that the integrals of four of the resonances are seen to covary within acceptable experimental error as two distinct pairs of resonances and possibly represent two species.

6.2.11. Vanadium Chemical Shifts

In isostructural species and at comparable positions the ^{51}V NMR shifts of V atoms in tungstovanadates are generally more negative than those observed for the molybdovanadates. Table 48 bears this out.

Table 48. A comparison of vanadium shifts (at 20°C/ppm) in analogous tungstovanadate and molybdovanadate species .

Species	δ_V	Species	δ_V
cis-$[Mo_4V_2O_{19}]^{4-}$	-498[a]	*cis*-$[W_4V_2O_{19}]^{4-}$	-511.4
$[Mo_5VO_{19}]^{3-}$	-506.4[a]	$[W_5VO_{19}]^{3-}$	-526.5

[a] From reference [154]

We can interpret these shift differences as follows. As described in Chapter 5, tungsten [VI] is known to form stronger bonds to oxygen, which are more covalent in character than molybdenum [VI]. Consequently, because of this greater covalency between tungsten and oxygen, and some delocalisation through the metal-to-oxygen $d\pi$-$p\pi$ bonding network, the ^{51}V NMR shifts of the vanadium atoms in tungstovanadates are more negative. With the exception of peak 5, a similar vanadium shift trend (Table 37) is observed for the species (1,9): $[WV_9O_{28}]^{5-}$ and $[MoV_9O_{28}]^{5-}$. The greatest shift differences are observed at the vanadium sites adjacent to the substituted vanadium and minimal differences are observed at sites

remote from the substitution site. It would therefore appear that the delocalisation is restricted to some extent in these larger anions.

It is also seen in Table 48 that the vanadium shifts of the (5,1) species are more negative than those for *cis*-(4,2) species. This clearly demonstrates that both W and Mo form much stronger, covalent bonds than V. Moreover, the fact that the difference in vanadium shift is greater for the tungstovanadate species shows that W is indeed more covalent than Mo.

7. CONCLUSION

The systematic approach adopted in the present study shows the ability of multi-nuclear solution-state NMR spectroscopy to identify species and elucidate their chemical relationships. The low sensitivity of the ^{183}W nucleus precluded any two-dimensional correlated spectroscopy nor any control of the ionic strength, but the large chemical shift range did compensate to a certain extent and the effect of the Li^+ concentration was quickly established. Also complementary ^{17}O NMR spectroscopy confirmed many of the proposed structures and aided us in locating the protonation sites. However, the application ^{17}O NMR spectroscopy was still restricted even with 5% ^{17}O enrichment because of overlapping resonances. ^{95}Mo nucleus yielded spectra with very broad resonances even at 89°C and only served as additional complementary information. The more sensitive ^{51}V nucleus permitted both two-dimensional correlation spectroscopy and control of the ionic strength, although it was necessary to raise the temperature of the solutions to 89°C to reduce the linewidths.

7.1. Isopolytungstates

Figure 85 shows the species identified and Scheme 3 summarises their chemical relationships. Even though both molybdenum and tungsten have the same charge and approximately the same octahedral and tetrahedral radii [36] their chemistry is markedly different. For example, in contrast to the isopolymolybdates, isopolytungstates (see Figure 85) are strictly composed of octahedrally coordinated metal atoms and are slow to attain equilibrium. In fact, the only common polymeric species in aqueous solution is the heptametallate anion and even here there is a contrast in stability. The heptatungstate decomposes before its first protonation step whereas, the molybdo analogue is stable. Evidently the isopolytungstate species prefer to bear a higher anionic charge, perhaps because of stronger π-bonding from oxygen to tungsten.

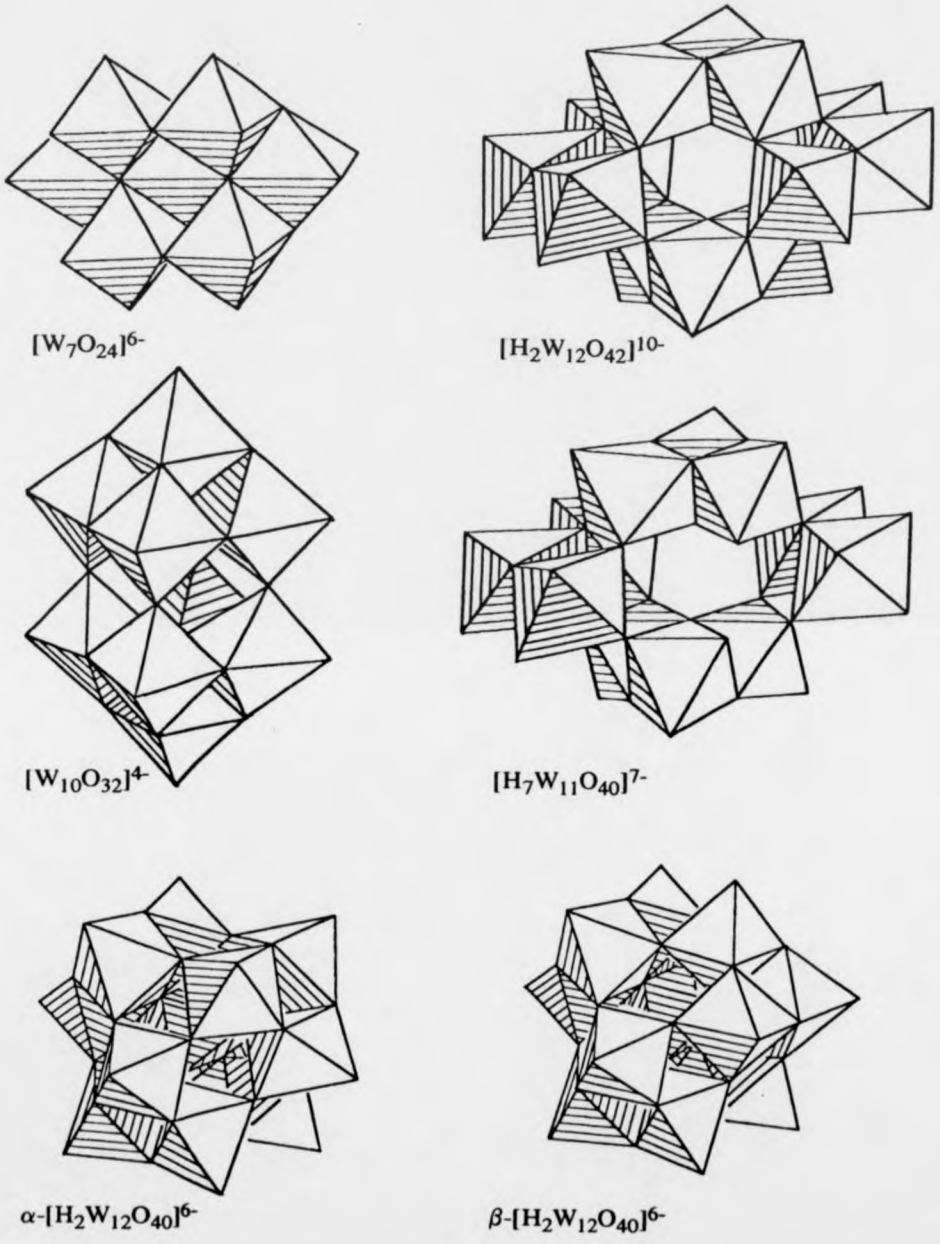

Figure 85. Isopolytungstates identified in aqueous solution.

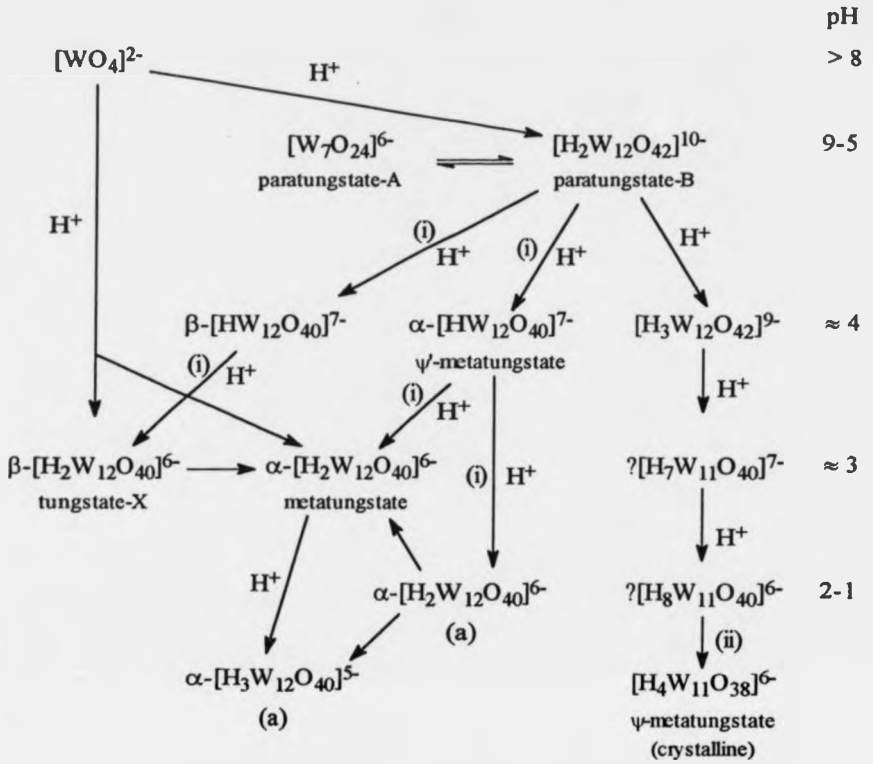

Scheme 3. The interconversion of isopolytungstates in aqueous solution. (i) Heat; (ii) crystallisation; (a) one proton is attached to the exterior of the anion.

7.2. Molybdotungstates

Molybdenum substitutes into paratungstate-A forming a range of isomers $[Mo_xW_{7-x}O_{24}]^{6-}$ (x=1 to 6) with a positional preference for the "ends" (site III) and least for the "central" W atoms (site I). On increasing Mo substitution the stability of the resulting heptametallate increases at lower pH values. Also by maintaining constant total metal and Li^+ concentrations it was possible to perform calculations of relative equilibrium constants, over a limited range of pH, using the LAKE program [154]. We only have evidence for single substitution in both the paratungstate-B and the α-Keggin species.

Molybdenum evidently has a clear preference to substitute the tungsten atom sites with the highest electron density. We have no evidence at all for tungsten substitution into $[Mo_8O_{26}]^{4-}$, nor for any other mixed metal species.

Following the kinetics of these substitutions proved very difficult because this required short accumulations of ^{183}W NMR data and the signal to noise ratio of these spectra were too poor to integrate reliably.

7.3. Tungstovanadates

Although the tungstovanadate species mirror the molybdovanadates in many ways, there are also significant differences. Judging from the relative proportions of species under comparable conditions, tungsten fits somewhat less readily into the decavanadate structure than does molybdenum. Indeed, we have very little evidence for (2,8) tungstovanadate species. In contrast, tungstovanadate Keggin species are more stable than molybdovanadate Keggins.

Also, in all the cases where isostructural species exist, the pK_a is lower in the tungsten case [(1,9), 2.1 *vs.* 2.8; *cis*-(4,2) 2.1 *vs.* 3.9] [25,26]. Concomitantly, (3,3) species are only found with tungsten. As above the tungstovanadate species again prefer to bear a higher anionic charge.

7.4. Avenues for Further Research

The present work has largely unravelled some of the associated fundamental chemistry and in particular, gained a greater understanding of metal substitution and tungsten chemical shifts.

Since NMR spectrometers are constantly improving it may be possible to perform ^{183}W-^{183}W two-dimensional correlation spectroscopy and confirm our assignments and assign those of $[H_7W_{11}O_{40}]^{7-}$ and the mixed molybdotungstates. Also by varying parameters such as the ionic strength and counter ion it may be possible to

control which species forms in solution and which precipitates out. For example one might crystallise $[WV_9O_{28}]^{5-}$ from a mixture of $[WV_9O_{28}]^{5-}$ and $[V_{10}O_{28}]^{6-}$.

The chemistry of these systems in non-aqueous media is still largely unknown. This area is of great importance because most organic reactions occur in non-aqueous media and certain polyoxometallates act as very good selective catalysts for a variety of syntheses. Very little is known how these catalysts operate, but a similar investigation to the one outlined in this thesis in non-aqueous media might improve our understanding of the stable polyoxometallate species that form. Also the exchangeable protons in aqueous media would now be visible. Indeed some very interesting protonation chemistry has been unravelled for the $[V_{10}O_{28}]^{6-}$ anion [53].

References

1). D. L. Kepert, *Prog. Inorg. Chem.*,1962, **4**, 199.

2). A. Hüllen, *Angew. Chem.*, 1964, **76**, 588.

3). W. N. Lipscomb, *Inorg. Chem.*, 1965, **4**, 132.

4). I. Lindqvist, *Acta Cryst.*, 1952, **5**, 667.

5). R. Allmann, *Acta Cryst. Sect. B*, 1971, **27**, 1393.

6). H.T. Evans Jr. and O. W. Rollins, *Acta Cryst. Sect. B*, 1976, **32**, 1565.

7). Y. H. Tsay and J. V. Silverton, *Z. Krist.*, 1973, **137**, 256.

8). J. Fuchs, H. Hartl, W. Schiller and U. Gerlach, *Acta Cryst. Sect. B*, 1975, **31**, 740.

9). J. Fuchs and E. P. Flindt, *Z. Naturforsch. Sect. B*, 1979, **34**, 412.

10) T. Lehmann and J. Fuchs, *Z. Naturforsch., Sect. B*, 1988, **43**, 89.

11). M. T. Pope, *Heteropoly and Isopoly Oxometallates*, Springer, Berlin, 1983.

12). D. L. Kepert, *Inorg. Chem.*, 1969, **8**, 1556.

13). P. B. Moore, *Neues Jahrb. Mineral. Abh.*, 1974, **120**, 205.

14). A. Goiffen, B. Spinner, *Rev. Chim. Minérale*, 1975, **12**, 316.

15). L. C. W. Baker, *Advances in the Chemistry of the Coordination Compounds*, ed. S. Kirschner, Macmillan, New York, 1961.

16). L. C. W. Baker, L. Lebioda, J. Grochowski, H. G. Mukherjee, *J. Am.Chem. Soc.*, 1980, **102**, 3274; L. Lebioda, M. Ciechanowicz-Rutkowska, L. C. W. Baker and J. Grochowski, *Acta Cryst. Sect. B*, 1980, **36**, 2530.

17). K. H. Tytko, *Angew. Chem., Internat. Ed.*, 1971, **10**, 860.

18). K. H. Tytko, *Z. Naturforsch. Sect. B*, 1973, **28**, 272.

19). K. H. Tytko and O. Glemser, *Chimia*, 1969, **23**, 494.

20). K. H. Tytko and O. Glemser, *Z. Naturforsch. Sect. B*, 1971, **26**, 659.

21). K. H. Tytko and O. Glemser, *Adv. Inorg. Chem. Radiochem.*, 1976, **19**, 239

22). H. T. Evans Jr. , *Perspec. Struct. Chem.*, 1971, **4**, 1.

23). L. G. Sillén, *Quart. Rev. Chem. Soc.*, 1959, **13**, 146.

24). A. T. Harrison and O. W. Howarth, *J. Chem. Soc. Dalton Trans.*, 1985, 1953.

25). O. W. Howarth, L. Pettersson and I. Andersson, *J. Chem. Soc. Dalton Trans.*, 1989, 1915.

26). O. W. Howarth, L. Pettersson and I. Andersson, *J. Chem. Soc. Dalton Trans.*, 1991, 1799.

27). C. Rocchiccioli-Deltcheff and R. Thouvenot, *Spectrosc. Lett.*, 1979, **12**, 127.

28). C. Rocchiccioli-Deltcheff, R. Thouvenot and M. Dabbabi, *Spectrochim. Acta Sect. A*, 1977, **33**, 143.

29). J. Aveston, *J. Inorg. Chem.*, 1964, **3**, 981.

30). J. Aveston, E. W. Anacker and L. S. Johnson, *J. Inorg. Chem.*, 1964, **3**, 735.

31). K. H. Tytko and B. Schoenfeld, *Z. Naturforsch. Sect. B*, 1975, **30**, 471.

32). K. H. Tytko, B. Schoenfeld, B. Buss and O. Glemser, *Angew. Chem. Internat. Ed.*, 1973, **12**, 330.

33). M. T. Pope and G. M. Varga Jr., *J. Chem. Soc. Chem. Comm.*, 1966, 653.

34). W. G. Klemperer, *Angew. Chem. Internat. Ed.*, 1978, **17**, 246.

35). O. Lutz, W. Nepple and A Nolle, *Z. Naturforsch. Sect. A*, 1976, **31**, 978.

36). R. R. Vold and R. L. Vold, *J. Chem. Phys.*, 1974, **61**, 4360.

37). L. P. Kazanskii, Sov. *J. Coord. Chem.*, 1977, **3**, 240.

38). M. A. Fedotov and R. I. Maksimovskaya, *Dokl. Phys. Chem.*, 1978, **240**, 431.

39). W. G. Klemperer and W. Shum, *J. Am. Chem. Soc.*, 1977, **99**, 3544.

40). M. Filowitz and W. G. Klemperer, *J. Chem. Soc. Chem. Comm.*, 1977, 201.

41). W. G. Klemperer and W. Shum, *J. Am. Chem. Soc.*, 1978, **100**, 4891.

42). W. G. Klemperer and W. Shum, *J. Chem. Soc. Chem. Comm.*, 1979, 60.

43). J. V. Hatton, Y. Saito and W. G. Schneider, *Can. J. Chem.*, 1965, **43**, 47.

44). O. W. Howarth and M. J. Jarrold, *J. Chem. Soc. Dalton Trans.*, 1978, 503.

45). O. W. Howarth and R.E. Richards, *J. Chem. Soc.*, 1965, 864.

46). L. P. Kazanskii, M. A. Fedotov, M. N. Ptushkina and V. I. Spitsyn, *Dokl. Phys. Chem.*, 1975, **224**, 1029.

47). L. P. Kazanskii and V. I. Spitsyn, *Dokl. Phys. Chem.*, 1975, **223**, 721.

48). O. Lutz, W. Nepple and A. Nolle, *Z. Naturforsch. Sect. A*, 1976, **31**, 1046.

49). R. I. Maksimovskaya, M. A. Fedotov, V. M. Mastikhin, L. I. Kuznetsova and K.I. Matveev, *Dokl. Phys. Chem.*, 1978, **240**, 422.

50). S. E. O'Donnell and M. T. Pope, *J. Chem. Soc. Dalton Trans.*, 1976, 2290.

51). E. Heath and O. W. Howarth, *J. Chem. Soc. Dalton Trans.*, 1981, 1105.

52). O. W. Howarth, *Prog. Nucl. Magn. Reson. Spectrosc.*, 1990, **22**, 453.

53). V. W. Day, W. G. Klemperer and D. J. Maltbie, *J. Am. Chem. Soc.*, 1987, **109**, 2991.

54). W. D. Kautt, H. Krueger, O. Lutz, H. Maier and A. Nolle, *Z. Naturforsch. Sect. A*, 1967, **31**, 351.

55). R. R. Vold and R. L. Vold, *J. Magn. Reson.*, 1975, **19**, 365.

56). R. Acerete, Ph. D. Thesis, Georgetown University, 1981; R. Acerete, C. F. Hammer and L. C. W. Baker, *J. Am. Chem. Soc.*, 1982, **104**, 5384.

57). R. Acerete, C. F. Hammer and L. C. W. Baker, *J. Am. Chem. Soc.*, 1979, **101**, 267.

58). R. Acerete, S. P. Harmalker, C. F. Hammer, M. T. Pope and L. C. W. Baker, *J. Am. Chem. Soc. Chem. Comm.*, 1979, 777.

59). R. G. Finke, M. Droege, J. R. Hutchinson and O. W. Gansow, *J. Am. Chem. Soc.*, 1981, **103**, 1587.

60). O. W. Gansow, R. K. C. Ho and W. G. Klemperer, *J. Organomet. Chem.* , 1980, **187**, C27.

61). Y. Jeannin and J. Martin-Frère, *J. Am. Chem. Soc.*, 1981,**103**, 1664.

62). J. Lefebvre, F. Chauveau, P. Doppelt and C. Brévard, *J. Am. Chem. Soc.*, 1981, **103**, 4589.

63). P. R. Sethuraman, M. A. Leparulo, M. T. Pope, F. Zonnevijlle, C. Brèvard and J. Lemerle, *J. Am. Chem. Soc.* , 1981, **103**, 7665.

64). R. I. Maksimovskaya and K. G. Burtseva, *Polyhedron*, 1985, **4**, 1559.

65). M. T. Pope and A. Müller, *Angew, Chem. Internat. Ed.*, 1991, **30**, 34.

66). M. Misono, *Catal. Rev. Sci. Eng.*, 1987, **29**, 269.

67). J. B. Moffat, *Chem. Eng. Comm.*, 1989, **83**, 9.

68). M. Misono, T. Okuhara and N. Mizuno, *Stud. Surf. Sci. Catal.*, 1989, **44**, 267.

69). E. M. Serwicka, J. B. Black and J. B. Goodenough, *J. Catal.*, 1987, **106**, 23.

70). S. Ahmed and J. B. Moffat, *Appl. Catal.*, 1988, **40**, 101.

71). A. R. Siedle, R. A. Newmark, W. B. Gleason, R. P. Skarjune, K. O. Hodgson, A. L. Roe and V. W. Day, *Solid State Ionics*, 1988, **26**, 109.

72). I. V. Kozhevnikov, *Russ. Chem. Rev.*, 1987, **56**, 811.

73). R. Neumann and M. Lissel, *J. Org. Chem.*, 1989, **54**, 4607.

74). C. L. Hill and D. A. Bouchard, *J. Am. Chem. Soc.*, 1985, **107**, 5148.

75). E. Papaconstantinou, *Chem. Soc. Rev.*, 1989, **18**, 1.

76). T. Yamase, *Polyhedron*, 1986, **5**, 79.

77). M. Faraj and C. L. Hill, *J. Chem. Soc. Chem. Comm.*, 1987, 1487.

78). I. V. Kozhevnikov and K. I. Matveev, *Appl. Catal.*, 1983, **5**, 135.

79). O. Nakamura, *Prog. Batteries Sol. Cells*, 1982, **4**, 230.

80). D. Dormont, B. Spire, F. Barre-Sinoussi, L. Montagnier and J. C. Chermann, *Ann. Inst. Pasteur/Virol. Sect. E*, 1985, **136**, 75.

81). R. H. Glew, M. S. Czuczman, W. F. Diven, R. L. Berens, M. T. Pope and D. E. Katsoulis, *Comp. Biochem. Physiol. Sect. B*, 1982, **72**, 581.

82). T. Yamase, H. Fujita and K. Fukushima, *Inorg. Chim. Acta*, 1988, **151**, 15.

83). F. Bussereau, M. Picard, J. Blancou and P. Sureau, *Acta Virol.*, 1988, **32**, 33.

84). R. H. Kimberlin and C. A. Walker, *Arch. Virol.*, 1983,**78**, 9.

85). J. Fisher, L. Ricard and R. Weiss, *J. Am. Chem. Soc.*, 1976, **98**, 3050.

86). K. G. Burtseva, L. A. Voropanova and L. A. Kochubei, *Russ. J. Inorg. Chem.* , 1984, **29**, 841.

87). L. A. Woodard and H. L. Robert, *Trans. Farad. Soc.*, 1956, **52**, 615; M. Theodorescu, *C. R. Acad. Sci., Ser.*, 1943, **216**, 117.

88). E. K. Simons, *Inorg. Chem.*, 1964, **3**, 1079.

89). K. G. Burtseva, T. S. Chernaya and M. I. Sirota, *Sov. Phys. Dokl.*,1978, **23**, 784.

90). H. T. Evans Jr. , B. M. Gatehouse and P. Leverett, *J. Chem. Soc. Dalton Trans.*, 1975, 505.

91). O. W. Howarth and P. Kelly, *J. Chem. Soc. Chem. Comm.*, 1988, 1236.

92). H. D' Amour and R. Allmann, *Z. Krist.*, 1972, **136**, 23; 1973, **138**, 5.

93). H.T. Evans Jr. and E. Prince , *J. Am. Chem. Soc.*, **105**, 1983, 4838.

94). K. I. Lunk, V. F. Chuvaev, I. D. Kolli and V. I. Spitsyn, *Dokl. Chem.*, 1968, **181**, 627.

95). J. P. Launay, M. Boyer and F. Chauveau, *J. Inorg. Nucl. Chem.*, 1976, **38**, 243.

96). M. J. Boyer and P. Souchay, *Electroanal. Chem.*, 1972, **38**, 169.

97). F. Chauveau, M. Boyer and B. LeMeur, *C. R. Acad. Sci. Ser. C*, 1969, **268**, 479.

98). P. Souchay, M. Boyer and F. Chauveau, *Kgl. Tek. Hoegsk. Handl. No. 259*, 1972 (Contributions to Coordination Chemistry in Solution, Stockholm, 1972, 159).

99). E. Birkholz, J. Fuchs, W. Schiller and H. P. Stock, *Z. Naturforsch. Sect. B*, 1971, **26**, 365.

100). S. C. Termes and M. T. Pope, *Inorg. Chem.*, 1978, **17**, 500.

101). M. Filowitz, R. K. C. Ho, W. G. Klemperer and W. Shum, *Inorg. Chem.*, 1979, **18**, 93.

102). H. Copaux, *Ann. Chim. Phys.*, 1909, **17**, 256.

103). R. Signer and H. Gross, *Helv. Chim. Acta*, 1934, **17**, 1076.

104). V. F. Chuvaev, K. I. Lunk and V. I. Spitsyn, *Dokl. Chem.*, 1968, **180**, 423.

105). J. P. Launay, Thesis, University of Paris VI, 1974

106). M. Boyer and P. Souchay, *Rev. Chim. Minérale*, 1971, **8**, 591.

107). M. J. Boyer, *Electroanal. Chem.*, 1971, **31**, 441.

108). M. Haeringer and J. P. Schwing, *Bull. Soc. Chim. France*, 1967, 708.

109). Y. Sasaki and L. G. Sillén, *Arkiv Kemi*, 1968, **29**, 253.

110). K. Matsumoto, A. Kobayashi and Y. Sasaki, *Bull. Chem. Soc. Japan*, 1975, **48**, 1009.

111). O. Nagano, *Acta Cryst. Sect. B*, 1979, **35**, 465.

112). A. Thiele and J. Fuchs, *Z. Naturforsch. Sect. B*, 1979, **34**, 145.

113). I. Lindqvist, *Arkiv Kemi*, 1950, **2**, 325; H. T. Evans Jr., *J. Am. Chem. Soc.*, 1968, **90**, 3275.

114). K. Sjöbom and B. Hedman, *Acta Chem. Scand. Sect. A*, 1973, **27**, 3673.

115). G. Johansson, L. Pettersson and N. Ingri, *Acta Chem. Scand. Sect. A*, 1979, **33**, 305.

116). O. W. Howarth, P. Kelly and L. Pettersson, *J. Chem. Soc. Dalton Trans.*, 1990, 81.

117). J. Fuchs, Conference on Polyoxometallates: From Platonic Solids to Anti-Retroviral Activity, Bielefeld, 1992.

118). P. Courtin, *Bull. Soc. Chim. France*, 1974, 2747.

119). P. Courtin, *Bull. Soc. Chim. France*, 1974, 2751.

120). P. Courtin and J. Lefebvre, *Bull. Soc. Chim. France*, 1975, 1983.

121). R. I. Maksimovskaya, S. M. Maksimov, A. A. Blokhin and V. P. Taushanov, *Russ. J. Inorg. Chem.*, 1991, **36**, 575.

122). K. G. Burtseva and L. A. Kochubei, *Russ. J. Inorg. Chem.*, 1991, **36**, 691.

123). H. Siebert, *Z. anorg. Chem.*, 1954, **275**, 225.

124). W. P. Griffith and I. D. Wickens, *J. Chem. Soc. Sect. A*, 1966, 1087.

125). R. N. Lindquist, J. L. Lyon Jr. and G. E. Lienhard, *J. Am. Chem. Soc.*, 1973, **95**, 8762.

126). K. Schiller and E. Thilo, *Z. anorg. Chem.*, 1961, **310**, 261.

127). F. Brito, *An. Quim. Sect. B*, 1966, **62**, 123, 193; *Acta Chem. Scand.*, 1967, **21**, 1968.

128). H. P. Stock and M. Engel, *Colloid Polym. Sci.*, 1978, **256**, 161.

129). J. Simon and K. F. Jahr, *Z. Naturforsch. Sect. B*, 1964, **19**, 165.

130). J. Fuchs, S. Mahjour and J. Pickardt, *Angew. Chem. Internat. Ed.*, 1976, **15**, 374.

131). H. T. Evans Jr., *Inorg. Chem.*, 1966, **5**, 967.

132). N. Pullman, Ph. D. Theseis, Rutgers University, 1966.

133). Y. N. Saf'yanov and N. V. Belov, *Sov. Phys. Dokl.*, 1976, **21**, 176.

134). Y. N. Saf'yanov, E. A. Kuz'min and N. V. Belov, *Sov. Phys. Dokl.*, 1977, **22**, 350.

135). A. G. Swallow, F. R. Ahmed and W. H. Barnes, *Acta Cryst.*, 1966, **21**, 397.

136). C. J. Besecker, W. G. Klemperer, D. J. Maltbie and D. A. Wright, *Inorg. Chem.*, 1985, **24**, 1027.

137). L. Pettersson, I. Andersson and O. W. Howarth, *Inorg. Chem.*, 1992, **31**, 4032.

138). C. M. Flynn Jr., M. T. Pope, *Inorg. Chem.*, 1971, **10**, 2524.

139). A. Rosenheim and M. Pieck, *Z. anorg. Chem.*, 1916, **98**, 230.

140). D. F. Takezhanova, *Dokl. Chem.*, 1974, **215**, 250.

141). C. M. Flynn Jr., S. E. O'Donnell and M. T. Pope, *Inorg. Chem.*, 1974, **13**, 831.

142). C. M. Flynn Jr., M. T. Pope, *Inorg. Chem.*, 1971, **10**, 2745.

143). M. A. Leparulo-Loftus and M. T. Pope, *Inorg. Chem.*, 1987, **26**, 2112.

144). P. J. Domaille, *J. Am. Chem. Soc.*, 1984, **106**, 7677.

145). R. I. Maksimovskaya and N. N. Chumachenko, *Polyhedron*, 1987, **6**, 1813.

146). K. Nishikawa, A. Kobayashi and Y. Sasaki, *Bull. Chem. Soc. Japan*, 1975, **48**, 889.

147). A. K. Ilyasova, D. F. Takezhanova, D. U. Begalieva and A. B. Bekturov, *Dokl. Chem.*, 1974, **215**, 250.

148). R. I. Maksimovskaya, A. K. Ilyasova, D. U. Begalieva, D. F. Takezhanova and A. K. Akhmetova, *Bull. Acad. Sci. USSR Div. Chem. Sci.* , 1984, **33**, 1977.

149). C. M. Flynn Jr., M. T. Pope, *Inorg. Chem.*, 1972, **11**, 1950.

150). K. Nishikawa, A. Kobayashi and Y. Sasaki, *Bull. Chem. Soc. Japan*, 1975, **48**, 3152.

151). M. A. Fedotov, R. I. Maksimovskaya, D. U. Begalieva and A. K. Il'yasova, *Izv. Akad. Nauk SSSR, Ser. Khim.*, 1980, 1477.

152). R. I. Maksimovskaya and M. A. Fedotov, *Zh. Strukt. Khim.*, 1981, **22**, 160.

153). G. Eriksson, *Anal. Chim. Acta*, 1979, **112**, 375.

154). K. Holmstrõm, Ph.D. Thesis, Umeå University, 1988.

155). A. T. Harrison and O. W. Howarth, *J. Chem. Soc. Dalton Trans.*, 1986, 1405.

156). O. W. Howarth and J. J. Hastings, *Polyhedron*, 1990, **9**, 143.

157). J. J. Hastings and O. W. Howarth, *J. Chem. Soc. Dalton Trans.*, 1992, 209.

158). J. J. Hastings and O. W. Howarth, *Polyhedron*, 1993, **12**, 847.

159). *Multinuclear NMR*, ed. J. Mason, Plenum, New York and London, 1987.

160). R. K. Harris, *Nuclear Magnetic Resonance*, Pitman, 1983.

161). E. Fukushima and S. B. W. Roeder, *Experimental Pulse NMR, A Nuts and Bolt Approach*, Addison-Wesley, 1981.

162). J. Sandstrōm, *Dynamic NMR Spectroscopy*, Academic Press, 1982.

163). J. K. M. Sanders and B. K. Hunter, *Modern NMR Spectroscopy, A Guide for Chemists*, Oxford University Press, 1987.

164). R. Freeman, *A Handbook of Nuclear Magnetic Resonance*, Longman Scientific and Technical, 1987.

165). G. E. Martin and A. S. Zektzer, *Two-Dimensional NMR Methods for Establishing Molecular Connectivity, A Chemist's Guide to Experiment Selection, Performance, and, Interpretation*, VCH, 1988.

166). D. Neuhaus and M. Williamson, *The Nuclear Overhauser Effect In Structural and Conformational Analysis*, VCH, 1989.

167). G. A. Morris and R. Freeman, *J. Magn. Reson.*, 1978, **29**, 433.

168). A. S. Tracy and J. S. Jaswal, *J. Am. Chem. Soc.*, 1992, **114**, 3835.

169). R. Freeman and H. D. W. Hill, *J. Chem. Phys.*, 1971, **54**, 3367.

170). E. L. Hahn, *Phys. Rev.*, 1949, **76**, 145.

171). E. L. Hahn, *Phys. Rev.*, 1950, **80**, 580.

172). H. Y. Carr and E. M. Purcell, *Phys. Rev.*, 1954, **94**, 630.

173). J. W. Akitt, J. M. Elders and O. W. Howarth, *J. Chem. Soc. Faraday Trans. 1*, 1989, **85**, 2035.

174). A. Bax and R. Freeman, *J. Magn. Reson.*, 1981, **63**, 454.

175). R. M. Smith and A. E. Martell, *Critical Stability Constants*, Plenum, New York and London, 1976.

176). J. Fuchs, H. Hartl, W. Schiller and U. Gerlach, *Acta Crystallogr. Sect B*, 1976, **32**, 1565.

177). *Transition Metal Nuclear Magnetic Resonance, (Studies in Inorganic Chemistry Vol. 13)*, ed. P. S. Pregosin, Elsevier Science, Amsterdam, 1991.

178). J. -Y. Kempf, M. -M. Rohmer, J. -P. Poblet, C. Bo and M. Bénard, *J. Am. Chem. Soc.*, 1992, **114**, 1136.

PUBLISHED PAPERS NOT FILMED FOR COPYRIGHT REASONS

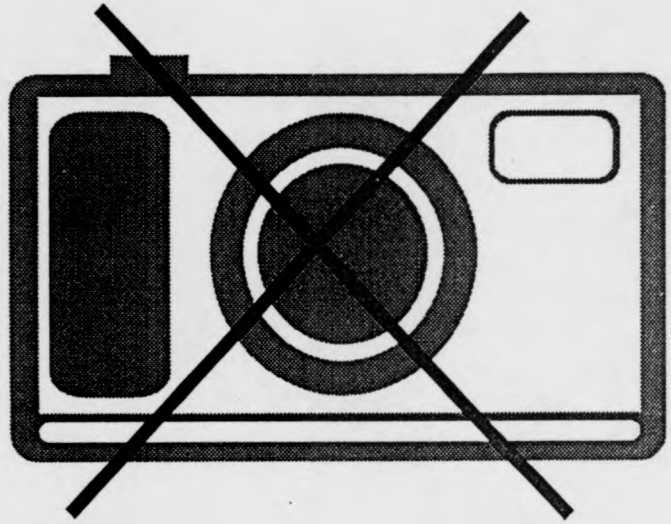

173 – END